Master thesis report

Conformable High-Pressure Type IV Hydrogen Storage System: Conceptual Design for Urban Air Mobility Applications

In collaboration with Expleo Group

M. Rodriguez

Expleo Group Toulouse

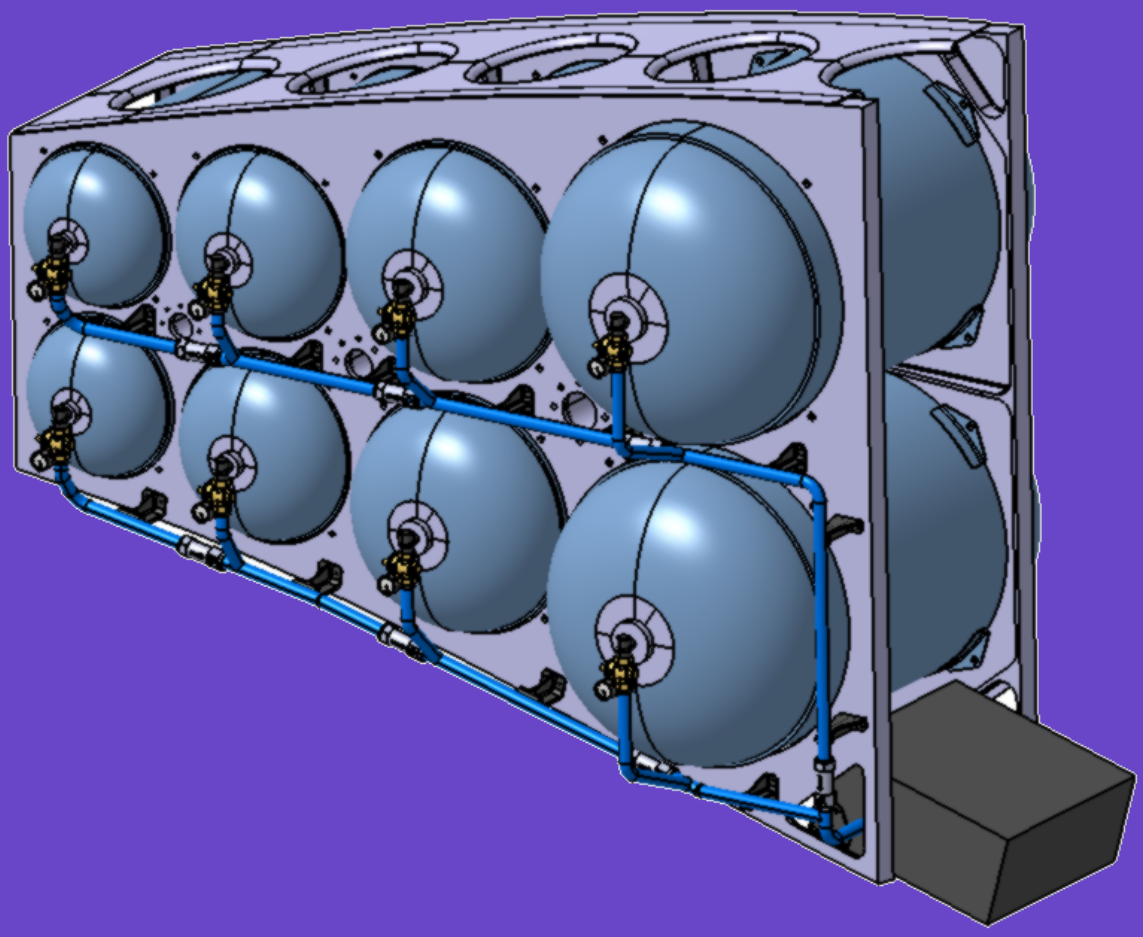

expleo
Think bold, act reliable

TU Delft

Master thesis report

Conformable High-Pressure Type IV Hydrogen Storage System: Conceptual Design for Urban Air Mobility Applications

by

M. Rodriguez

to obtain the degree of Master of Science at the Delft University of Technology,
to be defended publicly on the 20th of June 2024.

Company supervisor:	V. Bruere
TU Delft supervisor:	J. van Campen
Company:	Expleo Group
Place:	Bureau d'études Expleo Group St-Martin-du-Touch
Project Duration:	October, 2023 - June, 2024

Cover Image:	Render of conformable design
LaTeX template:	Adapted from the *TU Delft unofficial template*

[expleo]

Think bold, act reliable

TU Delft

Preface and acknowledgements

This thesis explores the potential of Type IV conformable compressed hydrogen pressure vessels to enhance the efficiency and performance of Urban Air Mobility (UAM) vehicles, specifically focusing on the Varuna EVTOL. The motivation for this research stems from the pressing need for sustainable and environmentally friendly propulsion systems in the aerospace industry. Hydrogen, with its high energy density and zero carbon emissions, presents a promising solution, but its storage poses significant challenges, particularly in weight-sensitive applications like UAM.

The journey to completing this thesis has been both challenging and rewarding. It involved an extensive literature review, conceptual design, and theoretical analysis. The collaboration with TU Delft and Expleo Group was instrumental in providing the necessary resources and expertise to conduct this research.

This thesis represents not only the culmination of my academic efforts but also my contribution to advancing sustainable aerospace technologies. I hope that the findings and recommendations presented here will pave the way for further innovations in hydrogen-powered aviation.

I would like to extend my deepest gratitude to all those who have supported and guided me throughout this research journey.

First and foremost, I would like to thank my supervisor, Julien van Campen, for their invaluable guidance, encouragement, and constructive feedback. Their expertise and insights were crucial in shaping the direction of this research.

I am also grateful to the TU Delft and Expleo Group for their collaboration and support. Special thanks to Valentin Bruere and Benoit Courouble at Expleo Group for providing access to the Varuna EVTOL and sharing their industry knowledge, which greatly enriched this study.

Finally, I would like to express my deepest appreciation to my family and friends for their unwavering support and understanding throughout this journey. To my parents, for their constant encouragement and belief in my abilities, and to my friends, for their patience and support during the challenging times.

Thank you all for being a part of this journey.

M. Rodriguez
Delft, June 2024

Contents

Nomenclature

Abbreviations

Abbreviation	Definition
BOP	Balance-Of-Plant
CAD	Computer-Aided Design
CFD	Computational Fluid Dynamics
CFRP	Carbon Fiber Reinforced Polymer
CTE	Coefficient of Thermal Expansion
EOL	End-of-Life
EU	European Union
EVTOL	Electric Vertical Take Off and Landing
FEM	Finite Element Method
FPF	First-Ply-Failure
HDPE	High Density PolyEthylene
ID	Identifier
L/D	Length-to-Diameter ratio
NIST	National Institute of Standards and Technology
PA6	PolyAmide6
SHC	Specific Heat Capacity
SPC	Single Point Constraint
UAM	Urban Air Mobility

Symbols

Symbol	Definition	Unit
A	Surface area	[m^2]
a	Van der Waals constant	[Pam^6mol^{-2}]
a_i	Virial constant	[-]
b	Van der Waals constant	[m^3mol^{-1}]
b_i	Virial constant	[-]
c_i	Virial constant	[-]
c_{str}	Structure mass coefficient	[-]
E_{req}	Energy required	[J]
e_{H2}	Hydrogen specific energy	[Jkg^{-1}]
h	Specific enthalpy	[Jkg^{-1}]
L_{cyl}	Cylinder length	[m]
$\frac{L}{D}$	Length to diameter ratio	[-]
LHV_{H2}	Hydrogen lower heating value	[Jkg^{-1}]
M_{H2}	Hydrogen molar mass	[$kgmol^{-1}$]
M_{incr}	Mass increase	[%]
m	Mass	[kg]
$\dot{m}$	Mass flow	[kgs^{-1}]
m_e	Empty hydrogen mass	[kg]
m_{EVTOL}	EVTOL mass	[kg]
m_f	Filled hydrogen mass	[kg]
m_{H2}	Hydrogen mass	[kg]
m_{req}	Required hydrogen mass	[kg]

Symbol	Definition	Unit
m_{tot}	Total concept mass	[kg]
N_θ	Hoop membrane load	[Nm^{-1}]
N_ϕ	Axial membrane load	[Nm^{-1}]
n_{gd}	Non-geodesic exponent	[-]
n_α	Number helical layers	[-]
n_θ	Number hoop layers	[-]
P	Pressure	[Pa]
P_e	Empty pressure	[Pa]
P_e	Filled pressure	[Pa]
p_{adj}	Adjusted power	[W]
p_{avg}	Average power	[W]
R	Local radius	[m]
R_0	Polar/boss radius	[m]
R_{cyl}	Cylinder radius	[m]
R_i	Inner radius	[m]
R_{tl}	Dome-cylinder tangent radius	[m]
R_g	Gas constant	[$JK^{-1}mol^{-1}$]
r_m	Radius of meridian	[mm]
SF	Safety factor	[-]
T_{H2}	Hydrogen temperature	[K]
t_{flight}	Flight time	[s]
t_0	Initial flight time	[s]
t_0	Thickness at cylinder junction	[mm]
t_{adj}	Adjusted flight time	[s]
t	Thickness	[mm]
t_α	Helical thickness	[mm]
t_θ	Hoop thickness	[mm]
t_{ply}	Ply thickness	[mm]
u	Specific internal energy	[Jkg^{-1}]
V_{avbl}	Available volume	[m^3]
V_{cyl}	Cylinder volume	[m^3]
V_{dome}	Dome volume	[m^3]
V_{H2}	Hydrogen volume	[m^3]
V_t	Tank volume	[m^3]
V_{tail}	Tail volume	[m^3]
V_{tot}	Total concept volume	[m^3]
x	Distance from cylinder junction	[m]
Z_e	Empty compressibility factor	[-]
Z_f	Filled compressibility factor	[-]
Z_v	Virial compressibility factor	[-]
α	Local winding angle	[deg]
α_0	Cylindrical winding angle	[deg]
β	Compressibility fitting coefficient	[KPa^{-1}]
δ	Non geodesic winding factor	[deg]
η_{grav}	Gravimetric efficiency	[-]
η_{vol}	Volumetric efficiency	[gL^{-1}]
η_{fill}	Fill efficiency	[-]
η_{FC}	Fuel cell efficiency	[-]
ϕ	Azimuth angle of R_m	[deg]
ρ	Density	[kgm^{-3}]
σ_f	Failure stress	[MPa]
γ	Ratio specific heat capacities	[-]
Ψ	Dome azimuth angle	[deg]

List of Figures

List of Tables

1. Introduction

The aerospace industry is increasingly focusing on developing sustainable and environmentally friendly propulsion systems. Hydrogen, as a clean energy carrier, offers a promising solution due to its high energy density and zero carbon emissions when used in fuel cells. However, effective storage of hydrogen poses a significant challenge, particularly in the weight-driven environment of aerospace.

Reducing the weight of aerospace systems is essential for improving fuel efficiency, increasing payload capacity, and enhancing overall performance. This necessity drives the demand for lighter systems, which can be achieved through the use of composite materials. Composites, such as carbon fiber-reinforced polymers (CFRPs), provide an excellent strength-to-weight ratio, corrosion resistance, and design flexibility. These materials enable the creation of complex shapes, making them ideal for innovative structural designs in hydrogen storage systems.

Type IV pressure vessels are a class of composite pressure vessels with a polymer liner fully wrapped with a composite material such as CFRPs. They are designed to withstand high-pressure hydrogen storage while being significantly lighter than their metal counterparts. The use of advanced composites in Type IV pressure vessels not only reduces the overall weight but also enhances their durability and performance, making them a preferred choice for hydrogen storage in aerospace applications.

Urban Air Mobility (UAM) represents a transformative vision for future urban transportation, utilizing electric or hybrid-electric vertical takeoff and landing (EVTOL) aircraft to move people and goods within urban areas. These aircraft require highly efficient and lightweight energy storage solutions to maximize range and payload while ensuring safety and performance standards. Hydrogen fuel cells, with their higher energy density compared to batteries, are a promising technology for powering UAM vehicles.

Traditional cylindrical compressed hydrogen pressure vessels, while effective for stationary applications, present challenges in the transportation sector. Their shape and limited volumetric efficiency result in sub-optimal use of space within vehicles, complicating integration and impacting performance. Moreover, the weight of these pressure vessels can offset some of the advantages offered by hydrogen fuel cells.

Conformable compressed hydrogen storage systems, designed to fit irregular spaces within a predetermined structure, offer a potential solution to these challenges. By optimizing the shape and distribution of storage tanks, these systems can enhance volumetric efficiency and integrate seamlessly into aircraft design. Additionally, the use of composite materials in these conformable tanks can further reduce weight, improving the overall performance and feasibility of hydrogen-powered UAM vehicles.

1.1. Research scope & goals

In collaboration with TU Delft and Expleo Group, this research project will propose a conformable compressed hydrogen storage solution for the Varuna EVTOL. Expleo aims to convert its existing electric passenger drone to a hydrogen-powered vehicle and increase its expertise in novel composite hydrogen storage solutions while minimizing the impact on the existing design. The project will focus on the preliminary design phase. The goal of this project is to develop a large-scale conformable Type IV compressed hydrogen storage design for a small air passenger vehicle. This project seeks to push the boundaries of hydrogen storage technology. By using advanced composite materials and innovative design methodologies, the objective is to create a storage system that optimizes volumetric efficiency, integration flexibility, and overall performance. This research aims to contribute to the advancement of clean energy technologies in the aerospace industry, paving the way for efficient and eco-friendly hydrogen-powered aviation.

1.2. Varuna EVOL

The Expleo EVTOL Varuna vehicle is one of the key aspects of the research project. The Varuna project aims to develop a small aircraft capable of taking off and landing using electrical propulsion [1]. The

purpose of the project is to investigate the recent developments in electrical technology that make such a project possible as of 2023.

Varuna is a system that aims to meet the growing need for Urban Air Mobility (UAM) and so-called ”Flying taxis”. Given the recent major advancements in electrical propulsion such as motors, batteries, fuel cells, and electronic control systems, this technology has garnered much interest and investment in recent times [1].

The solution proposed by Expleo aims to investigate most of these aspects. The system is going to be a 4-seater quad-rotor running on batteries. The system shall be able to take off and land from both sea and ground and shall be multipurpose (aerial surveillance, medical, inspection, civil or VIP transport, and aerial freight) [1]. Furthermore, the system shall include innovative technologies to improve safety, performance, and operational costs.

At this stage in the project the system uses a battery system to store the energy required to operate the EVTOL [1]. This research project aims to develop an innovative hydrogen storage system so that the current system can be powered using hydrogen fuel cells with onboard hydrogen storage. In the figure below a render of the current system can be seen. Note that as the project progresses several design changes may occur as this is an internal research project for Expleo Group [1].

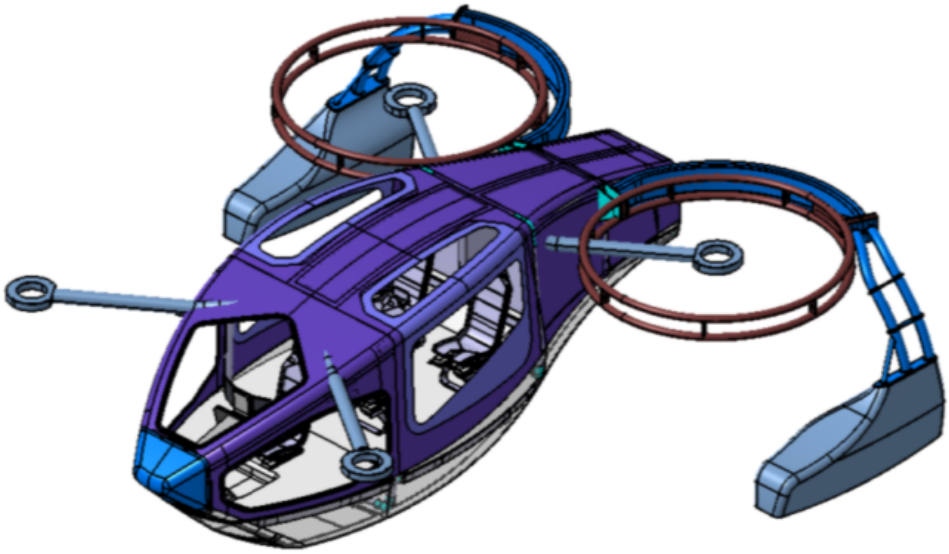

Figure 1.1: Overview of Varuna EVTOL

1.3. Research questions

To achieve the project goals, the research will address several key questions that explore the potential benefits and challenges of implementing conformable pressure vessels in UAM vehicles. The main research question guiding the research project is:

“**To what extent can Type IV conformable compressed hydrogen pressure vessels enhance the efficiency and performance of Urban Air Mobility (UAM) vehicles compared to conventional Type IV pressure vessels?**”

To answer this research question several sub-questions need to be addressed. These can be found in the list below.

- How much can conformable pressure vessels increase the hydrogen mass stored within a predetermined volume compared to conventional pressure vessels?

- To what extent can conformable pressure vessels make better use of available space in UAM vehicles compared to conventional pressure vessels?
- How do conformable pressure vessels affect the operational range of UAM vehicles compared to conventional pressure vessels?
- How does the weight of conformable pressure vessels affect the overall weight and balance of UAM vehicles compared to conventional pressure vessels?

These questions aim to comprehensively evaluate conformable hydrogen storage solutions and their implications for the efficiency, performance, and design of UAM vehicles like the Varuna EVTOL.

2. Methodology

The first step of the research project is to establish the design methodology. This can be done by identifying the goals and philosophy of the project as well as the aims of the various stakeholders. The research project aims to explore conformable Type IV pressure vessel solutions for vehicular design. This will be achieved by developing a toolbox for conceptual design and comparing existing solutions to the proposed solution. This toolbox will be developed for pre-existing vehicles to develop solutions with minimal impact on the original vehicle and structure.

As such the research project will follow an unconventional design approach. This is mainly due to the dual requirement of developing both a conformable compressed hydrogen storage solution and a comprehensive toolbox for preliminary design. The first part of the research project will focus on developing the toolbox and relevant models required for conceptual design. To do this a conventional Type IV pressure vessel will be designed and used as a baseline for verification. The research project will focus on the preliminary design stage.

The first step will be to perform a functional analysis of the Varuna EVTOL while considering all stakeholder needs and requirements. This will be useful to determine the various performance requirements of the hydrogen system while establishing a set of system requirements. These requirements can then be used to compare the conventional and conformable design while ensuring that they apply to the current Varuna design.

The outcome of the functional analysis will be used to develop the preliminary sizing model, which will serve to design a conventional Type IV pressure vessel according to the performance requirements. This model will provide a first-level estimate of hydrogen mass, that can then be used to define the various geometrical dimensions of the pressure vessel. At this stage, a list of material candidates will be identified for the various components of the pressure vessel. The materials will be chosen during the preliminary design. Additionally, various dome designs and manufacturing processes will be considered. Finally, the preliminary sizing will conclude with an initial structural sizing. At this stage, a conceptual design of a Type IV pressure vessel will be finished and can be used as the baseline for verification and comparison with the conformable solutions.

The next step of the design project is to develop a thermal and structural analysis model that can be used to verify the outcome of the preliminary sizing. This can also be used to quickly iterate through a variety of designs and solutions later on. The thermal and structural models will be verified using data available in the literature before being applied to the conventional design. At this stage, the hydrogen state modeling will also be verified using a variety of models and equations of state for gaseous hydrogen.

Once the conventional design is completed, a performance and efficiency analysis will be performed. This will be used to define the various criteria used to compare the different solutions. Here, the capability of a hydrogen-powered Varuna with a conventional pressure vessel will be determined. This will be the final step in the design of the conventional pressure vessel. At this stage, the preliminary design of the conventional tank and the toolbox for conceptual design are completed and verified.

The next step is to explore different conformable storage solutions, which will be done by generating a list of concepts and selecting the best candidate via a tradeoff. Once a concept has been chosen, it will be designed using the toolbox and models previously developed. The chosen concept's performance and efficiency will be evaluated to compare it with the conventional design. This will be done via a comparative analysis. This comparative analysis will determine whether conformable solutions are advantageous for the given application.

The research project will conclude by determining the next steps to transform the conceptual design into a detailed design which will be integrated into the Varuna EVTOL. The design will be expanded upon within Expleo Group and will serve as a baseline for future designs within the company.

3. Functional analysis

The first step of the research project, as seen in the project timeline and design methodology (See Chapter 2), is to perform a functional analysis. This starts by identifying the stakeholder needs and need statement. These can then be translated into a set of clear requirements with corresponding identifiers (IDs). The next part of the functional analysis consists of deriving the constraints imposed on the design. Finally, the stakeholder requirements and design constraints can be translated into a set of technical system requirements which can be used to verify the design at a later stage.

3.1. Requirement identification

In order to generate a set of clear stakeholder requirements the research project need statement must be identified. Furthermore, it is necessary to organize the requirements using IDs such that they can be readily accessed. Finally, the stakeholder requirements are generated from the various stakeholder needs. There are two main stakeholders for this research project: the TU Delft and Expleo Group are represented by Julien Van Campen and Valentin Bruere respectively.

3.1.1. Need statement

The need statement conveys the needs of the different stakeholders in a concise and clear way, that can be used to identify the scope and goal of the research project. Given that this is both a research and design project, the need statement consists of two main needs. The need statement for the research project is:

"**There exists a need for compressed hydrogen storage solutions with unconventional shapes for applications where the shape and geometry of the surrounding system cannot be altered. Additionally there exists a need for Expleo to increase its knowledge and expertise in conformable composite gaseous hydrogen storage solutions for aerospace applications**"

3.1.2. Requirement ID generation

Before the stakeholder needs can be translated into a set of unambiguous requirements it is necessary to establish a proper requirement identification method. Each requirement must be assigned an ID. Hence requirements IDs are generated according to this pattern:

AAA-BBB-XXX where AAA and BBB are alphabetic characters while XXX are numeric characters.

- In the AAA field, the requirement type is indicated as an acronym.
- In the BBB field, the requirement subtype is indicated as an acronym.
- In the XXX field, the requirement ID is indicated as a 2-digit number. IDs cannot be reused even if requirements are deleted.

The different requirement types and subtypes can be seen in Table 3.1.

Table 3.1: Requirement types, subtypes, and their corresponding acronyms

Types		**Subtypes**	
Acronym	**Term**	**Acronym**	**Term**
SHR	Shareholder	EXP	Expleo
SYS	System	TUD	TU Delft
		THERM	Thermal
		OPS	Operational
		SAFE	Safety
		MAT	Material
		GEN	General

3.1.3. Stakeholder requirements

The set of user requirements has been generated from the stakeholder needs. The main stakeholders of this project are Expleo Group and the TU Delft Faculty of Aerospace Engineering.

The Expleo Group stakeholder needs stem from the initial project proposal for the Varuna EVTOL [1]. The project needs are ever-evolving as this is an internal research project with a variable team and as such new needs might arise on Expleo's side. However, for the sake of the research project, the stakeholder needs will be fixed. The final version of the stakeholder needs will be those of January 2024.

Given that the project is a research project and not a conventional design exercise several requirements stem from the research gaps that were identified in the literature study. The TU Delft needs are those that originate from the literature study, discussions with the thesis coordinator, and the project goals. The TUD stakeholder requirements are specific to the hydrogen storage vessel while the EXP requirements refer to the Varuna EVTOL as a whole. The stakeholder requirements can be found in Table 3.2 and 3.3.

Table 3.2: Expleo stakeholder requirements

ID	Requirement
SHR-EXP-01	Varuna shall be a quadrotor system.
SHR-EXP-02	Varuna shall be fully powered by electricity.
SHR-EXP-03	Varuna shall be able to land on the ground and water.
SHR-EXP-04	Varuna shall have a low environmental and noise impact.
SHR-EXP-05	Varuna shall be multi-purpose: civil, military.
SHR-EXP-06	Varuna shall be a modular 4-seater vehicle depending on mission requirements.
SHR-EXP-07	Varuna shall have an endurance of 1 [h].
SHR-EXP-08	Varuna shall be able to fly at 100 [kmh^{-1}].
SHR-EXP-09	Varuna's energy shall be provided by batteries or hydrogen.
SHR-EXP-10	Varuna shall employ new innovative technologies and methodologies.
SHR-EXP-11	Varuna shall be safe.

Table 3.3: TU Delft stakeholder requirements

ID	Requirement
SHR-TUD-01	The hydrogen storage solution shall be a composite pressure vessel.
SHR-TUD-02	The hydrogen storage solution shall be a Type IV pressure vessel.
SHR-TUD-03	The hydrogen storage solution shall be a conformable pressure vessel.
SHR-TUD-04	The hydrogen storage solution shall control & distribute hydrogen to Varuna.
SHR-TUD-05	The hydrogen storage solution shall be efficient (volumetric/gravimetric).
SHR-TUD-06	The hydrogen storage solution shall be lightweight.
SHR-TUD-07	The hydrogen storage solution shall be a high-pressure storage vessel (70 [MPa]).
SHR-TUD-08	The hydrogen storage solution shall operate within a safe temperature range.
SHR-TUD-09	The hydrogen storage solution shall be durable and reliable.

3.2. Design constraint analysis

Before the system technical requirements can be drafted, it is necessary to perform an analysis of the design to identify the various constraints. These constraints are mainly geometrical since most of the operative requirements can be found in Table 3.2. To identify the constraints, a spatial breakdown of Varuna must be performed. The various dimensions of the spatial breakdown can then be specified.

3.2.1. Varuna EVTOL spatial breakdown

A global view of Varuna can be found in Figure 1.1 In order to identify the potential design spaces and constraints Varuna must be split into multiple sections. This is done in Figure 3.1 where the vehicle is

split into three main sections: cabin, cargo, and tail. Each section is represented by a bounding box and volume in CATIA which are simplification of the original structure.

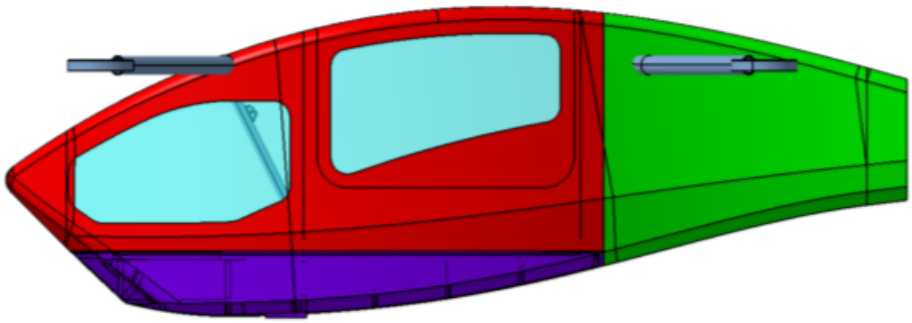

Figure 3.1: Overview of Varuna sections. Cabin in red, tail in green and cargo in purple

Each bounding box represents the design space for each section, individual subsystems must be contained within a single section for structural reasons. The cabin (See Figure 3.2) is where the navigation and control subsystem are contained. It is where the pilot and passengers are located as well as the main structural components such as rotor arms and floor. This section cannot be used as the location for the hydrogen storage system. This is because it is already encumbered and the passengers or pilot cannot be moved to another section. Furthermore, the hydrogen storage system needs to be distanced from the passengers to ensure their safety in case of pressure vessel failure.

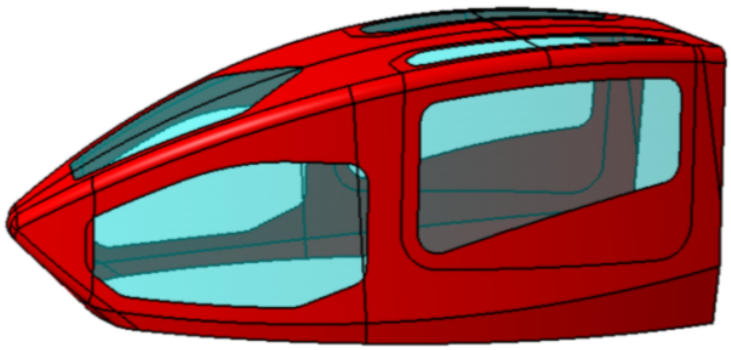

Figure 3.2: Bounding box of cabin section

The cargo area (See Figure 3.3) is where the current battery arrays are stored, this section is relatively large. The batteries are located in this section to lower the center of gravity of the vehicle while distributing the center of gravity over the vehicle footprint. This section would be the ideal location for the fuel cell array when transforming Varuna from a battery-powered vehicle to a hydrogen fuel cell vehicle. This is because the fuel cell array exhibits similar properties to the battery array in terms of mass and volume. Furthermore, this location is not ideal for the hydrogen storage subsystem in case

of a crash as the passengers are situated right above the cargo area. The crash might lead to failure of the pressure vessel and an explosion below the passengers.

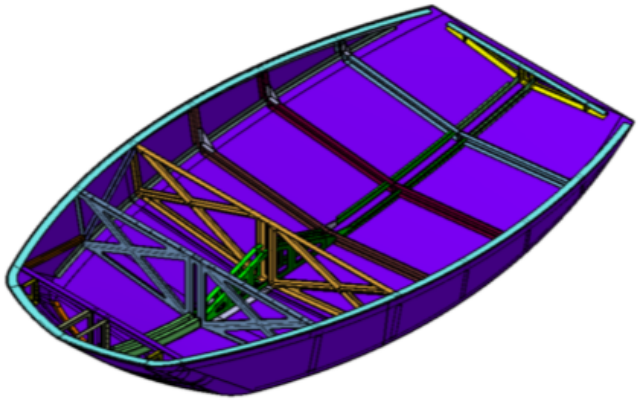

Figure 3.3: Bounding box of cargo section

The final section is the tail section (See Figure 3.4), this is where the hydrogen storage system will be located. It is a large and relatively empty section. Furthermore, it is safer in terms of crashes than the other sections. It can be separated from the cabin via a strong divider. The limitation of having the storage system in the tail is that it increases the height of the center of gravity and shifts it backward which is undesirable for control purposes.

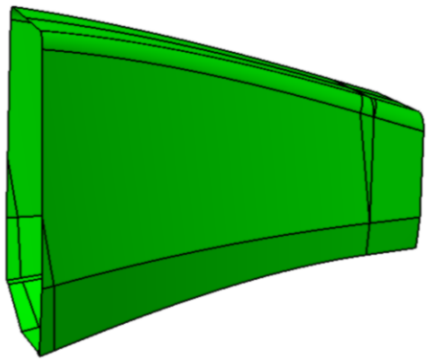

Figure 3.4: Bounding box of tail section

3.2.2. Varuna EVTOL dimensions

Now that the different sections have been identified, it is important to measure the various sections. These dimensions will determine the maximum volume and shape of the subsystem as the bounding box is considered to be fixed for this vehicle and cannot be changed. Top-level estimates can then be derived from these dimensions and used in Chapter 4. An overview of all dimensions can be found in Figure 3.5

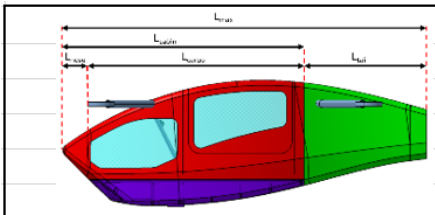

Description	Property	Value	Unit
Total vehicle length	Lmax	6650	mm
Cabin length	Lcabin	4410	mm
Nose length (up to cargo bay)	Lnose	426	mm
Cargo bay length	Lcargo	3940	mm
Tail length (from end of cabin)	Ltail	2240	mm

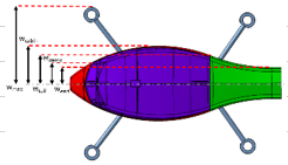

Maximum vehicle width	wmax	2426	mm
Maximum cabin width	wcabin	1190	mm
Maximum tail width	wtail	1780	mm
Minimum cargo bay width	wcargo	1380	mm
Minimum tail width (end width)	wend	1000	mm

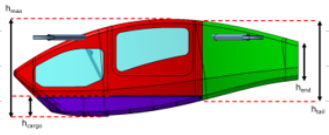

Maximum vehicle height	hmax	2300	mm
Maximum cargo bay height	hcargo	465	mm
Maximum tail height	htail	1860	mm
Minimum tail height (end height)	hend	890	mm

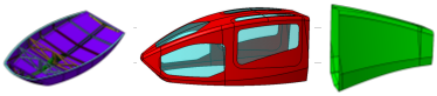

Cargo bay bounding volume	Vcargo	2360	L
Cabin bounding volume	Vcabin	12600	L
Tail bounding volume	Vtail	3520	L

Figure 3.5: Varuna breakdown dimensions

3.3. Technical system requirements

Using the stakeholder requirements and the constraint analysis, a list of top-level system technical requirements can be generated. These requirements can be used to verify and validate the design in Chapter 8. Given that the research project will provide a preliminary design for a modular hydrogen storage system, the list of requirements does not contain all technical requirements. The list of requirements focuses on the primary needs and requirements of the system. They are broken down by subsystem and can be found in Table 3.4

Table 3.4: System technical requirements

ID	Requirement
SYS-THERM-01	The maximum vessel temperature shall be less than 85 [°C].
SYS-THERM-02	The minimum vessel temperature shall be less than -40 [°C].
SYS-OPS-01	The nominal storage pressure shall be 70 [MPa].
SYS-OPS-02	The empty storage pressure shall be 2 [MPa].
SYS-OPS-03	The storage vessel's usable hydrogen mass shall be at least 33.34 [kg].
SYS-OPS-04	The maximum filling pressure shall be less than 125 [%] of nominal pressure.
SYS-SAFE-01	The storage vessel burst pressure safety factor shall be above 2.25 [-].
SYS-SAFE-02	The storage vessel shall have a permeation rate of less than 46 [mLh^{-1}]
SYS-MAT-01	The storage vessel wall material shall be a composite material.
SYS-MAT-02	The storage vessel liner material shall be a polymer material.
SYS-GEN-01	The storage vessel shall be positioned inside the tail zone of Varuna.
SYS-GEN-02	The storage vessel shall provide enough hydrogen to complete the mission.

The aforementioned requirements are driven by regulations, stakeholder requirements and design constraints. Requirements SYS-THERM-01, SYS-THERM-02, and SYS-OPS-04 directly stem from the SAE J2601 fueling protocol [2]. Requirements SYS-OPS-01, and SYS-OPS-02 are driven by current technology in composite material capabilities and fuel cell inlet pressure requirements respectively [3, 4]. An empty pressure of 2 [MPa] ensures sufficient inlet pressure for the fuel stack array [5]. Requirement SYS-OPS-03 is directly taken from Chapter 4 and is generated from the vehicle energy

requirements. SYS-SAFE-01 and SYS-SAFE-02 are directly taken from industry standards ISO/TS 15869 and R314 which define safety factor and permeation rates for compressed hydrogen storage solutions. The material and general system requirements are generated from stakeholder requirements SHR-TUD-01, SHR-TUD-02, SHR-EXP-07, SHR-EXP-08, and SHR-EXP-09 as well as the constraint analysis in Section 3.2.

Now that the system functional analysis is completed, the next step of the research project, the system preliminary sizing, can be started. This will be covered in the next chapter.

4. Preliminary sizing

Using the set of unambiguous technical requirements a preliminary sizing of the hydrogen storage vessel can be performed. Note that the preliminary design will be set up for the conventional single tank configuration and that the tools and models developed can then be used to design the multi-cellular configuration in Chapter 9.

The preliminary design phase starts with a performance analysis of the Varuna system, and then the required hydrogen mass and volume can be derived. This can then be used to compute the geometrical dimension and shape of the system. Finally, netting analysis [6, 7] can be used to derive the required structural thicknesses. An overview of the preliminary design can be found in Chapter 7.

4.1. Varuna performance breakdown

In order to derive the required hydrogen mass and volume for Varuna to perform its mission it is necessary to look at its power and energy requirements. Varuna is currently a quad-rotor electric vehicle. Its total mass is 3200 [kg] including 1000 [kg] of batteries.

The power and energy requirements have been obtained by exchanging with the power and propulsion team of the Varuna EVTOL project. Since the technical maturity of the project is relatively low, they are estimates. The hovercraft requires 1.3 [MW] of power for takeoff and an average power of 0.9 [MW] for hovering. Furthermore, it is known that the takeoff and climb phase takes 5 [min] of the total flight time. An overview of the flight parameters can be found in Table 4.1.

Table 4.1: Varuna flight parameters

Property	Value	Unit
Vehicle mass	3200	kg
Battery mass	1000	kg
Takeoff power	1.3	MW
Hover power	0.9	MW
Flight time	60	min
Takeoff/Climb time	5	min

Figure 4.1 shows the required power over the flight time. Using these flight parameters, the required hydrogen mass and volume can be derived. This will be done in the next section.

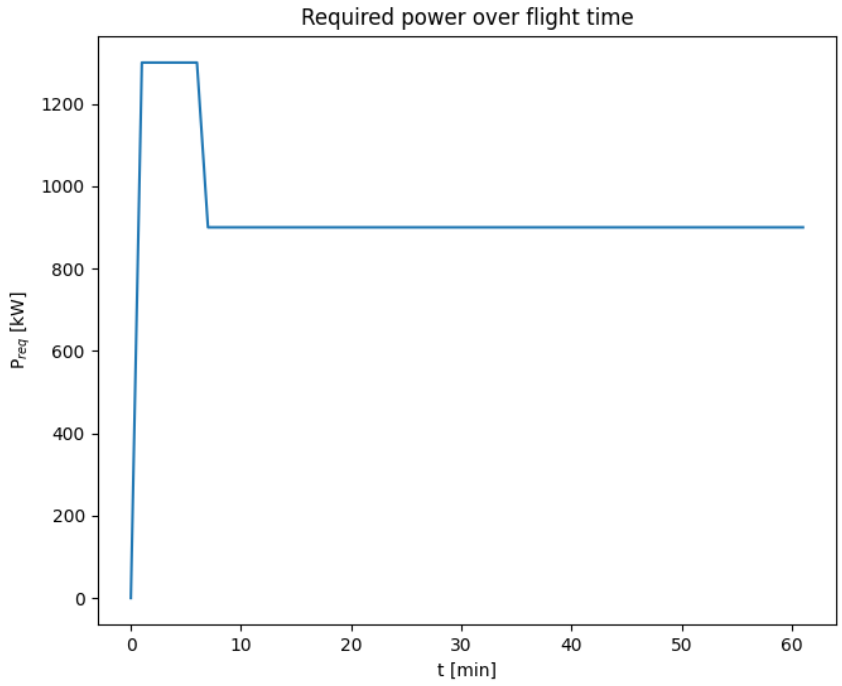

Figure 4.1: Graph of required power versus flight time

4.2. Hydrogen mass & volume sizing

To obtain the required hydrogen mass and volume, the overall energy requirements of the Varuna EVTOL must be derived. This can be done using the flight parameters from Section 4.1 and Equation 4.1.

$$m_{H2} = \frac{E_{req}}{e_{H2} \cdot \eta_{FC}} = \frac{p_{avg} \cdot t_{flight}}{\eta_{FC} \cdot LHV_{H2}} \tag{4.1}$$

Where m_{H2} is the required hydrogen mass, E_{req} is the required energy, e_{H2} is the specific energy of hydrogen, η_{FC} is the fuel cell efficiency, p_{avg} is the average power required, t_{flight} is the flight time and LHV_{H2} is the lower heating value of hydrogen.

A few assumptions are made for this equation to be true. First of all the fuel cells are the only components that contribute to the system energy losses, other losses are neglected. The fuel cell efficiency is taken at End-of-Life (EOL) Next the lower heating value of hydrogen gas is used as the specific energy, this is in accordance with the European Union (EU) convention for fuel cell design [8]. Finally, the power required is taken as constant throughout the flight with a value of 1 [MW], 7 [%] higher than the actual average power of 0.933 [MW]. This is done to provide a conservative estimate of the required mass to account for electrical losses and permeation.

The mass obtained in Equation 4.1 represents the required usable hydrogen mass. The pressure vessel shall never be fully emptied such that a constant flow of hydrogen can be fed to the fuel cell array throughout the flight time. As the hydrogen mass inside the tank decreases so does the pressure. It is assumed that the mass outflow is constant throughout the flight time. In order to ensure that the fuel cell stack receives a steady supply of hydrogen, a minimum empty pressure of 2 [MPa] is required [5].

With a given empty and nominal pressure, a required hydrogen mass, and an assumed storage temperature the required tank volume can be derived from Equation 4.2, 4.3, 4.4 and 4.5. These equations

can also be used to derive the empty and filled hydrogen masses. Here it is assumed that the hydrogen temperature is constant and it is stored at normal temperature (293.15 [K]). In reality, the hydrogen temperature will increase during filling which will lead to a slight overpressurization, this will be covered in Section 8.1.

$$P_e = \frac{Z_e \cdot m_e \cdot R_g \cdot T_{H2}}{V_t \cdot M_{H2}} \tag{4.2}$$

$$P_f = \frac{Z_f \cdot m_f \cdot R_g \cdot T_{H2}}{V_t \cdot M_{H2}} \tag{4.3}$$

$$m_f = m_{H2} + m_e \tag{4.4}$$

$$Z_i = 1 + \frac{\beta P_i}{T_i} \tag{4.5}$$

Where subscript e stands for empty, subscript f stands for full, P_e is empty pressure, P_f is filled pressure, Z_e is the empty compressibility factor, Z_f is the filled compressibility factor, m_e is the empty hydrogen mass, m_f is the total hydrogen mass, m_{H2} is the usable hydrogen mass, R_g is the gas constant, T_{H2} is the hydrogen temperature, V_t is the tank volume, M_{H2} is the molar mass of hydrogen and β is a fitting coefficient.

Here the equation of state is taken from [9]. This is because at high-pressure hydrogen does not behave like an ideal gas, the compressibility factor accounts for the variation between ideal and real gas laws at a given pressure and temperature. A comparison between the ideal gas laws and different real gas equations of states can be found in Section 8.1. With the required hydrogen masses and tank volume, the tank dimensions can be derived. This will be covered in the next section.

4.3. Geometrical dimensioning

The next step of the preliminary sizing is to estimate the tank dimensions in order to get a top-level estimate of the total system volume inside the Varuna tail section. This section is related to Section 4.4 as the wall thickness is required to compute the various tank dimensions.

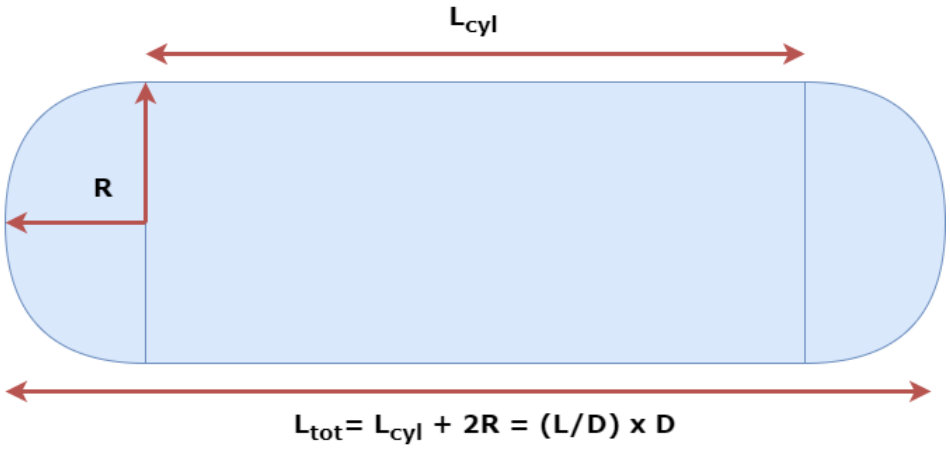

Figure 4.2: Diagram of assumed tank shape

The storage vessel is assumed to be a standard cylindrical pressure vessel with hemispherical end caps. Furthermore, a certain length-to-diameter (L/D) ratio is assumed. This way the tank length, cylinder length, and inner diameter can be computed from the required tank volume of Section 4.2. This is done via Figure 4.2 and Equation 4.6.

$$V_{dome} = \frac{4}{6}\pi R_i^3 \qquad V_{cyl} = \pi R_i^2 L_{cyl} \qquad V_t = 2V_{dome} + V_{cyl} \qquad L_{cyl} = (\frac{L}{D} - 1) \cdot 2R_i \tag{4.6}$$

Where V_{dome} is dome volume, V_{cyl} is cylinder volume, V_t is tank volume, R_i is inner tank radius, L_{cyl} is cylinder length and $\frac{L}{D}$ is the assumed L/D ratio.

The next step is to compute the volume of the liner which is taken to be 5 [mm] to prevent hydrogen permeation [4]. It is assumed that the thickness of the liner is constant. Hence the liner volume is considered to be a 5 [mm] shell around the hydrogen volume. A similar approach is taken to estimate the wall volume, this time taking the thicknesses obtained Section 4.4. Figure 4.3 shows how the tank is separated into three sections with corresponding radii. By taking the material densities of the liner and wall material, a top-level estimate of mass can be derived.

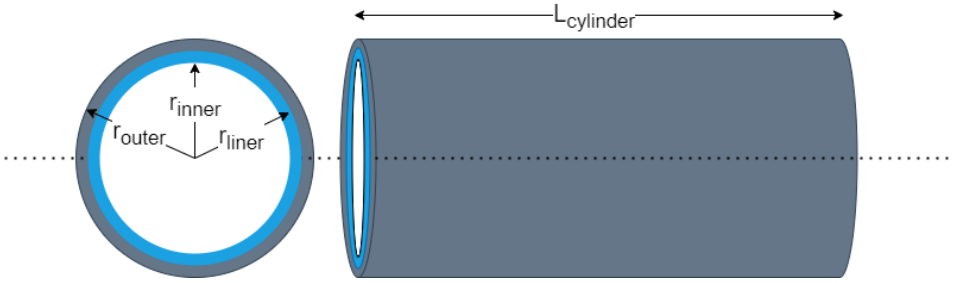

Figure 4.3: Tank volume and section breakdown by radius and material

With the inner radius obtained from Equation 4.6, the wall thickness can be computed according to netting analysis. This will be done in the next section and will be the final step in the preliminary design of the pressure vessel.

4.4. Structural sizing

To conclude the preliminary sizing an estimate of the wall thickness for the cylindrical and dome sections must be generated. The pressure vessel will be filament wound, the manufacturing process is important in the design of composite structures since it influences the mechanical properties of the structure [10]. Netting analysis can be used during the initial sizing of filament wound pressure vessels [6, 7, 11].

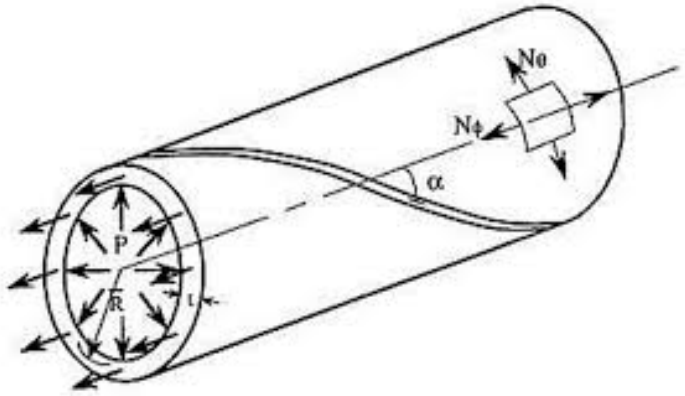

Figure 4.4: Free body diagram of a filament wound pressure vessel [6]

Figure 4.4 shows the free body diagram of a filament wound pressure vessel sized using netting analysis. The fibers are wound around the pressure vessel at an angle α with respect to the tank axis. Note that the material is orthotropic with axial and transverse mechanical properties. In netting analysis, a few assumptions are made. The first is that the pressure vessel is thin-walled $\left(\frac{R}{t} > 10\right)$. Secondly, the wall acts as a membrane, which means there are no shear loads or out-of-plane bending loads [6]. Finally, netting analysis assumes that the fibers provide all the stiffness and strength which makes this sizing method conservative [12].

Filament wound pressure can be wound in a geodesic or non-geodesic winding pattern according to Equation 4.7 [12, 13]. The winding consists of helical layers at a given winding angle and circumferential layers. Circumferential layers can only be wound on the cylindrical part of the cylinder due to slippage. The winding pattern determines the winding angle along the cross-section, a geodesic winding pattern is one where δ is 0. This pattern requires no additional friction during manufacturing to prevent the filament bands from slipping [13]. Geodesic wound pressure vessels have a constant angle α_0 in the cylindrical section and a variable angle in the domes. This winding pattern results in a hole at the crown, this happens when the filament band reaches an angle of 90° with respect to the meridional contour. At the location of the hole, an aluminum insert called a boss is installed to close the cylinder and reinforce the area locally. On one side the insert contains a valve such that the tank can be filled and emptied. The pressure vessel will be wound with a geodesic pattern, this will be discussed further in Chapter 6. Hence the constant angle α_0 in the cylindrical section is determined by the boss diameter according to Equation 4.7.

$$\alpha(R) = \text{arcsin}\left(\frac{R_0}{R}\right) \pm \delta\left(\frac{R - R_0}{R_{tl} - R_0}\right)^{n_{gd}} \qquad \alpha_0 = \text{arcsin}\left(\frac{R_0}{R_{cyl}}\right) \tag{4.7}$$

Where α is winding angle, α_0 is winding angle in cylindrical section, R_0 is the boss radius, R is the local radius, R_{tl} is the radius at the dome cylinder tangent line, R_{cyl} is the cylinder radius, δ and n_{gd} are constants related to the non-geodesic winding pattern.

Thin-walled pressure vessels experience two principal stresses caused by the hoop and axial membrane loads (See Equation 4.8, 4.9, 4.10) [6, 7]. The helical layers at angle α_0 provide stiffness and strength in both axial and hoop directions. Meanwhile, the hoop layers only provide stiffness and strength in the hoop direction. The required thickness in helical and hoop layers can be computed according to Equation 4.11. Note that the dome thickness and cylinder thickness are taken to be constant and equal to the sum of the helical and hoop thicknesses. Even though hoop layers cannot be wound around the dome this assumption is taken for the top-level mass estimations and is conservative. In reality, the dome thickness varies along the length, this will be covered in Chapter 6. Finally, the number of layers can be computed according to Equation 4.12

$$N_\theta = PR \qquad N_\phi = \frac{PR}{2} \tag{4.8}$$

$$N_\theta = \sigma_f \cdot t \sin(\alpha)^2 \qquad N_\phi = \sigma_f \cdot t \cos(\alpha)^2 \tag{4.9}$$

$$\sigma_\theta = \frac{N_\theta}{t} \qquad \sigma_\phi = \frac{N_\phi}{t} \tag{4.10}$$

$$t_\theta = \frac{PR}{2\sigma_f \cdot SF} \cdot \left[2 - \tan(\alpha)^2\right] \qquad t_\alpha = \frac{PR}{2\sigma_f \cdot SF \cdot \cos(\alpha)^2} \tag{4.11}$$

$$n_\theta = \left\lfloor \frac{t_\theta}{t_{ply}} \right\rfloor \qquad n_\alpha = \left\lfloor \frac{t_\alpha}{t_{ply}} \right\rfloor \tag{4.12}$$

Where N_θ is hoop membrane load, N_ϕ is axial membrane load, P is pressure, R is the radius, t is thickness, t_α is helical thickness, t_θ is hoop thickness σ_f is the failure stress of the material, SF is the safety factor, α is the winding angle, n_α is the number of helical layers, n_θ is the number of hoop layers and t_{ply} is the ply thickness.

The thicknesses can be used as an input in Section 4.3 to compute the wall mass. This is the final step of the preliminary sizing. By choosing an appropriate material the mass, volume, and shape of the pressure vessel can be determined. The material choice and design will be discussed in the next chapter.

5. Composite pressure vessel material selection & stacking sequence design

It is necessary to establish a material choice and design methodology to complete the design of the standard pressure vessel. To use the tools and models developed in Chapter 4, a material must be chosen for the liner, tank wall, and tank bosses. First, a list of material candidates will be identified, then the material design model will be detailed. Finally, the material and laminate choices will be discussed.

5.1. Material candidates

In the design of Type IV pressure vessels, it is important to choose high strength low-density temperature resistant material to achieve designs capable of withstanding up to 70 [MPa] of pressure with a high gravimetric efficiency (See Section 10.1.1). Type IV pressure vessels are made up of multiple materials for different components.

Each Type IV pressure vessel contains two bosses which are inserted at the dome crowns, this is due to the filament wound manufacturing process which leaves a gap at the crown. One boss often contains a valve such that it can be connected to the hydrogen control and delivery system, meanwhile the other side is a closed boss. The bosses are inserted and fixed to the composite layers during the filament winding process. Figure 5.1 shows the typical design of a Type IV pressure vessel with each component. Typically the bosses are made of metal; this is because the bosses have a complex shape which would be costly to manufacture in composite material. Furthermore, they exhibit good thermal properties which is desirable for filling and emptying (See Section 8.2). In general, the bosses are made up of aerospace-grade metals due to their high strength-to-weight ratio, and environmental and heat resistance [14]. The main candidates for boss material are aluminum and titanium alloys, the vast majority of bosses are made from aluminum due to its high strength-to-weight ratio and high machinability at low cost [14].

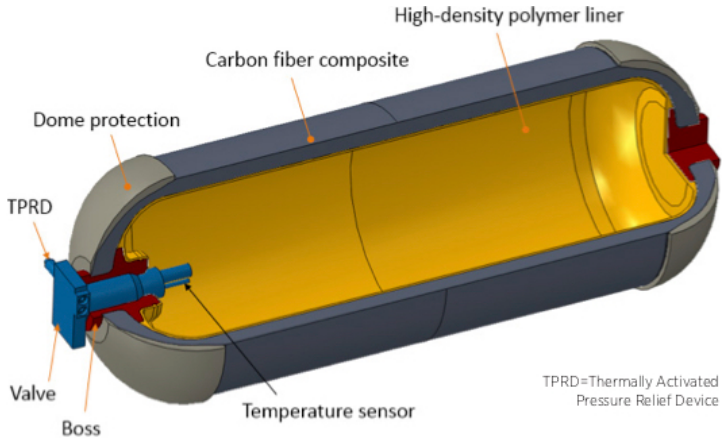

Figure 5.1: Cross-sectional view of a standard Type IV pressurized vessel [15].

The choice of liner material is important in the design of Type IV pressure vessels. The liner must be able to withstand a large temperature range, have a high failure strain and a low permeation rate [16]. The large temperature range is due to the high difference in temperature of the hydrogen during operations. The high failure strain allows the liner to follow the shape of the wall as it deforms due to the pressure inside the tank without failing or collapsing [17]. Finally, the main purpose of the liner is to prevent hydrogen leakage through the skin therefore it must have a low permeation rate. High-Density Polyethylene (HDPE) is used in the vast majority of cases due to its presence in compressed natural gas applications and high technical maturity. Recently, polyamide liners, most notably PolyAmide6

(PA6), have appeared at the forefront of research due to their increased barrier properties and higher resistance to blistering [18, 19]. Figure 5.2 shows an example of a polyamide liner.

Figure 5.2: Polyamide6 Type IV liner [20].

Finally, the choice of wall material is vital in the design of Type IV pressure vessels. The main goal of Type IV pressure vessel research is to increase the gravimetric and volumetric efficiency of hydrogen storage systems. As such, high-strength low-density materials are the main candidates. Furthermore, the materials must be able to handle high-temperature variations [21]. When looking at composite materials it is important to distinguish between matrix and reinforcement. In the case of filament wound pressure vessels, continuous fibers are used as reinforcement, often in the form of prepreg bands [22] These are then wound around a mandrel before curing in an autoclave. In general, carbon, glass, and Aramid fibers are the most promising reinforcement materials due to their high tensile strength [21]. These materials are often costly but provide a massive increase in gravimetric efficiency.

The matrix material can be a thermoplastic or thermoset, its function is to support the reinforcement material by introducing loads within the fiber. Furthermore, it provides environmental protection and impact resistance to the reinforcement. In Type IV pressure vessels a high yield strength coupled with high temperature resistance is desirable. There are many candidates including Epoxy, Polyetheretherketone, PA6, and polypropylenes.

Now that the main material candidates for each component of the Type IV pressure vessel have been identified, the material choice can be selected. However, the material design and philosophy must first be discussed due to their impact on the final material choice. This will be covered in the next section.

5.2. Material design

When selecting a material for the pressure vessel design several factors, such as the manufacturing process, drive the selection. The modeling method also plays a critical role in the material choice. These factors will be discussed in the following subsections.

5.2.1. Material philosophy & modelling

Typically, standard Type IV pressure vessels are manufactured using filament winding. This is due to the relative speed and ease of the process [12]. Manufacturing Type IV pressure vessels require a polymer liner, which acts as a mandrel, onto which the fibers are spun. The liner is usually roto- or blow-molded with the boss inserts added during the manufacturing process [23]. The prepreg fibers are then wound in helical and hoop directions around the liner before being cured in an autoclave. The helical layers must not slip during manufacturing, especially on the dome sections. This requires the addition of friction or specific winding patterns to avoid slippage [24]. A typical winding pattern that does

not require added friction is a geodesic winding [12]. For the design, a geodesic dome and winding pattern have been chosen in Chapter 6.

Another key factor in the material design is the analysis method. Here the design will be verified using FEM software HyperWorks, which uses a ply-based modeling method that simulates the composite material at the ply level. As such, each ply is represented by a material and stacked up into a laminate. The material type is orthotopic with material properties in fiber-dominant and transverse directions.

Several other factors drive the material choice and design such as heat resistance, environmental resistance, cost, and sustainability. However, these factors don't have an immediate impact on the material design and philosophy but act as choice criteria when selecting the material. By considering these factors during material selection an appropriate choice of material can be made.

5.2.2. Material choices & properties

Now that the different material candidates and the design philosophy have been identified, a choice of material can be made for each component. For the preliminary design of the pressure vessel, several material properties are of interest. These differ for each component.

First, the boss material can be chosen. As previously mentioned aluminum alloys show the most promise due to their high strength-to-weight ratio and machinability at a low cost. As such an aerospace-grade aluminum alloy has been chosen as the boss material. The properties of interest for the boss are summarized in Table 5.1. The mechanical properties such as tensile strength, elastic modulus, and shear strength are necessary for the structural analysis. Meanwhile, the thermal properties such as Coefficient of Thermal Expansion (CTE) and Specific Heat Capacity (SHC) are required for the thermal and environmental analysis.

Table 5.1: Boss material properties - AL2024 [25]

Material property	Value	Unit
Tensile strength	324	MPa
Elastic modulus	73.1	GPa
Shear strength	283	MPa
Shear modulus	28	GPa
CTE	23.2	$\mu mm^{-1}C°^{-1}$
SHC	0.875	$Jg^{-1}C°^{-1}$
Thermal conductivity	121	$Wm^{-1}K^{-1}$
Density	2780	kgm^{-3}

Secondly, the liner material has been chosen to be PA6, this is mainly due to its higher tensile strength and barrier properties compared to HDPE which also comes at an increased cost. Overall the weight of a PA6 liner is similar to an HDPE liner, this is because PA6 liners are thinner than HDPE liners despite a higher material density. For the liner material, the strain at failure is an important material property to prevent liner collapse and blistering [17]. Furthermore, thermal and mechanical properties are of key interest for structural analysis. The material properties of interest are summarized in Table 5.2. Note that the material degradation temperature is of key interest for the thermal analysis. Furthermore, PA6 liners can be reinforced with glass fibers and material properties depend on the manufacturing process. Here an unreinforced cast PA6 liner is assumed.

Table 5.2: Liner material properties - Cast Polyamide6 [26]

Material property	Value	Unit
Tensile strength	66.5	MPa
Elastic modulus	2.4	GPa
Shear strength	62	MPa
Elongation at yield	10	%
CTE	120	$\mu mm^{-1}C°^{-1}$
SHC	1.3	$Jg^{-1}C°^{-1}$
Thermal conductivity	0.32	$Wm^{-1}K^{-1}$
Maximum service temperature	120	C°
Density	1150	kgm^{-3}

Finally, the choice of wall material has been chosen to be a combination of high-strength carbon fiber with an epoxy matrix. This is mainly due to the very high mechanical properties at a low weight. Furthermore, the epoxy reinforcement provides good temperature and environmental resistance with relatively low-temperature dependence on mechanical properties. Furthermore, a commercially available prepregged unidirectional lamina has been chosen to simulate a behavior close to reality. To follow the material design philosophy and modeling method, orthotopic material properties are of interest and these have been summarized in Table 5.3. Finally, the material thermal properties are necessary for the thermal analysis. The material Poisson ratio and thermal properties have been assumed from the literature. The material manufactured by Toray is suitable for filament winding [27]. The properties are taken at room temperature ambient.

Table 5.3: Wall material properties - P173EBN-19 (T11100G UD) [27]

Material property	Axial value	Transverse value	Unit
Tensile strength	3941	67.6	MPa
Elastic modulus	175	9.17	GPa
Compressive strength	2048	258	MPa
In-plane shear strength	107		MPa
In-plane shear modulus	5.37		GPa
Fiber volume	56.8		%
Ply thickness	0.183		mm
CTE	21.3		$\mu mm^{-1}C°^{-1}$
SHC	1.2		$Jg^{-1}C°^{-1}$
Thermal conductivity	78.8		$Wm^{-1}K^{-1}$
Maximum service temperature	127		C°
Density	1573		kgm^{-3}

Now that the material selection is done, the stacking sequence can be chosen. This will conclude the material selection chapter and will be covered in the next subsection.

5.2.3. Stacking sequence

The final step of the material selection process is to define the laminate stacking sequence, this is required to model the material in a ply-based FEM software. As mentioned in Section 4.4, the composite material will be made up of helical and hoop plies in the cylindrical section and only helical plies in the domes. The goal of the stacking sequence is to have a balanced and symmetrical laminate. A balanced laminate is one where there is an equal number of positive and negative α plies. This results in a laminate without stretching and shear coupling which reduces the material stress. A symmetrical laminate is symmetric about its midplane. This cancels out many of the diagonal elements of the stiffness matrix which are responsible for bend, twist, shear extension... This results in a simpler laminate which significantly lowers distortion [28].

Another important consideration is the order of plies between hoop and helical layers. In this case, the

hoop layers are chosen to surround the helical layers. This provides a strengthening effect and yields a stronger laminate [29]. This is impossible in the domes where the plies are only helical.

In order to ensure that the laminate is symmetric and balanced, additional plies will be provided on top of the number of required plies obtained in Section 4.4. Note that the stacking sequence will not be provided as it contains over 100 plies. However, an example of a symmetric balanced laminate can be seen below.

$$\text{Cylinder stacking} : [90/+\alpha/-\alpha/90]s \tag{5.1}$$

$$\text{Dome stacking:} : [+\alpha/-\alpha]s \tag{5.2}$$

Using the selected materials and the following stack-up sequence, the vessel preliminary design can be completed. To do this, the dome must first be designed. This will be covered in the next chapter.

6. Pressure vessel dome

The dome design is one of the most important aspects of Type IV pressure vessel design. It is a broad area of research with many active researchers looking to advance this field even further. The dome design is complex as it is driven by manufacturing capabilities and has a significant impact on the stress state of the pressure vessel [30].

In Section 4.3, the dome was assumed to be hemispherical with a constant thickness. This was done to achieve a reasonable sizing and mass estimation at an early stage. However, spherical domes are structurally and volumetrically inefficient which leads to a reduction in gravimetric capacity [31]. As such more efficient dome designs have been proposed, mainly geodesic and non-geodesic domes. Geodesic windings require no additional friction during manufacturing and follow the Clairaut trajectories (See Section 4.4).

Overall geodesic domes are more efficient than hemispherical domes as they are shorter than hemispherical domes which results in a shorter tank for a constant hydrogen mass and tank radius. An added benefit of geodesic winding is that no additional friction is required during manufacturing, unlike non-geodesic domes. As such, a geodesic winding has been chosen for the pressure vessel. The winding path and dome model will be discussed in the next section.

6.1. Geodesic path algorithm

As previously mentioned, geodesic winding patterns follow the Clairaut trajectories (See Equation 6.1) this means that the polar radius determines the winding angle in the cylindrical section. This is because the roving bands must be tangent to the polar hole. Netting analysis indicates that a 54.7 [deg] winding angle is ideal. However, this leads to a large boss radius which is undesirable [6]. As such the winding angle is usually reduced to achieve a smaller opening, even smaller boss radii can be achieved with non-geodesic winding patterns. A lower winding angle means that more hoop layers are required in the cylindrical section.

$$\alpha\left(R\right) = \text{arcsin}\left(\frac{R_0}{R}\right) \tag{6.1}$$

The dome shape, thickness, and contour are driven by the geodesic winding pattern, which can be computed via numerical integration. This is done step by step, starting at the dome cylinder junction and progressing until the polar opening. An overview of the geodesic dome profile and its corresponding notation can be found in Figure 6.1 [7]

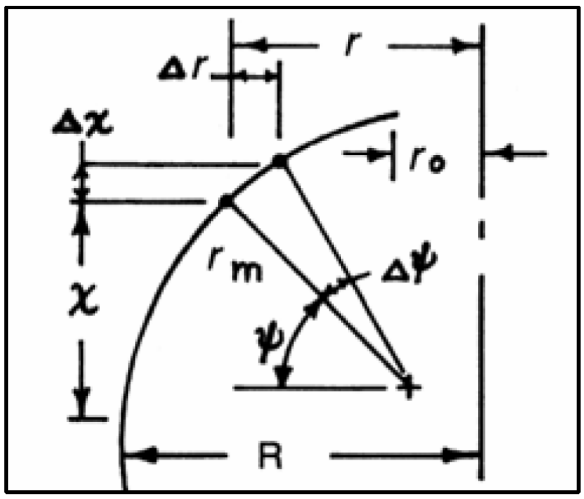

Figure 6.1: Dome profile breakdown

The dome path algorithm starts at the dome-cylinder junction. Either the winding angle in the cylindrical junction or the polar radius must be assumed. In this case, the polar radius is chosen and can be varied. The initial conditions can be found in Equation 6.2 and 6.3.

$$\Psi = 0 \qquad x = 0 \qquad r = R_{cyl} \tag{6.2}$$

$$t_0 = t_\alpha \qquad \alpha = \arcsin\left(\frac{R_0}{R_{cyl}}\right) \tag{6.3}$$

Where Ψ is the azimuth angle at which r_m is taken, x is the distance from the cylinder junction, r is the local radius, t_0 is the thickness at the cylinder junction and R_0 is the polar opening radius.

For the dome to be in equilibrium Equation 6.4 must be true:

$$N_\phi = \frac{PR}{2\cos\Psi} \qquad \frac{N_\phi}{r_m} + \frac{N_\theta}{r}\cos\Psi = P \tag{6.4}$$

Where r_m is the radius of curvature of the meridian.

Using Equation 6.4 the radius of curvature of the meridian can be obtained for a given winding angle and azimuth angle. This results in the following equation:

$$r_m = \frac{r}{\cos\Psi\left(2 - \tan^2\alpha\right)} \tag{6.5}$$

To determine the dome profile, a constant value of $\Delta\Psi$ must be set by which Ψ is incremented at every step, from there the increment for r and x can be computed according to Equation 6.6. The dome profile can be obtained by summating all the increments as shown in Equation 6.7.

$$\Delta\Psi = \text{constant} \qquad \Delta r = r_m \Delta\Psi \cos\Psi \qquad \Delta x = r_m \Delta\Psi \sin\Psi \tag{6.6}$$

$$\Psi = \sum \Delta\Psi \qquad r = R_{cyl} - \sum \Delta r \qquad x = \sum \Delta x \tag{6.7}$$

Finally, the winding angle can be computed according to Equation 6.1. T his combined with the local radius can be used to compute the local dome thickness according to Equation 6.8.

$$t = \frac{R_{cyl}}{r} \frac{\cos \alpha_0}{\cos \alpha} \tag{6.8}$$

Other methods can be used to generate the dome profile. These tend to be more complex and provide more accurate results, especially in the vicinity of the polar radius. However, the accuracy of the proposed method is sufficient for preliminary design. Next, an overview of the dome contour and profile will be provided.

6.2. Dome analysis

The aforementioned method can be used to generate several dome contours for a given cylinder radius as long as the winding angle or polar radius is assumed. Typically the winding angle is chosen to be between 15 and 25 [deg] to have a relatively small polar radius. It is worth noting that there is an asymptote in Equation 6.5 when $\alpha \approx 54.7$ [deg], this occurs when $r = 1.22R_0$. At that point, the curvature has an inflection point and the method is not valid. A tangent or ellipse approximation must be done to continue the curvature. To account for this, a polar insert of radius $r > 1.22R_0$ will be added so the dome thickness will not tend to infinity. More complex computational methods could be used such as Wang's cubic interpolation method for greater accuracy near the polar opening. However, this is out of the scope of the research project [32]. An example of a dome contour generated using this method can be found in Figure 6.2.

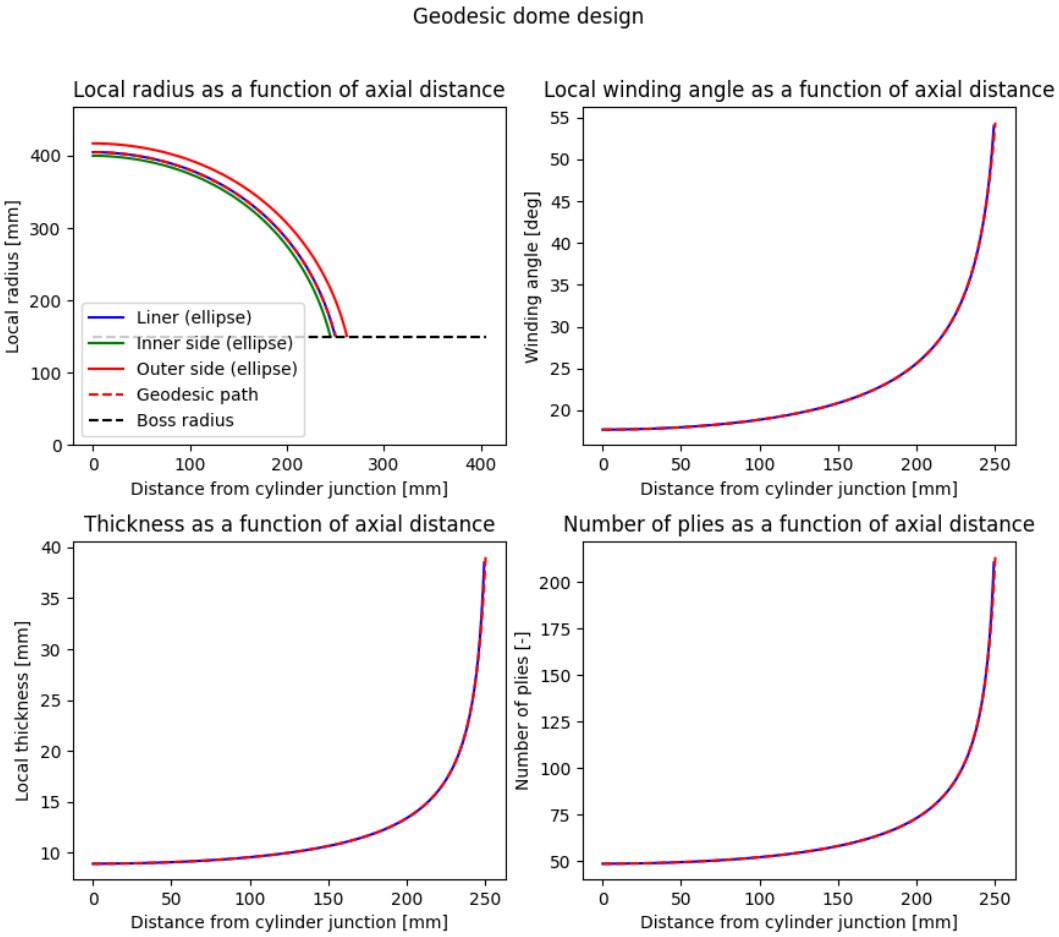

Figure 6.2: Example of dome contour and corresponding profiles

As can be seen in Figure 6.2, the thickness varies along the length and goes to infinity near the polar

opening. This is inaccurate therefore the average thickness of the dome is taken in the mass and volume estimates. For the structural analysis, the dome will be sectioned into multiple rings where the average winding angle and thickness will be taken for increased accuracy.

Note that the dome is simplified as an ellipse, by finding the closest ellipse via the least square regression method. This is done so the dome can be modeled in 3D CAD software. Furthermore, by subtracting the liner thickness or adding the average dome thickness to the ellipse approximation, the inner and outer surfaces of the pressure vessel can be modeled (See Figure 6.3). By doing an integral revolution about the X-axis, the hydrogen, liner, and wall volume can be computed accurately. This can then be used to refine the first level estimates of Section 4.3 where the dome is assumed to be hemispherical. With the new dome length and dome hydrogen volume, the cylinder length can be adjusted such that the required hydrogen volume stays constant. This in turn can be used to compute the actual L/D ratio. Once the tank dimensions have been recalculated with the actual dome dimensions the preliminary sizing is completed.

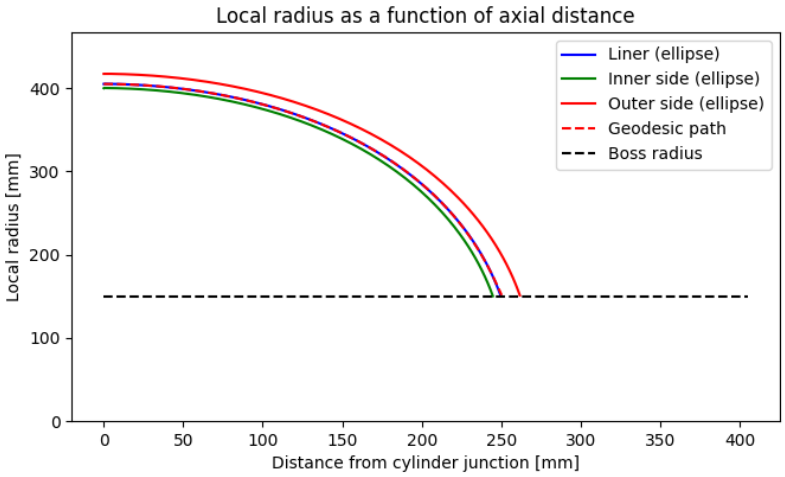

Figure 6.3: Plot of dome contour with each component.

7. Conventional pressure vessel design overview

At this stage, the preliminary design of the pressure vessel is finished. The need and technical requirements have been used to generate a set of performance criteria which were used as inputs during the preliminary sizing. The preliminary sizing assumes that the pressure vessel is composed of hemispherical domes with a cylindrical section. Later in Chapter 6, this assumption is revised and a geodesic dome is built using the geodesic path algorithm. A render of the preliminary design can be found in Figure 7.1. As discussed in Chapter 2, the preliminary design is a conventional pill-shaped Type IV pressure vessel made up of carbon-epoxy with a PA6 liner and aluminum bosses.

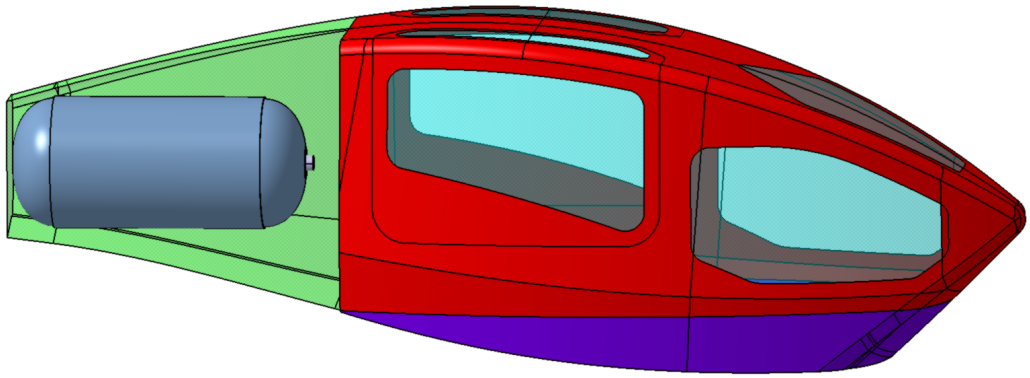

Figure 7.1: Render of preliminary single tank design inside Varuna EVTOL

7.1. Design parameters & assumptions

As shown in Figure 7.1 the standard tank fits within the intended section of the EVTOL, and there is sufficient clearance between the bounding box and the pressure vessel. Figure 7.2 and 7.3 provide an isometric render and a side view of the preliminary design.

Figure 7.2: Isometric render of the preliminary single tank design

Figure 7.3: Side view of the preliminary single tank design

At this stage of the design process, it is important to note that requirement SHR-EXP-07 has been revised. The required 1 hour of endurance has been reduced to 30 minutes, after a discussion with

Expleo Group. The reason for this reduction in endurance can be seen in Figure 7.4. The volume of hydrogen required for 1 hour of endurance is too large to fit within the tail section of the EVTOL, this is true for any L/D ratio, the single tank configuration is too long and large. Therefore, to make the design feasible, the endurance requirement has been reduced by 50 [%], which is acceptable for Expleo Group as the hydrogen version of the EVTOL will be able to refuel much faster than its electric counterpart. Note that this will double the number of life cycles and impact the fatigue characteristics of the pressure vessel. From this point forward the design will be sized for 30 minutes of flight time before refueling.

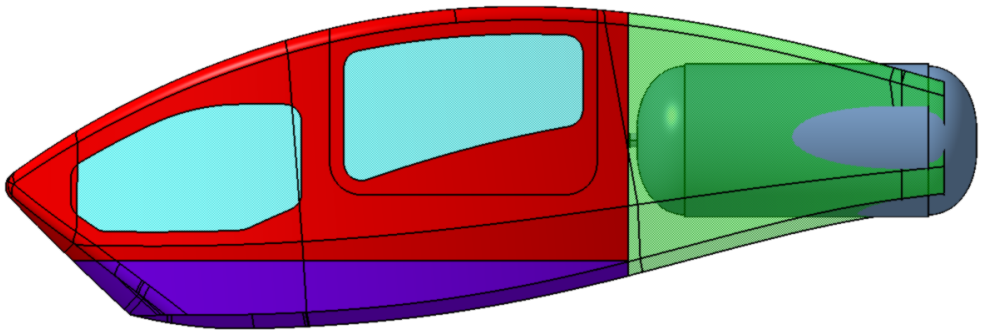

Figure 7.4: Render of initial single tank design inside Varuna EVTOL

The various model assumptions used throughout the preliminary sizing will now be broken down. The first assumption that was used is that the hydrogen mass flow in and out of the tank is constant. In reality, the mass flow will decrease as the pressure inside the tank decreases. It is necessary to keep sufficient pressure and mass flow out of the tank even when the hydrogen mass is low. This will be achieved using a pressure regulator.

Another key assumption is that the hydrogen temperature stays constant at 20 [°C]. This is done to simplify the mass and hydrogen volume sizing. In reality, the hydrogen temperature will increase during filling, leading to an overpressurization after filling. This overpressurization will be discussed in Section 8.1.

Furthermore, using netting analysis during the preliminary structural sizing means that the fibers are assumed to take up all the loads. In reality, the stresses are also taken up by the matrix material. This assumption is conservative and yields accurate results for initial sizing [6]

For the pressure vessel dimensioning and mass estimates the domes are assumed to have a constant thickness. In reality, the thickness varies and increases in the vicinity of the polar opening due to the winding pattern. The average dome thickness is taken during sizing. This is a conservative estimate since the dome thickness is mostly constant and lower than the average (See Figure 7.5). Furthermore, the geodesic algorithm leads to an asymptote near the polar opening which is not accurate compared to reality.

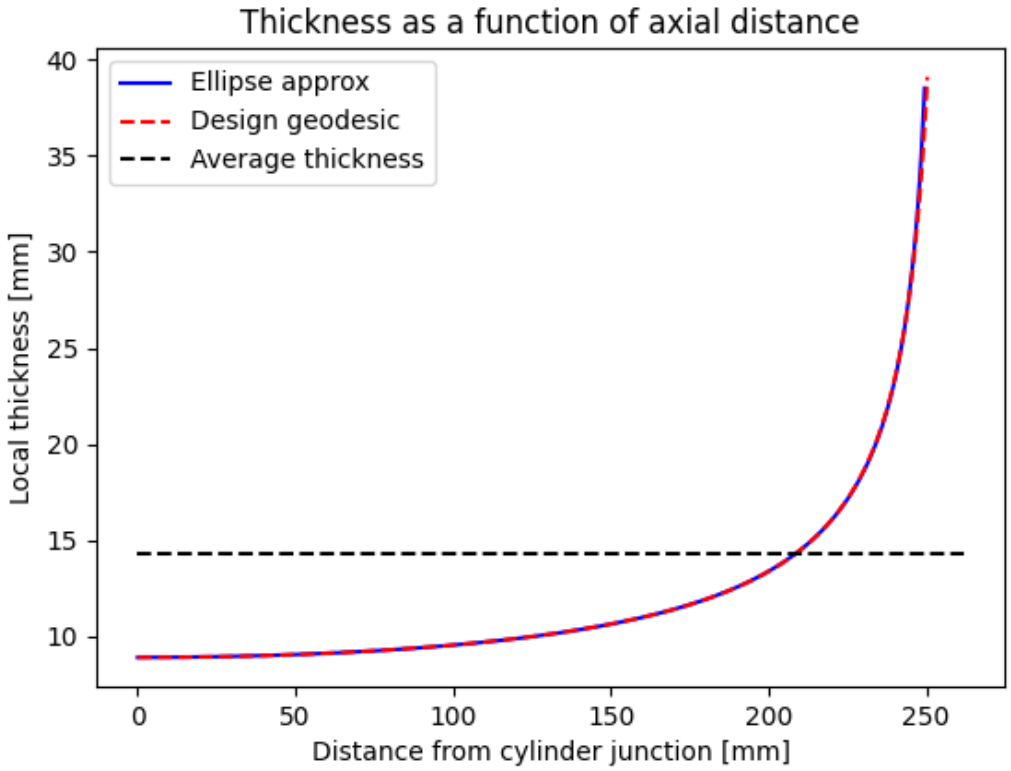

Figure 7.5: Dome thickness as a function of axial distance from cylinder junction

Another assumption is made during dimensioning. The domes are assumed to be perfect hemispheres to compute the required tank diameter and length. This assumption does not have a significant impact on the design since the dome is then designed using geodesic winding. This assumption is necessary to compute the radius which is an input for the geodesic winding algorithm. The tank dimensions are then updated using the result of the geodesic analysis.

Moreover, the pressure vessel length to diameter is assumed to be 2.5. The impact of shape on tank mass and volume will be discussed in Section 9.2.1. The L/D ratio of 2.5 is a reasonable estimate compared to the dimension of the tail section, furthermore in the composite pressure vessel industry L/D ratio is usually between 1.5 and 5 [4]. Using all these assumptions, the preliminary design of the single tank configuration can now be generated.

The hydrogen mass and volume parameter can be found on Table 7.1. The vehicle power, endurance, and storage parameters are the main inputs to compute the hydrogen volume (See Chapter 4).

Table 7.1: Overview of hydrogen mass and volume parameters including relevant inputs

Property	Value	Unit
Inputs		
Average power	1	MW
Flight time	30	min
EOL efficiency	0.45	-
”Empty” pressure	2	MPa
Nominal pressure	70	MPa
Storage temperature	293.15	K
Outputs		
Total hydrogen mass	34.77	kg
Usable hydrogen mass	33.34	kg
Required tank volume	870.7	L

The first estimate of tank radius can be obtained using the hydrogen mass and volume. This is done by using the assumed L/D ratio and required tank volume. Here is where the hemispherical assumption is used. The structural sizing can be performed by taking the required tank radius and assuming a polar radius. The results of the structural sizing and its inputs can be found in Table 7.2.

Table 7.2: Overview of structural parameters including relevant inputs

Property	Value	Unit
Inputs		
Tank inner radius	400	mm
Liner thickness	5	mm
Polar opening radius	150	mm
Safety factor	2.25	-
Ultimate tensile strength	3941	MPa
Ply thickness	0.183	mm
Nominal pressure	70	MPa
Outputs		
Winding angle	17.67	deg
Required helical thickness	8.91	mm
Required hoop thickness	15.36	mm
Number helical layers	49	-
Number hoop layers	84	-
Actual cylinder thickness	24.34	mm
Thin-walled ratio	16.7	-

The geodesic dome can be sized by using the data obtained from the preliminary structural sizing. The outputs of the geodesic path algorithm can then be used to update the dome dimensions and conclude the preliminary sizing. The tank dimensions are used to compute the mass and volume of each component which will be done in the next section. An overview of the main tank dimensions can be found in Table 7.3. The difference between the input and actual L/D ratio is caused by the hemispherical assumption, the tank length is reduced by using geodesic domes.

Table 7.3: Overview of geometric parameters including relevant inputs

Property	Value	Unit
Inputs		
Tank (input) LD ratio	2.5	-
Outputs		
Total tank length	1861	mm
Dome length	249	mm
Dome volume	91.1	L
Inner radius	399.92	mm
Liner radius	404.92	mm
Cylinder radius	429.25	mm
Actual LD ratio	2.33	-

7.2. Mass and volume breakdown

With the preliminary sizing completed and the tank dimensions known, some first-level estimates of system volume and mass can be obtained. By assuming that the dome thickness is constant and taking the densities of the laminate and Polyamide6, the volume and mass of each component can be computed.

The pressure vessel is divided into 5 main components: wall, liner, hydrogen, aluminum bosses, and balance-of-plant (BOP) components. The BOP components are the necessary equipment for hydrogen control and delivery, the design of the BOP falls outside the scope of the research project. However, to provide accurate system mass and volume estimates an average mass and volume fraction of the BOP components was taken from literature [4]. An overview of the system mass and volume parameters can be found in Table 7.4.

Table 7.4: Overview of mass parameters including relevant inputs

Property	Value	Unit
Inputs		
Wall material density	1573	kgm^3
Liner material density	1100	kgm^3
BOP mass fraction	0.17	-
BOP volume fraction	0.03	-
Outputs		
Total system mass	275.5	kg
Hydrogen mass	34.8	kg
Wall mass	166.9	kg
Liner mass	23.6	kg
Bosses mass	3.4	kg
BOP mass	46.8	kg
Total system volume	249	L
Hydrogen volume	870.7	L
Wall volume	106.1	L
Liner volume	24.7	L
Bosses volume	1.2	L
BOP volume	31.0	L

By computing the various component masses and volumes, the overall system can be broken down and its efficiency measured. In general Type IV pressure vessel efficiencies are measured in terms of gravimetric and volumetric efficiency. The gravimetric efficiency indicates the mass of stored hydrogen over the total system mass. Similarly, the volumetric efficiency indicates the mass of hydrogen

stored over the total system volume. An additional efficiency, defined as fill efficiency representing the volume of hydrogen over the available storage volume, is considered during this research project. An overview of the performance and efficiency parameters as well as target values will be provided in Section 10.1.1. Figure 7.6 and 7.7 provide the system mass and volume breakdown including the total system efficiencies. An overview of the efficiencies for the standard design can be found in Table 7.5

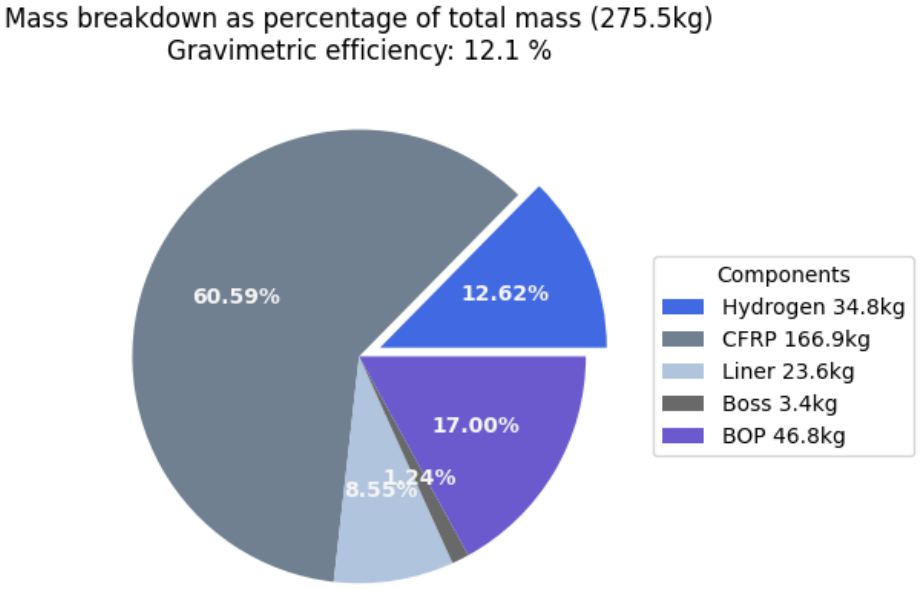

Figure 7.6: Preliminary single tank design mass breakdown

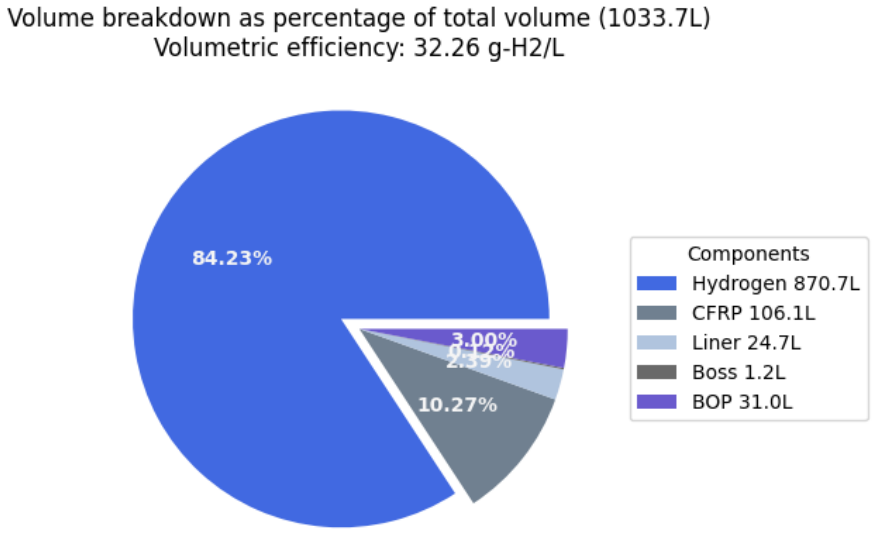

Figure 7.7: Preliminary single tank design volume breakdown

Table 7.5: Overview of system efficiencies for the standard pressure vessel design

Efficiency	Value	Unit
Gravimetric	12.1	[%]
Volumetric	32.3	[g-H2L^{-1}]
Fill	24.7	[%]

This concludes the preliminary design of the single tank configuration. This design will now be used as a baseline to verify and validate the preliminary sizing model. The design will be verified with a thermal and structural analysis. This will be the topic of the next chapter.

8. Design verification & validation

Now that the preliminary design of the single tank configuration has been completed the design must be verified. First, the hydrogen mass and volume state modeling will be compared to other models from the literature. This is necessary to ensure that the pressure profile and required volume estimates are accurate.

Furthermore, a thermal model will be developed to ensure that the current design stays within the appropriate temperature range as specified within the system requirements. The thermal model will be verified with available literature data, then it will be applied to the current design to simulate the actual temperature and pressure profile.

Finally, a FEM model will be developed to verify the preliminary structural sizing using netting analysis. This will give an estimate of the burst pressure and verify the applied safety factor.

8.1. Hydrogen mass & behaviour

The first verification step is to check that the equation of state used during the preliminary sizing provides an accurate estimate of the required hydrogen mass and tank volume. This will be done by comparing the design method to other methods available in the literature.

8.1.1. Compressed hydrogen equations of state

The equation of state used to simulate the hydrogen pressure and volume can be found in Section 4.2. This method uses a linear compressibility factor which depends on pressure, temperature, and a fitting coefficient. According to the literature, the method yields a maximum error of 3.8 [%] as long as the hydrogen temperature stays within 173 < T_{H2} < 393 [K].

Several other models can be used to simulate the hydrogen pressure and volume. The first model is the ideal gas law (See Equation 8.1), valid at low pressures and high temperatures. The hydrogen inside the pressure vessel is at low temperature and high pressure hence the ideal gas law should underestimate the actual pressure [9].

$$PV_t = nR_gT_{H2} \tag{8.1}$$

Where n is the number of hydrogen moles.

Another method that can be used to simulate hydrogen pressure and temperature is the real gas law, also known as the van der Waals equation of state. This method uses two constants to account for the attractive force between molecules and the effective volume occupied by a molecule. This equation should be valid for all gases at any temperature and pressure. In reality, the van der Waals equation tends to overestimate the pressure at high pressure compared to experimental data [33]. Equation 8.2 shows the van der Waals equation for hydrogen gas.

$$\left(P + \frac{an^2}{V_t^2}\right)(V_t - nb) = nR_gT_{H2} \qquad a = 0.0254 \qquad b = 0.0002651 \tag{8.2}$$

Where a and b are the van der Waals constants for hydrogen.

Finally, another method can be used to model hydrogen pressure and volume. This method is a truncated virial-type equation that uses 30 constants to model hydrogen gas [34], fitted on experimental data from the National Institute of Standards and Technology (NIST). This method is accurate within 0.01 [%] for pressures up to 70 [MPa] and temperatures between 220 to 1000 [K]. This method is similar to the design method since it computes a corrective compressibility factor which is then applied to the

ideal gas law. The equation for the compressibility factor and corrected ideal gas law can be found in Equation 8.3. The corresponding constants can be found in [34].

$$PV_t = Z_v n R_g T_{H2} \qquad Z\left(p,T\right) = 1 + \sum_{i=1}^{9} a_i \cdot \left(\frac{100\ \text{K}}{T}\right)^{b_i} \cdot \left(\frac{P}{1\ \text{MPa}}\right)^{c_i} \tag{8.3}$$

Where Z_v is the virial type compressibility factor, a_i, b_i and c_i are fitting coefficients.

Now that the available methods have been identified these will be compared to the design method from Section 4.2. This will be the subject of the next subsection.

8.1.2. Hydrogen state model comparison

To verify that the design method provides an accurate estimate of the hydrogen volume and pressure, each method will be modeled using a Python script and will be plotted on the same graph. Note that at this stage the hydrogen temperature is still assumed to be constant throughout filling. The hydrogen temperature profile will be modeled in Section 8.2. Figure 8.1 shows the pressure as a function of hydrogen mass inside the tank for each model.

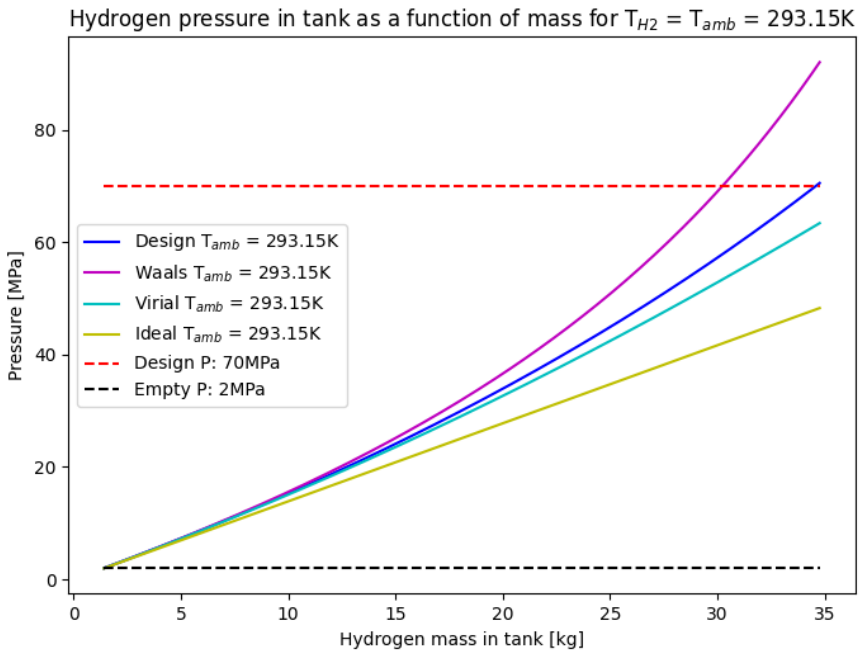

Figure 8.1: Hydrogen pressure as a function of mass inside the tank using different equations of state for hydrogen gas

From the figure above, it is clear that the ideal gas law is an inaccurate model for hydrogen pressure and volume. The pressure profile is similar to the other methods at low pressures however at higher pressures it severely underestimates the hydrogen pressure. Similarly, the van der Waals equation is also inaccurate when modeling hydrogen gas pressure; it holds until 30 [MPa] and tends to overestimate the hydrogen pressure at higher pressures. The error is larger than 25 [%] at 70 [MPa] and cannot be used to model hydrogen pressure. Finally, it is known that the truncated virial type equation is highly accurate with 0.01 [%] error for a large pressure and temperature range. When comparing the virial method to the design method which uses a simplified equation for computing the compressibility factor, it is clear that the design method leads to a slight overestimation of the hydrogen pressure. The difference in final pressure is less than 10 [%]. When using the design method, the hydrogen pressure is slightly higher than what is expected experimentally.

Overall, the design method tends to overestimate the hydrogen pressure at room temperature, meaning that the pressure estimate is slightly conservative. This is deemed acceptable since in reality the pressure inside the tank will be less than the design pressure. This means that the tank size can be reduced during detailed design which is desirable. Alternatively, this will yield a higher safety factor. Now that the hydrogen mass and pressure model has been verified, a thermal model of the tank will be developed. This will be the subject of the following section.

8.2. Pressure vessel thermal modeling

So far the hydrogen temperature has been assumed to be constant throughout filling and emptying, in reality, the hydrogen temperature will increase as the hydrogen is compressed while the temperature will decrease as the gas expands. To verify that the pressure vessel stays within the allowable temperature range specified in the requirements a thermal model must be developed. Here an adiabatic dual zone model has been chosen to model the temperature rise within the pressure vessel.

8.2.1. Hydrogen pressure vessel heat model

Modeling the temperature rise of hydrogen during refueling, dormancy, and emptying is of vital importance in the context of vehicular hydrogen storage. One of the key hurdles in the widespread commercialization of compressed hydrogen systems is safety. Overpressurization due to temperature increase during filling must be modeled accurately to prevent catastrophic failure.

As such a key area of research in compressed hydrogen technologies is the development and verification of accurate thermal models which can be used to model the pressure vessel wall and hydrogen temperature throughout operations. Several thermodynamic models exist with varying degrees of complexity. Typically pressure vessel thermal models are divided into thermal zones. The most basic model is a single-zone model which only considers the hydrogen temperature. These models offer accurate results for the hydrogen temperature variations but do not provide any information on the liner or wall temperature. More complex models such as dual-zone and triple-zone models also take into account the liner, wall temperature, and environmental interactions.

For the research project, a dual-zone model has been chosen. This model has been verified in the literature and compared with Computational Fluid Dynamics (CFD) and experimental data [35, 36]. It applies to Type III and IV pressure vessels and provides accurate estimates for hydrogen and wall temperature [35]. The dual-zone model aims to represent the hydrogen and wall temperature but neglects the contribution of the liner [35]. As such, the liner is considered part of the wall zone and its temperature is equal to the wall temperature.

Furthermore, the model is adiabatic and considers no heat transfer to the environment. This assumption holds as long as the filling and emptying of the vessel is over a short period and the specific heat capacity of the wall is high. The model breaks down the pressure vessel operation into three distinct phases: filling, dormancy, and emptying. Another key assumption is that the mass flow is constant throughout each phase. The model can be used to accurately predict hydrogen and wall temperature. Furthermore, the hydrogen temperature profile can then be used to accurately predict hydrogen pressure inside the tank.

The mass and energy balance equations model the hydrogen temperature, meanwhile, the wall temperature is modeled using the heat balance equation. The governing equations can be found in Equation 8.4, 8.5 and 8.6.

$$\frac{dm}{dt} = \dot{m_{in}} - \dot{m_{out}} \tag{8.4}$$

$$\frac{d\left(mu\right)}{dt} = \dot{m_{in}} h_{in} - \dot{m_{out}} h_{out} + A_{in} a_{in} \left(T_w - T\right) \tag{8.5}$$

$$\frac{d\left(m_w c_w T_w\right)}{dt} = A_{in} a_{in} \left(T - T_w\right) - A_{out} a_{out} \left(T_w - T_f\right) \tag{8.6}$$

Where m is the hydrogen mass, $\dot{m}$ is the mass flow, u is the specific internal energy of the gas, h is the

specific enthalpy of the gas, A is the surface area, a is the heat transfer coefficient, T is the hydrogen temperature T_w is the wall temperature, T_f is the ambient temperature, m_w is the wall temperature and c_w is the specific heat capacity of the wall.

Pressure vessel filling phase
The first phase of the thermal modeling is the filling process, this phase assumes a constant hydrogen inflow temperature. The hydrogen is provided by a large reservoir, so the input temperature and pressure should stay relatively constant. With the assumption that the hydrogen mass flow is constant during filling and the heat transfer to the environment is negligible, the governing equations become:

$$\frac{dm}{dt} = \dot{m} \tag{8.7}$$

$$\frac{d\left(mu\right)}{dt} = \dot{m}h + A_{in}a_{in}\left(T_w - T\right) \tag{8.8}$$

$$\frac{d\left(m_w c_w T_w\right)}{dt} = A_{in}a_{in}\left(T - T_w\right) \tag{8.9}$$

The hydrogen temperature as a function of time can be obtained by using the following simplifications and substitutions inside Equation 8.5.

$$m = m_0 + \dot{m}t \qquad u = c_v T \qquad h = c_p T_\infty \qquad t^* = \frac{m_0}{\dot{m}} \qquad \gamma = \frac{c_p}{c_v} \tag{8.10}$$

$$\gamma' = \frac{\gamma}{1+\alpha} \qquad \alpha' = \frac{\alpha}{1+\alpha} \qquad \alpha = \frac{a_{in}A_{in}}{c_v\dot{m}} \qquad T^* = \gamma' T_\infty + \alpha' T_w \qquad t_w^* = \frac{m_w c_w}{a_{in}A_{in}} \tag{8.11}$$

Where c_v and c_p are the specific heat capacities of hydrogen at constant volume and pressure respectively and T_∞ is the hydrogen in/outflow temperature.

This results in an equation for hydrogen temperature as a function of time and wall temperature (See Equation 8.12)

$$\frac{dT}{dt} = \left(1+\alpha\right)\frac{T^* - T}{t^* + t} \tag{8.12}$$

A similar approach is taken to obtain the wall temperature as a function of time and hydrogen temperature. Equation 8.6 can be simplified to Equation 8.13.

$$\frac{dT_w}{dt} = \frac{T - T_w}{t_w^*} \tag{8.13}$$

Equation 8.12 and 8.13 are coupled differential equations, they can be solved numerically or analytically. To solve Equation 8.12 analytically, it must be integrated with the assumption that the wall temperature is constant. A similar approach can be taken for Equation 8.13, this time assuming that the hydrogen temperature is constant. This yields the following analytical solutions.

$$T = f_g T_0 + \left(1 - f_g\right)T^* \qquad f_g = \left(\frac{m_0}{m}\right)^{1+\alpha} \tag{8.14}$$

$$T_w = f_w T_{w0} + \left(1 - f_w\right)T \qquad f_w = e^{-\frac{t}{t_w^*}} \tag{8.15}$$

Where T_0 is the initial temperature inside the tank and T_{w0} is the initial wall temperature. Note that these two equations are coupled by T^* and must be decoupled to obtain a solution in terms of initial parameters

Equation 8.14 and 8.15 can be used to solve the hydrogen temperature analytically during refueling under the dual-zone adiabatic constant inflow assumptions. Next, the hydrogen and wall temperature during emptying will be derived.

Pressure vessel emptying phase
During the emptying phase, another assumption is made; instead of assuming the outflow temperature to be constant, it is assumed to be equal to the hydrogen temperature inside the tank. This accurately represents the emptying phase. All other assumptions stay unchanged. The derivation is similar to the previous case with slight changes. The hydrogen and wall temperatures can be modeled using Equation 8.17.

$$T^* = \frac{\alpha T_w}{1+\alpha-\gamma} \qquad T_\infty = T \tag{8.16}$$

$$\frac{dT}{dt} = (1+\alpha-\gamma)\frac{T^*-T}{t^*+t} \qquad \frac{dT_w}{dt} = \frac{T-T_w}{t_w^*} \tag{8.17}$$

Similarly, coupled analytical solutions can be obtained via integration (See Equation 8.18 and 8.19).

$$T = f_g T_0 + (1-f_g)\,T^* \qquad f_g = \left(\frac{m_0}{m}\right)^{1+\alpha-\gamma} \tag{8.18}$$

$$T_w = f_w T_{w0} + (1-f_w)\,T \qquad f_w = e^{-\frac{t}{t_w^*}} \tag{8.19}$$

Pressure vessel dormancy phase
The final phase of the thermal model is the period of dormancy. Here, the hydrogen mass stays constant and the governing equations can be seen in Equation 8.20.

$$\frac{d\,(mu)}{dt} = A_{in}a_{in}\,(T_w - T) \qquad \frac{d\,(m_w c_w T_w)}{dt} = A_{in}a_{in}\,(T - T_w) \tag{8.20}$$

The relationship between hydrogen and wall temperature can be obtained by dividing the equations by each other. This equation can then be integrated with the given initial conditions ($T = T_0$ and $T_w = T_{w0}$ at $t = 0$) to obtain the following relation (See Equation 8.21).

$$\frac{mc_v}{m_w c_w}\frac{dT}{dT_w} = -1 \qquad k = \frac{m_w c_w}{mc_v} \qquad T = T_0 + k\,(T_{w0} - T_w) \tag{8.21}$$

An equation for wall temperature as a function of time can be obtained by substituting the relation between hydrogen and wall temperature into the governing equations and then integrating with the aforementioned initial conditions (See Equation 8.22).

$$T_w = \left(T_{w0} + \frac{B}{A}\right)e^{At} - \frac{B}{A} \tag{8.22}$$

Finally, Equation 8.22 can be substituted into Equation 8.21 to obtain the hydrogen temperature as a function of time and wall temperature. This is shown in Equation 8.23.

$$T = T_0 + k\left(T_{w0} - \left(T_{w0} + \frac{B}{A}\right)e^{At} - \frac{B}{A}\right) \tag{8.23}$$

Now that the governing equations for hydrogen and wall temperatures during each operational phase have been derived, the model can be used to simulate the hydrogen temperature inside any pressure vessel. This can be done both analytically and numerically. First, the model must be verified using data available from the literature to ensure its accuracy.

8.2.2. Heat model verification using literature

Before it can be used to determine the temperature profile of the preliminary design, the thermal model must first be verified. This can be done by using data available from the literature and comparing the model results. To do this, a similar tank configuration to the one in [35] has been chosen and used as input in the Python model. The hydrogen and wall temperature rises can then be plotted and compared. The model and literature results for hydrogen temperature can be found in Figure 8.3 and 8.2. Similarly Figure 8.5 and 8.4 show the results for wall temperature.

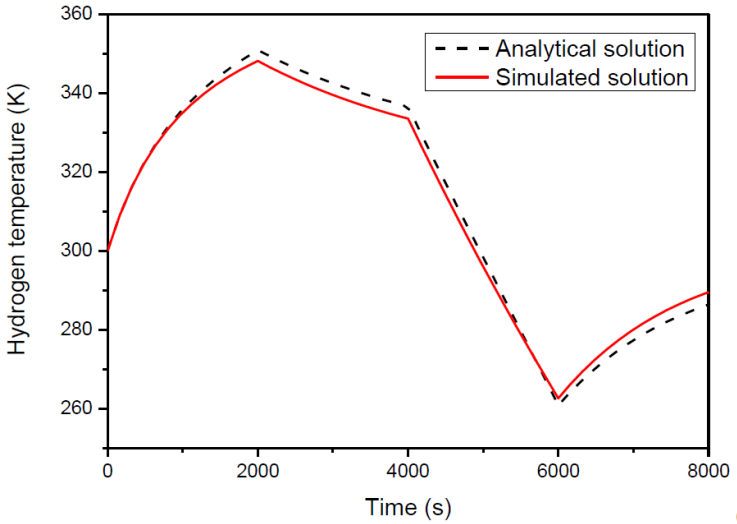

Figure 8.2: Hydrogen temperature profile literature test case

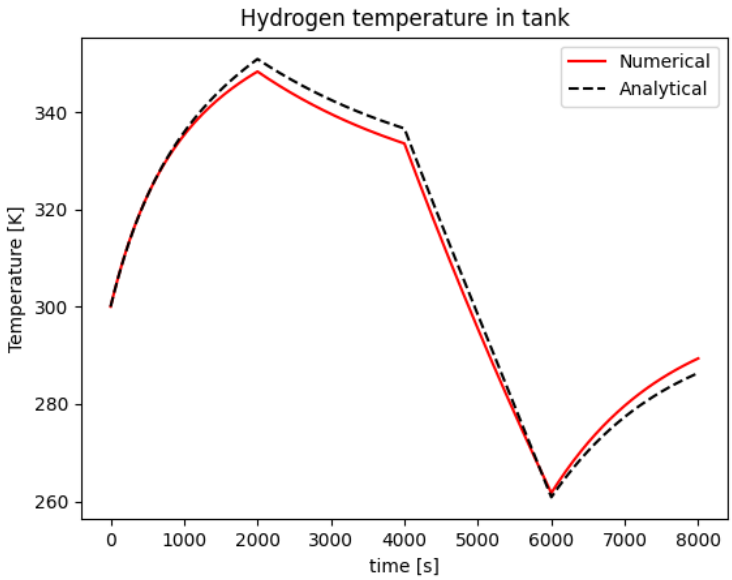

Figure 8.3: Hydrogen temperature profile model test case

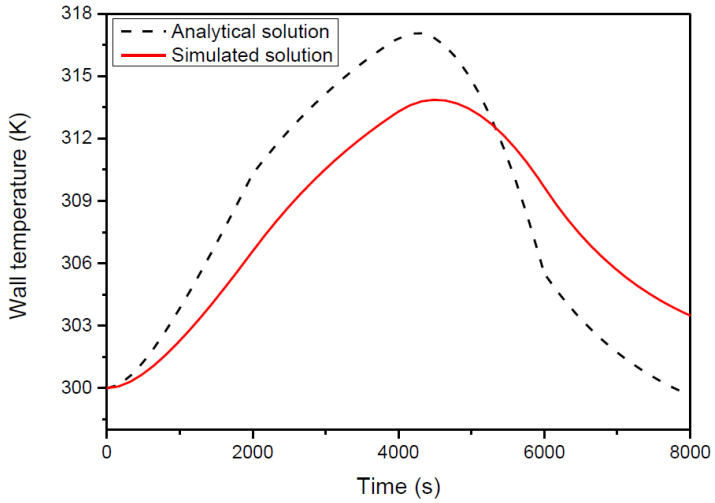

Figure 8.4: Wall temperature profile literature test case

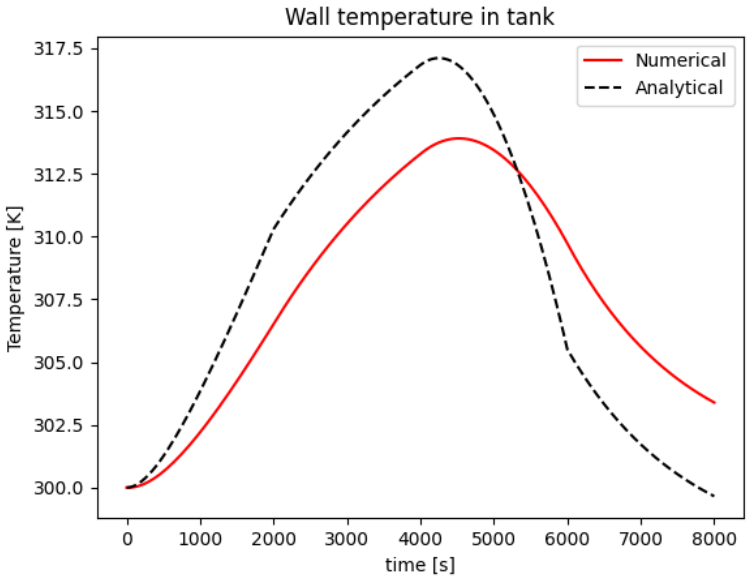

Figure 8.5: Wall temperature profile model test case

The model data is simulated for 8000 [s] with each phase lasting 2000 [s]. The first phase starts with pressure vessel filling, followed by a period of dormancy. Thereafter, the pressure vessel is emptied before another final dormancy period occurs. There is a discrepancy between numerical and analytical solutions which is caused by the assumption taken during integration. The numerical solution is more accurate.

The model data follows the data from the literature to a high degree of accuracy. This can be observed both in terms of magnitude and behavior. The temperature rise profile is similar and the model is verified. The next step is to apply this model to the design tank to observe the temperature profiles of both the wall and the hydrogen. This will be covered in the next subsection.

8.2.3. Thermal modelling results & discussion

To simulate the thermal behavior of the design vessel, its thermodynamic parameters must first be obtained. The hydrogen-related parameters such as specific heat capacity do not change. It is important to note that the vehicle operational parameters such as filling time and dormancy time must be assumed. After discussing with the EVTOL design team, a flight profile has been drafted. This flight profile is based on the standard EVTOL operational profile with a shorter refueling time. However, a dormancy period has been added, to settle the hydrogen temperature inside the vessel. An overview of the flight characteristics and thermodynamic parameters of the system can be found in Table 8.1.

Table 8.1: Thermal model parameters for single tank configuration

Property	Value	Unit
Refuel time	15	min
Dormancy time	10	min
Flight time	30	min
Wall mass	223.2	kg
Wall SHC	1.2	kg
Hydrogen inflow temperature	0	C°
Ambient temperature	20	C°
Initial pressure	2	MPa

At this stage, some assumptions and simplifications must be made. First, the initial hydrogen and wall temperatures are assumed to be equal to the ambient temperature. The wall mass is a combination of the wall mass and liner mass, to account for the contribution of the liner as a heat sink. Finally, the heat transfer coefficient is assumed to be constant throughout operations. In reality, the heat transfer coefficient varies throughout operations. The estimation of the heat transfer coefficient is a complex process that depends on the gas Reynolds number, hydrogen inlet velocity, and many more parameters. Several methods exist to compute the heat transfer coefficient however, this falls out of the scope of the research project [37, 38]. The heat transfer coefficient has been obtained from literature [39].

Several parameters can be changed to impact the temperature rise of the hydrogen and wall. These are mainly the refueling time, the discharge time, the hydrogen inflow temperature, and the initial pressure. If the design vessel does not meet the system requirements, these parameters can be changed to reduce the maximum and minimum operational temperature. Increasing the refueling time reduces the maximum temperature during filling. Similarly, increasing the discharge time leads to a higher minimum temperature during emptying. Reducing the hydrogen inflow temperature leads to an overall lower temperature profile with a lower maximum and minimum temperature. Finally, increasing the initial pressure leads to a lower maximum temperature. An overview of the hydrogen and wall temperature profile including mass and pressure over time can be found in Figure 8.6.

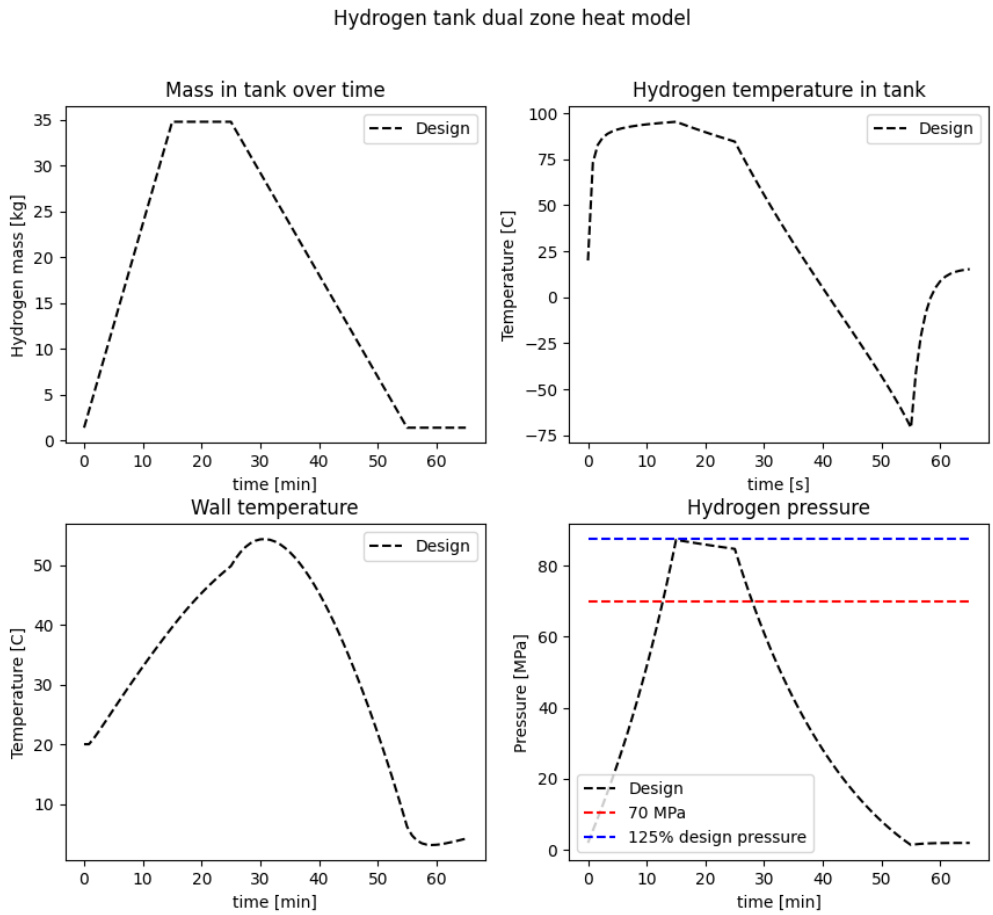

Figure 8.6: Single tank design thermal analysis results

From the figure above, it is clear that the temperature variations within the pressure vessel are significant, especially during filling and emptying. The hydrogen temperature reaches a maximum of 95 [C°] before settling under 85 [C°] after a short dormancy period. During discharge, the hydrogen temperature drops significantly to around -70 [C°] before rising back up quickly to around 10 [C°]. The filling results seem to model reality accurately and are within the allowable after a short dormancy period. It is necessary to pre-cool the hydrogen inflow to reduce the maximum temperature.

The discharge behavior is less accurate. This is most likely due to the adiabatic assumption which considers no heat loss or gain with the environment. Since the hydrogen mass expands significantly, the temperature drop is also significant. However, the leftover hydrogen mass is very small and cannot retain much heat. This explains why the temperature quickly shoots back up when in contact with the more massive wall. The wall temperature seems to follow the hydrogen temperature and behaves as expected.

The mass and SHC of the wall are much higher than that of hydrogen and it can store much more heat. This explains why the temperature variations are smaller.

Finally, the pressure inside the vessel goes beyond the nominal pressure of 70 [MPa] which is expected since the pressure vessel was designed assuming a constant hydrogen temperature of 20 [C°]. The pressure inside the tank increases when the temperature increases. However, the pressure does not go over 125 [%] of the design pressure which is allowed during filling. Over time the hydrogen pressure settles to 70 [MPa] as the temperature reaches the ambient level.

Overall, the thermal model can simulate the temperature profile of both the hydrogen and wall. It can

be used to size any pressure vessel and is sufficiently accurate for preliminary design. The model can be improved by accounting for environmental interactions. This way, the expansion and compression would not be adiabatic, which should reduce the maximum temperature and increase the minimum temperature due to heat loss and gain respectively. Furthermore, the model can be further improved by deriving and simulating the heat transfer coefficient accurately, yielding more accurate temperature results. Implementing a triple zone model would also yield the liner temperature which is important when considering liner degradation. The maximum service temperature of PA6 is over 100 [C°] and given the model results, it is not expected that the liner will degrade due to thermal interactions.

Now that the thermal analysis of the design has been performed and the thermal model verified, a FEM model of the design can be developed to verify the structural sizing and burst pressure of the preliminary design. This will be the subject of the next section.

8.3. Pressure vessel structural modeling

The final key verification step is to verify that netting analysis provides an accurate estimate of burst pressure for the preliminary design. Netting analysis is a simple sizing method that assumes that the fibers take up all the loads in the composite material. The netting analysis is based on a geodesic winding pattern. It takes the tensile strength of the laminate with an applied safety factor to compute the number of required layers. Netting analysis should provide a conservative estimate of burst pressure when applied correctly. This will be verified via a FEM model in HyperWorks using the Optistruct solver.

8.3.1. Pressure vessel FEM model

HyperWorks is a finite element modeling software that integrates a wide variety of solvers to obtain accurate modeling results. It can model composite materials and designs via the composite toolbox. This composite toolbox aims to integrate manufacturing in the analysis via ply-based modeling which simulates stresses at ply scale.

The analysis starts with a 2D shell model which is directly imported from the CAD modeling software CATIA. This surface represents the liner's outer surface onto which the fibers will be spun. A full model of the surface will be simulated without symmetry. An overview of the model can be found in Figure 8.7. The shell is made up of 14,000-panel elements with 14,000 nodes, the elements have a maximum size of 20 [mm] and a maximum aspect ratio of 5. The elements are smaller near the polar opening due to the curvature and decreased radius. The mesh is a panel mesh that keeps the number of elements constant at the boundaries, leading to a homogeneous mesh with quadrilateral elements only.

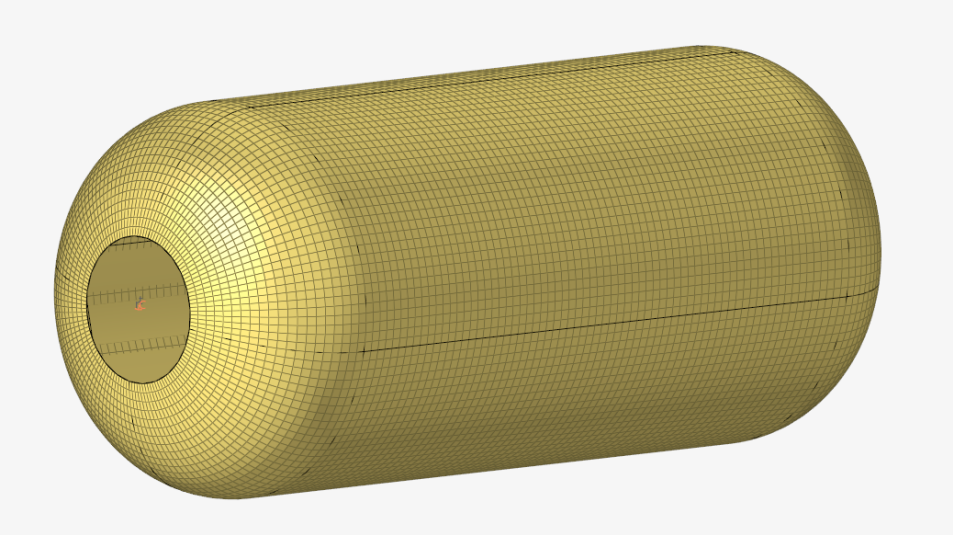

Figure 8.7: Pressure vessel shell FEM model

A cylindrical coordinate system is applied to all nodes and elements, resulting in radial displacements

without the need for coordinate transformation during result post-processing. The cylindrical coordinate Z-axis is lined up with the axial direction of the pressure vessel. To create a ply-based analysis, the element orientation and normals have to be defined. This is done using vectors that follow the vessel curvature. An analysis of all element normals and orientations was performed to ensure consistency, which can be seen in Figure 8.8. The element normals determine the stack-up direction while the orientation determines the fiber orientation over the elements.

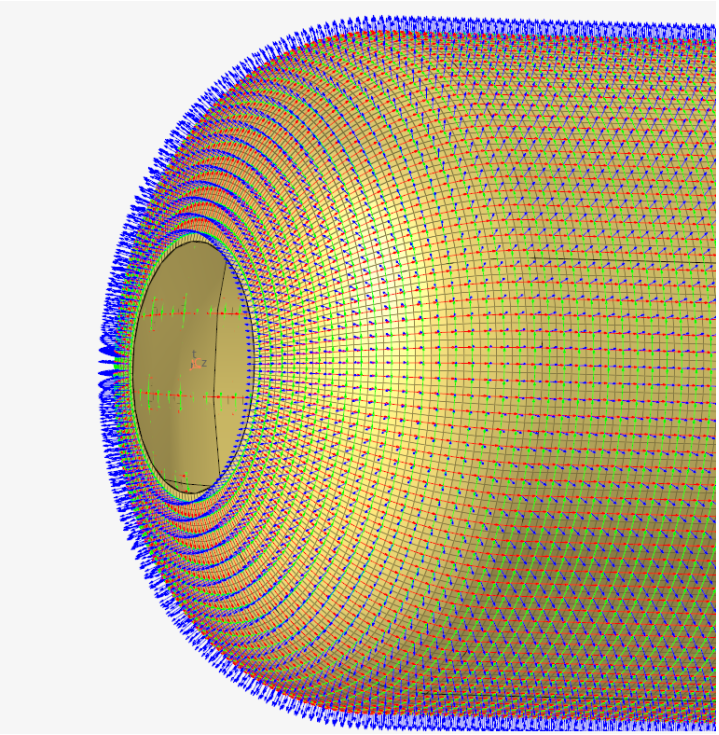

Figure 8.8: Cylindrical coordinate system and element orientation analysis

The material choice is a MAT8 element representing an orthotropic material. To fully define this material, the transverse & axial moduli, poison ratio, shear modulus, and material density are required. Furthermore, the tensile, compressive, and shear strengths can be input for first-ply failure analysis.

The composite material is applied using zonal composite modeling, this is done by applying the PCOMPG property to certain elements. A PCOMPG property contains information about the origin of the stack up (Z0) and the plies in that zone. Each ply is represented by a material, a ply thickness and an orientation. Furthermore, each ply is given a global ID, ensuring fiber continuity between neighboring zones. Zonal composite modeling is required since the winding angle and number of layers are not constant in the dome.

The dome must be sectioned since the winding angle has to be constant within a single zone. In this case, the model is sectioned into 6 zones. The first zone is the cylinder which is made up of helical and hoop layers. The domes are divided into 5 zones, each zone is 4 elements long in the axial direction. The zones close to the polar opening are smaller due to the dome profile (See Chapter 6). Since the winding angle and thickness rapidly increase near the polar opening, more zones are required to describe the vicinity of the polar opening accurately.

The dome is sectioned by taking the axial location of the first and last element of a given zone. Then, the thickness and winding angle are evaluated at each axial distance and an average value is computed. These average values are then applied to each zone. This divides the dome into discrete zones with different mechanical properties, as the number of zones increases the representation closely resembles reality. An overview of the composite zones can be found in Figure 8.9.

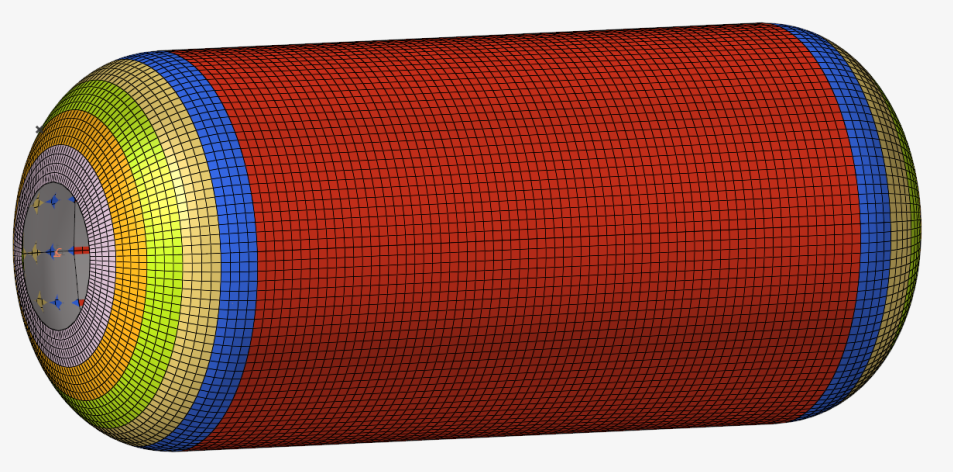

Figure 8.9: FEM model broken down using zonal composites.

To simplify the analysis and reduce the number of simulated plies, the number of plies is kept constant throughout the dome. The dome thickness increases rapidly near the polar opening due to the winding pattern. To represent this, the ”actual” ply thickness is increased. For example, in the cylindrical section, there are 56 helical plies with a thickness of 0.183 [mm] resulting in a helical thickness of 10.25 [mm]. Meanwhile, the helical thickness of zone 3 is 14.83 [mm] with 82 plies. To convert this to a 56-ply zone, the ply thickness is increased to 0.268 [mm] from 0.183 [mm]. This way the global ID of plies between zones matches and there is continuity between zones. An overview of the composite property per zone is given in Table 8.2.

Table 8.2: Overview of composite zones and their corresponding properties

Property	**Zone 1**	**Zone 2**	**Zone 3**	**Zone 4**	**Zone 5**	**Zone 6**
Colour	Red	Blue	Yellow	Green	Orange	Pink
Winding angle [deg]	17.67	18.33	20.46	24.76	33.15	54.60
Helical thickness [mm]	10.25	10.65	12.00	14.83	21.00	45.26
Number of helical plies [-]	56	59	66	82	115	248
Actual helical ply thickness [mm]	0.183	0.193	0.216	0.268	0.376	0.810
Hoop thickness [mm]	15.37	0	0	0	0	0
Number of hoop plies [-]	84	0	0	0	0	0
Actual hoop ply thickness [mm]	0.183	NA	NA	NA	NA	NA

Note that the need to section the dome into discrete zones with constant ply numbers is a limitation imposed by the use of HyperWorks. The analysis would be performed differently using other software such as Abaqus. On the other hand, the advantage of this method is that it closely resembles reality in terms of the manufacturing process and provides a clear layup.

The analysis will be a static linear analysis, the load applied is a constant pressure load with a magnitude of 70 [MPa] applied on every element. The pressure is applied on the inside of the pressure vessel and its direction is outwards.

A set of fixed constraints is added at the polar opening, these single-point constraints (SPC) are applied at every node on the open edge. They constrain all rotations but allow displacement in the axial, tangential, and radial directions. An overview of the SPC and the applied pressure load can be found in Figure 8.10.

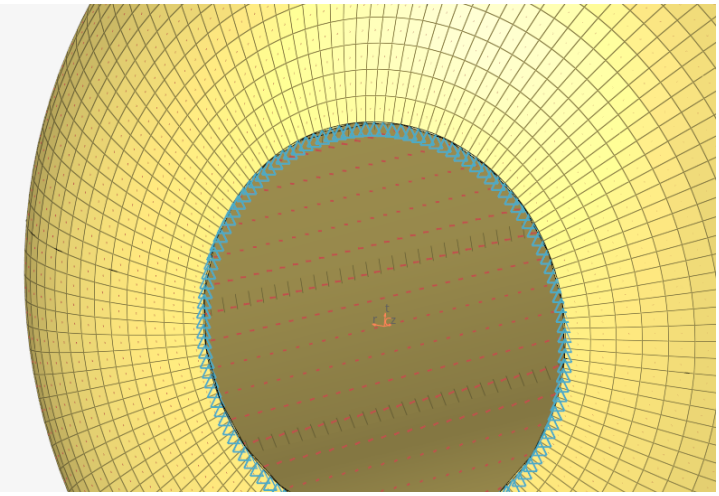

Figure 8.10: FEM model constraints and loads. Red: Pressure load, Blue: SPC

With the FEM model setup, the analysis can now be run and the results can be reviewed. This will be the subject of the next subsection.

8.3.2. Structural modelling results & discussion

The FEM analysis can now be solved using the Optistruct solver. It is a static linear analysis. The results are evaluated at the element level where the element stresses, element moments, element forces, and displacements are queried. The analysis aims to determine whether netting analysis is an accurate sizing method for the research project. An overview of the pressure vessel von Mises stress distribution can be seen in Figure 8.11.

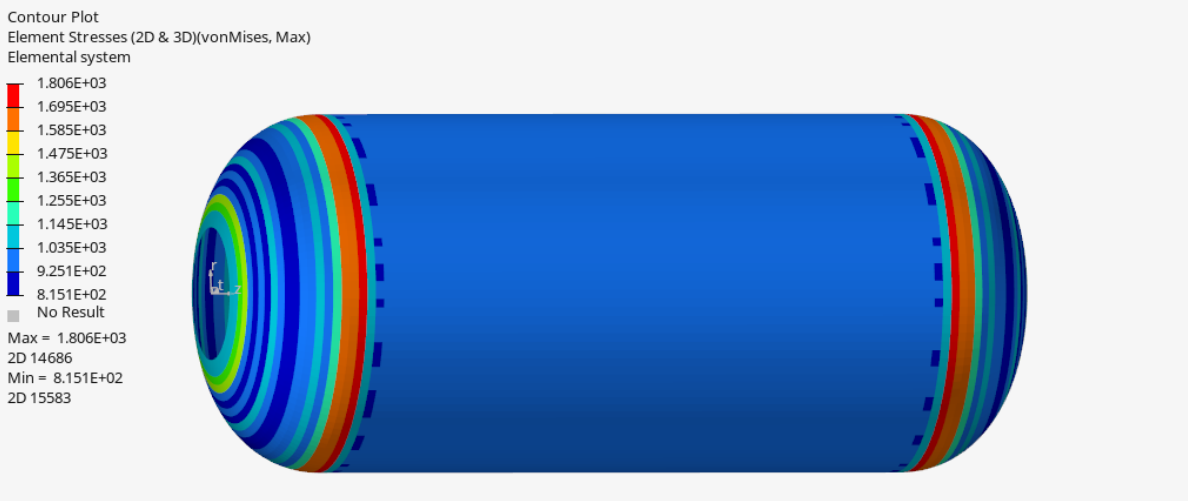

Figure 8.11: Von misses stress distribution in pressure vessel FEM analysis

Overall the von Mises stress distribution behaves as expected [40, 41]. The maximum stress is located at the cylinder-dome junction due to the jump in thickness and increased moment at the junction. The dome tends to fold open as it deforms whereas the cylinder expands, creating a stress concentration that leads to high stresses at the junction. The maximum stress is around 1806 [MPa]. The laminate has an ultimate tensile strength of 3941 [MPa] which reduces to 1751 [MPa] with an applied safety factor of 2.25. This means that there is a 3 [%] difference between the expected maximum stress and the FEM results. This shows that netting analysis is an appropriate sizing method for this type of pressure vessel and can be used to design a modular tank with cylindrical geodesic shapes.

There are several limitations to this analysis, mainly related to the dome. The stresses, forces, and moments in the dome do not behave as predicted. There is significant stress near the polar opening and the maximum moment is located around the polar opening (See Figure 8.12). This can be explained by several factors. Firstly, the dome is sectioned into individual sections with discrete jumps in winding angle and thickness, leading to several stress concentrations and a mismatch between zones. Furthermore, the polar opening is usually reinforced by the bosses whose diameter is greater than the opening and provides a reinforcing effect around the polar opening. Finally, the SPCs which constrain rotation at the edge of the polar opening, create a stiffening effect that induces a lot of moments inside the structure.

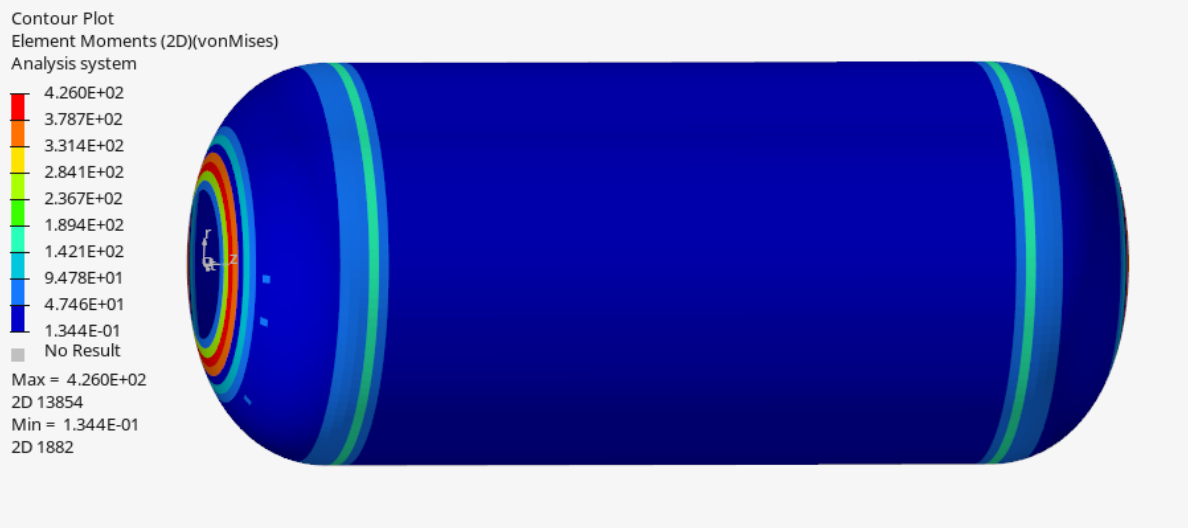

Figure 8.12: Internal moment distribution in pressure vessel FEM analysis

Overall, when the elements around the polar opening are neglected, the moment distribution resembles the expected results from the literature. The moment is highest at the cylinder dome junction where the pressure vessel is expected to fail. Figure 8.13 shows the moment distribution on every element besides those around the polar opening.

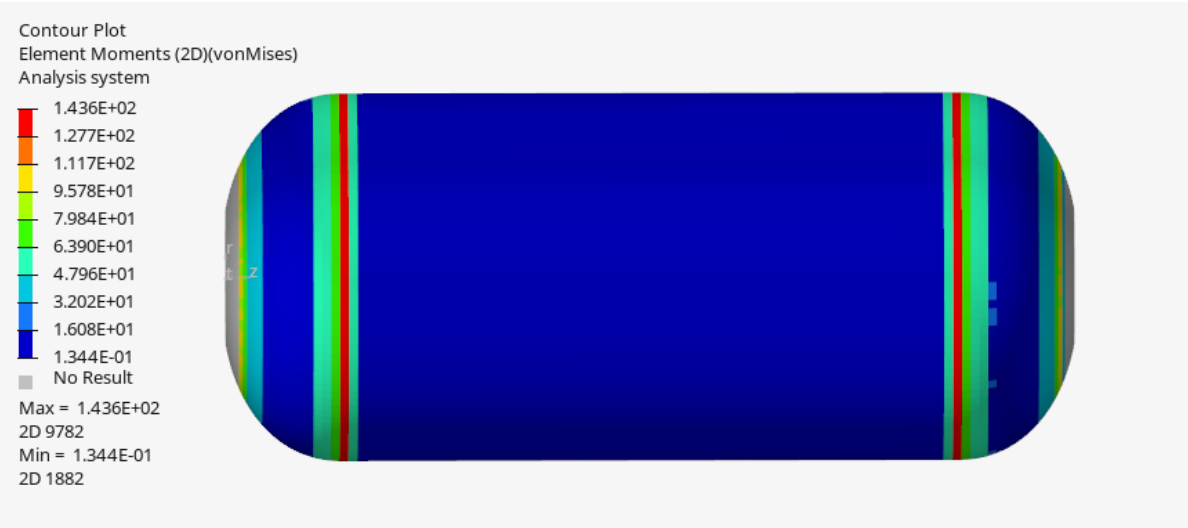

Figure 8.13: Internal moment distribution neglecting elements near the polar opening in pressure vessel FEM analysis

In order to obtain more accurate results an analytical model of the pressure should be developed to compare with the FEM model results. This will indicate whether the results are coherent with reality.

Furthermore, the full pressure vessel including liner and aluminum bosses needs to be modeled to provide a more accurate representation of reality.

To improve this analysis even further, a failure analysis using a variety of failure criteria needs to be performed to verify the burst pressure of the pressure vessel. A progressive damage analysis needs to be performed to fully characterize the failure of the pressure vessel. However, this falls out of the scope of this project.

Another improvement to this structural analysis would be to perform a fatigue analysis. This can be done by applying a damage factor based on the total number of cycles. Additionally, an impact analysis needs to be performed to ensure the safety of the pressure vessel. This also falls outside of the scope of this research project.

Overall, the FEM analysis of the pressure vessel is not comprehensive enough to verify the structural sizing of the pressure vessel to an accurate degree. It is necessary to assume that netting analysis is an accurate method for the preliminary sizing of Type IV composite vessels. This is supported by the von Mises stress distribution and the literature [6, 7, 40]

9. Conformable pressure vessel design

Now that the preliminary design of the standard tank has been completed and verified a conformable storage solution will be developed. This will begin by generating a list of concepts, these will be traded off qualitatively before a concept will be detailed and developed. An overview of the chosen conformable concept will conclude this chapter.

9.1. List of concepts

In literature, two main conformable compressed hydrogen storage solutions are being investigated to replace conventional pressure vessels. The main interest of conformable research is the ability to store hydrogen in non-cylindrical pressure vessels which comes at an increased system mass for an equivalent hydrogen mass. The main application for this technology is to implement hydrogen storage in preexisting designs particularly vehicles [42]

The first conformable concept is lattice-based pressure vessels. These pressure vessels can be made into any desired shape and rely on internal plates and struts to carry loads between the walls. The objective of the struts is to reduce the bending loads on the skin whose sole purpose becomes hydrogen containment [42]. An example of a lattice-based pressure vessel can be found in Figure 9.1.

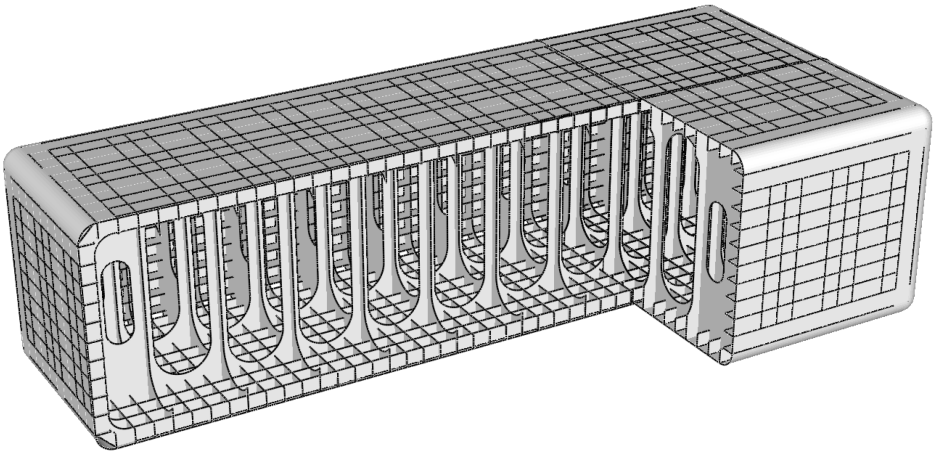

Figure 9.1: Lattice based pressure vessel concept [43]

Lattice-based pressure vessels are made up of a lattice pattern in all 3 cartesian directions with a thin skin, both the skin and lattice pattern are made of metals. They can be manufactured at a lower cost than composite pressure vessels with a much higher system mass.

The other concept is multi-cell pressure vessels, which are made up of individual cylinders that can be arranged in any pattern to fit a given volume. The individual cells are shaped like the standard pressure vessel and are then joined together. The cells can be assembled within an outer structure. Another option is for the individual cells to share the same walls resembling a porous structure. An overview of multi-cell pressure vessels can be found in Figure 9.2 and 9.3

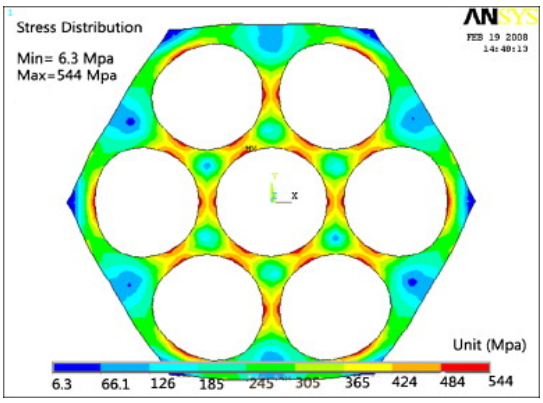

Figure 9.2: Porous multi-cell pressure vessel concept [44]

Figure 9.3: Joined multi-cell pressure vessel concept [45]

Porous multi-cell pressure vessels are more mass efficient than joined multi-cell pressure vessels as each cell shares adjacent walls and hence requires less material to be manufactured. However porous multi-cell pressure vessels can not be made of composite materials and are more difficult to manufacture.

Joined multi-cell pressure vessels can be made using filament winding and have a high potential for optimization. If the system is built using symmetric and similar cells the manufacturing cost and time are decreased severely. This is because the equipment can be reused and the manufacturing process can be automated [45]. Each cell is as optimal as the standard pressure vessel. They offer a high modularity with the possibility to fill any volume, this is particularly true as the cell size decreases. The addition of an external structure to joined the cells together increases the system mass.

Overall, the joined multi-cell pressure vessel shows the most promise for the research project. Firstly, it is the only concept that can be manufactured using composite material at a competitive cost. It is also the only Type IV pressure vessel concept. This is important as it is a stakeholder requirement. Furthermore, this concept can be manufactured using filament winding which means the thermal and structural verification and sizing models can be applied to this concept. Another advantage of this concept is that the outer structure required to join the cells can be used as a primary structure for attachments and load transferring in a vehicle. Finally, this concept has high modularity and conformability which can be integrated into any existing design.

It is worth noting that Expleo expressed its interest in the study of joined multi-cell pressure vessels compared to other technologies. As such, the joined multi-cell pressure vessel concept has been chosen and its design will be detailed in the following section.

9.2. Multi cellular pressure vessel design

The joined multi-cell pressure vessel concept has been chosen, this concept is made up of many individual cells which are then joined together using an outer structure. The goal of this concept is to increase the amount of hydrogen that can be taken on board vehicles. This is done by filling a given volume with many individual cells. Each cell can be seen as a standard filament-wound pressure vessel with geodesic domes, as such each cell can be designed using the toolbox developed in the previous chapters.

Before the multi-cell design can be developed a sensitivity analysis based on shape and number must be performed. This is necessary to find the optimal space-filling method. A compromise between size, number of tanks, fill efficiency, and total mass must be found.

9.2.1. Sensitivity analysis

To find the optimal arrangement of individual cells to fill the available volume with the lowest system mass possible a sensitivity analysis must be done. This analysis will be performed at constant hydrogen mass, the aim is to study the impact of shape and number of tanks on the total system mass.

The impact of the L/D ratio on total system mass can be seen in Figure 9.4. Note that this figure also indicates the impact of the geodesic winding angle on system mass.

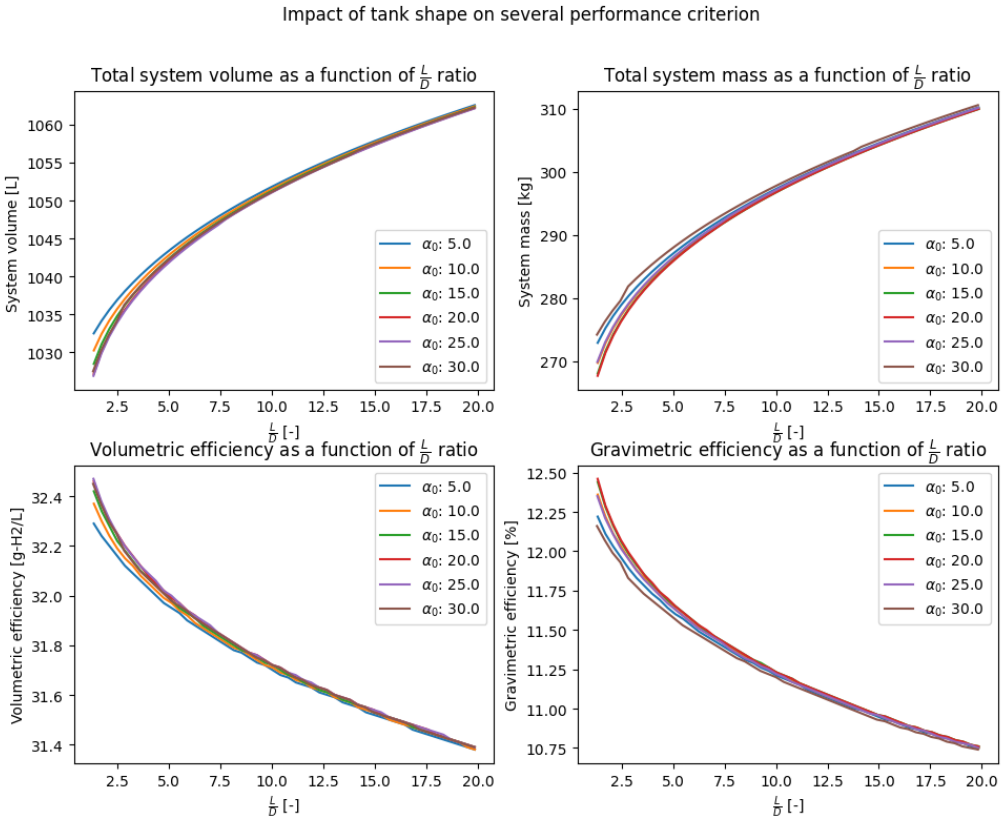

Figure 9.4: Impact of L/D ratio and winding angle on system mass

From the figure it is clear that as the L/D ratio increases the total mass of the system increases, this can be explained by the fact that the dome is overall less thick than the cylindrical section of a pressure vessel. Furthermore, it is known that the optimum shape for a pressure vessel is a sphere with an L/D ratio of 1. Meanwhile, the winding angle does not seem to have a significant effect on total system mass and can therefore be chosen as desired.

It can be said that in a joined multi-cell pressure vessel the L/D ratio of individual cells shall be minimized. However, this is not necessarily true when looking at the impact of the number of tanks on total system mass (See Figure 9.5).

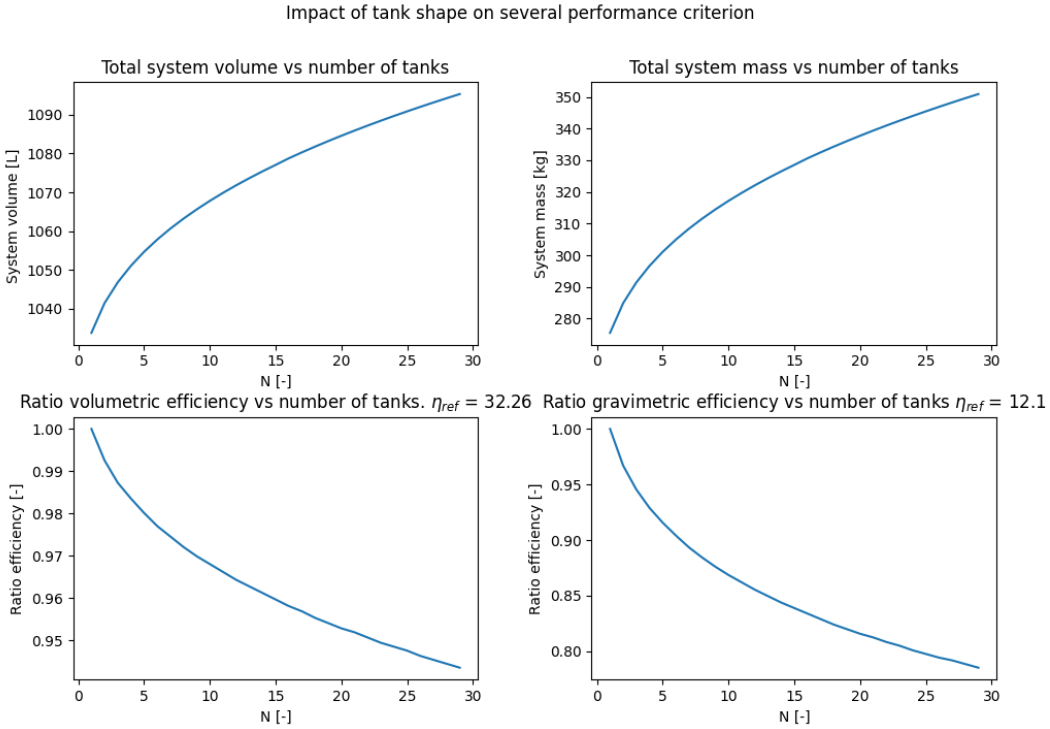

Figure 9.5: Impact of number of tanks on system mass

Here the total system mass and volume is plotted against the number of tanks within the system. An L/D ratio of 2.5 is chosen for this analysis. Furthermore, the efficiencies are plotted as ratios. The system efficiency for N tanks is divided by the reference efficiency of the single tank configuration.

From the figure, it is clear that total mass increases with the number of tanks at constant hydrogen mass, this is especially true for the gravimetric efficiency which is reduced by 20 [%] at 30 tanks. This means that a compromise between L/D and the number of tanks must be found. Using too many spheres with an L/D of 1 will lead to an increased system mass compared to multiple cylindrical cells.

9.2.2. Space filling method

The next step in the design of the joined multi-cell concept is to fill the target volume, this is done by taking the data from the sensitivity analysis. First, a section cut of the required volume is taken from CAD software. Next, the available length is evaluated along the cross-section (See Figure 9.6).

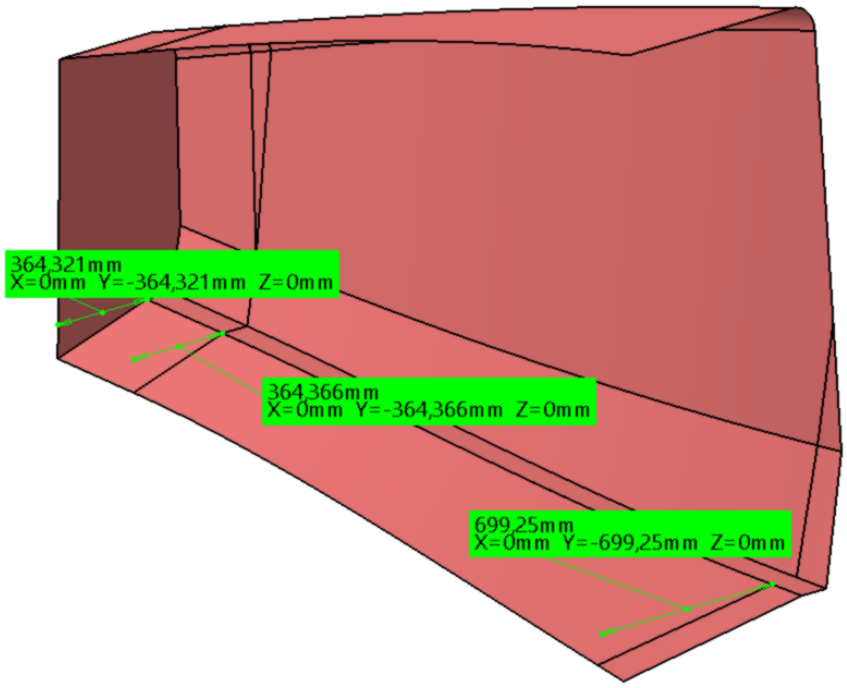

Figure 9.6: Section cut of the target volume with available lengths

At this stage it is important to set a range for the L/D ratios, a minimum and maximum L/D ratio needs to be defined. In this case, a range of 1.5 to 3 L/D ratio is chosen. Minimizing the L/D ratio is important for total system mass but it needs to be high enough such that the available length is filled using a single cell. This limits the total number of tanks while ensuring the volume is filled.

Then a clearance needs to be defined, this clearance is between the target volume bounding box and the individual cells. This clearance also applies to the distance between cells, this ensures there is no clash between the design and the vehicle. Furthermore, this leaves enough space for the outer support structure. Using the available lengths, L/D limits, clearances, and the volume cut the cell pattern can be defined. An example is shown in Figure 9.7.

Another condition that is imposed on the space-filling method is to keep the number of unique tanks as low as possible. This means that tanks should be the same size and length where possible, this decreases the fill efficiency. However, this leads to a much lower manufacturing cost and shorter processing time. In Figure 9.7 the bottom and top rows are made up of similar tanks which reduces the number of unique tanks by a factor of two.

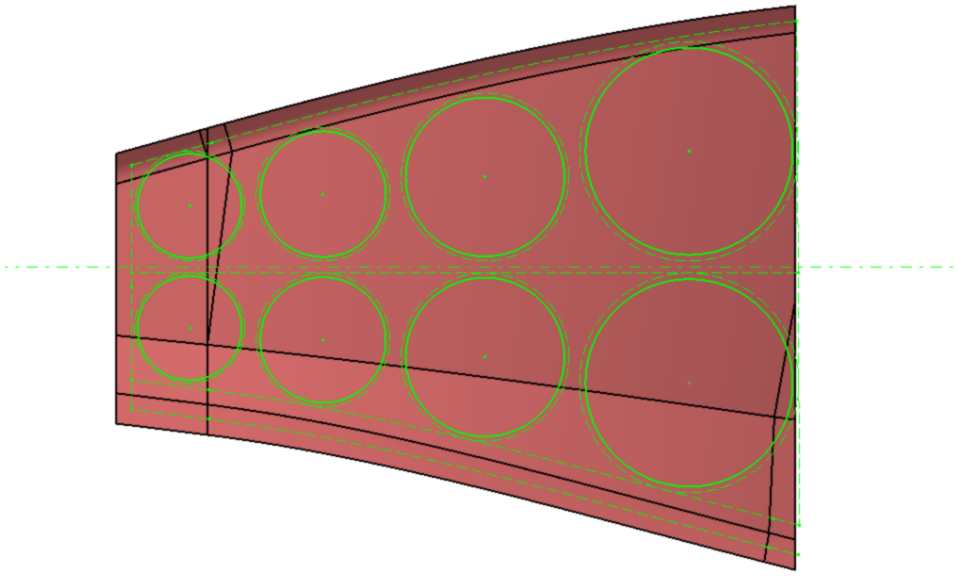

Figure 9.7: Cell pattern with clearances and imposed limits

This process can be automated with a Python script Then the individual cells can be sized and verified using the toolbox used for the standard design. Once the tanks have been sized using the conceptual design toolbox the BOP can be designed.

9.2.3. Balance-of-plant architecture

Now that the target volume has been filled with the optimum cell configuration and each cell has been designed according to the sizing module, the system BOP must be designed. As previously mentioned the detailed design of the BOP is out of the scope of this research project but some considerations and preliminary visuals will be given for future work.

The BOP mass and volume are taken as mass and volume fractions from literature similar to the conventional design. This is a conservative estimate as the BOP can be a central unit for all cells with minimal equipment per cell. In this case, a pressure regulator will be added to the end of each cell to ensure that the pressure out of the tank and inside the BOP components is controlled. A hydrogen line will run from each cell column or row and group all cells into one line, these lines will then be combined and input into the BOP central unit (See black box in Figure 9.8). Note there is a check valve at every intersection to ensure the flow is in the correct direction. This unit will ensure hydrogen control and delivery to the fuel cell stack. An example of the BOP architecture can be found in Figure 9.8

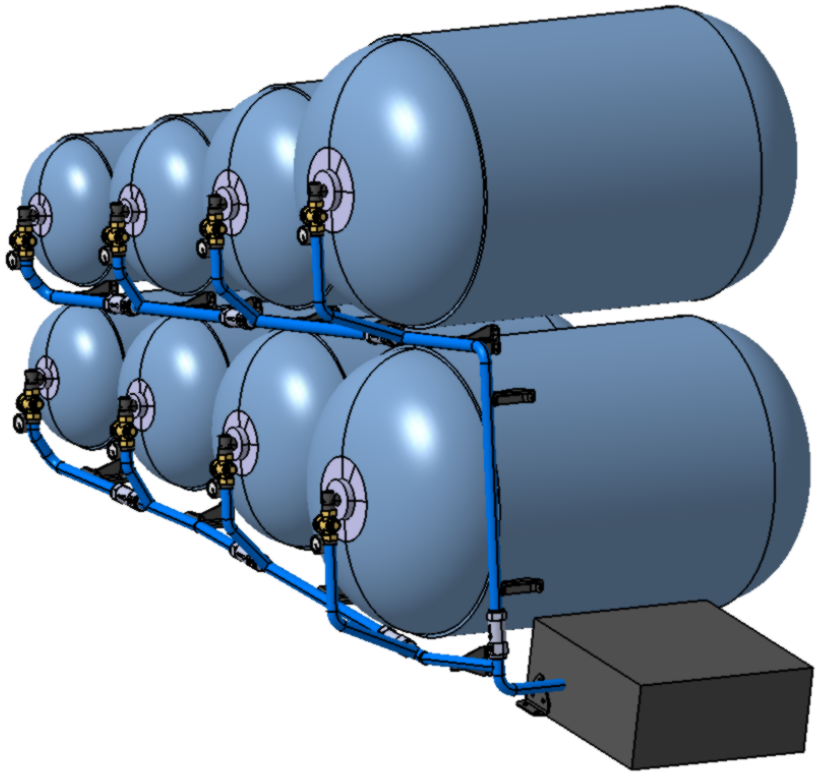

Figure 9.8: Preliminary BOP architecture with pressure regulators, check valves and central unit

9.2.4. System integration & attachment

Joined multi-cell pressure vessels require an outer structure to ensure that they are fastened within the target volume. This supporting structure needs to ensure that the cells stay together while allowing for some displacement due to the pressure inside the cells.

To reduce the vehicle and system mass the supporting structure will be a primary structure. As the system will be installed inside the tail section, the structure will also be used to mount the vehicle skin and required systems. The supporting structure can be seen in Figure 9.9.

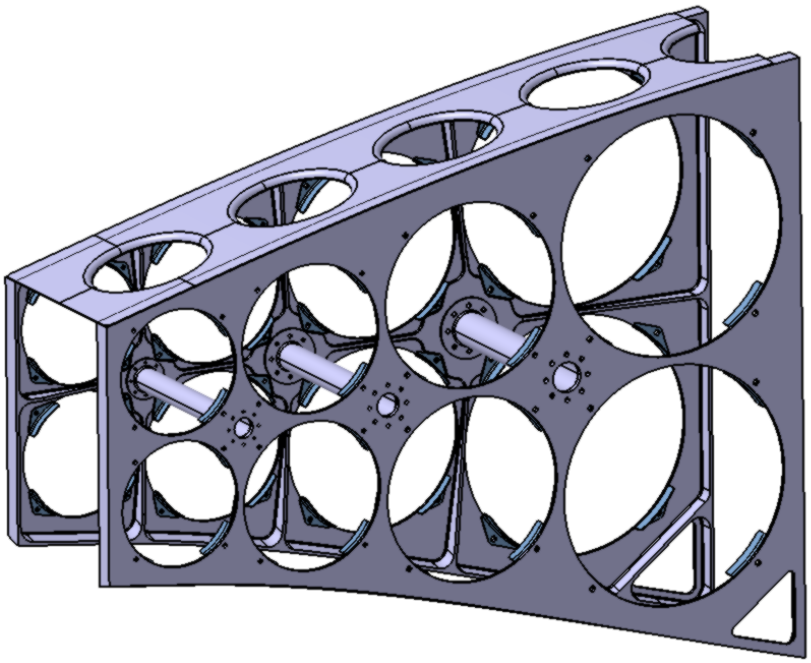

Figure 9.9: Overview of multi-cell concept outer structure

It is made up of two large aluminum ribs with a top skin. These ribs follow the skin of the tail with holes for the cells. Each hole has a 5 [mm] clearance such that the cell wall is not flush with the structure and can deform. A series of aluminum spacers are used to keep the ribs at a fixed distance (See Figure 9.10), this also ensures the lateral loads are not transferred by the cells.

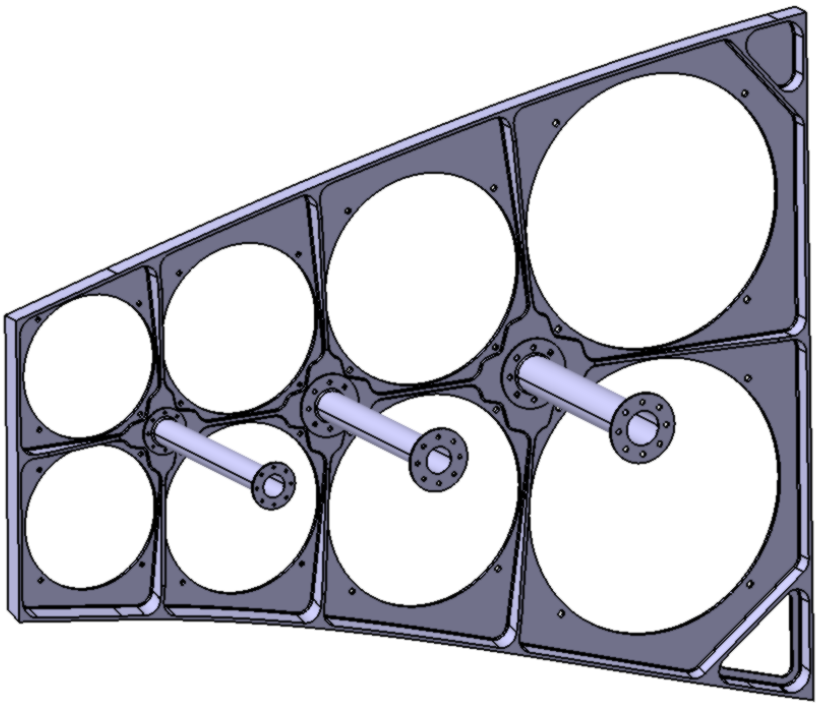

Figure 9.10: Multi-cell concept structure with aluminum spacers

The cells are mounted onto the supporting structure using four symmetric composite brackets, these can be co-cured to the cells during curing or simply fixed using adhesive during mounting. These brackets ensure the cell is fastened onto the structure. A series of silent blocs is used to dampen vibrations and allow cell deformation within the structure. An example bracket can be seen in Figure 9.11.

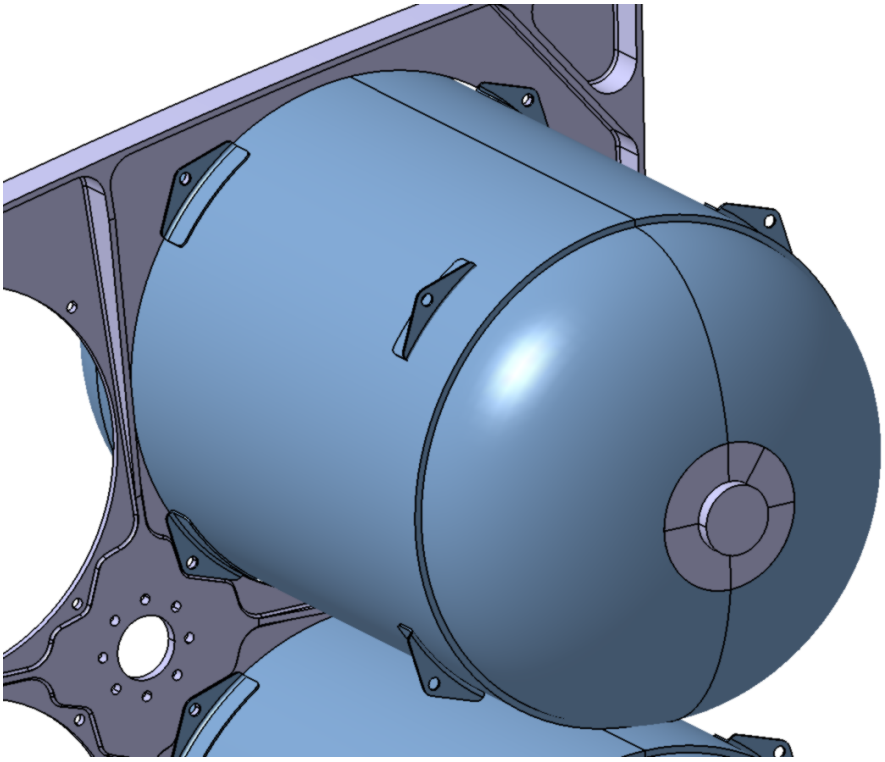

Figure 9.11: Multi-cell concept cell attachment brackets

With the supporting structure and system integration finished an overview of the multi-cell design will be given. This will be the subject of the next section.

9.3. Multi cell design overview

At this stage, the multi-cell of the pressure vessel is finished. The multi-cell design is made up of several Type IV pressure vessels with geodesic domes, these are called cells. Each cell has been designed using the toolbox for conceptual design. Then a supporting structure and BOP architecture have been proposed which completes the joined multi-cell concept. The goal of the multi-cell configuration is to increase the amount of on-board hydrogen. An overview of the multi-cell concept within the Varuna EVTOL can be found in Figure 9.12. The cells are made up of the same materials as the standard design. They are numbered from left to right and then up and down.

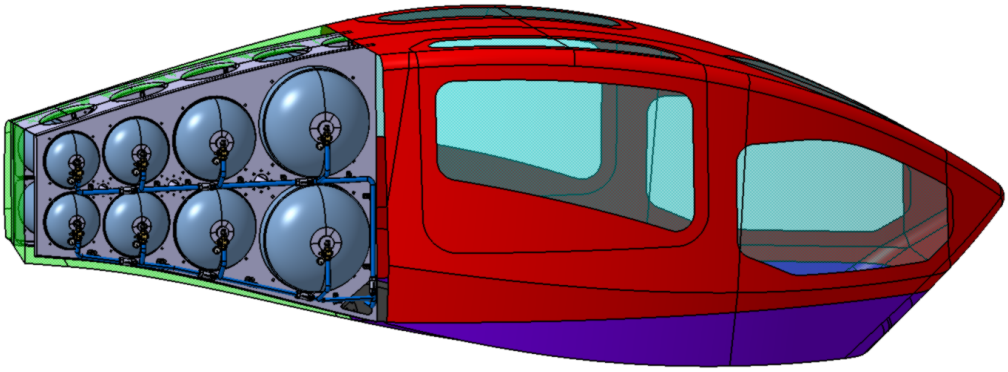

Figure 9.12: Render of joined multi-cell design inside Varuna EVTOL

The number of cells in the design is 8, it is the result of the space-filling method. Note that even more hydrogen can be brought on-board by decreasing the size of the cells and including many more cells. However, as the number of cells increases the mass of the system increases as well. The mass of the system increases linearly with the number of cells but the amount of hydrogen increases asymptotically. This means that a small increase in hydrogen comes at a high cost in mass. The 8-cell design is a compromise between mass and on-board hydrogen. A detailed view of the design can be found in Figure 9.13.

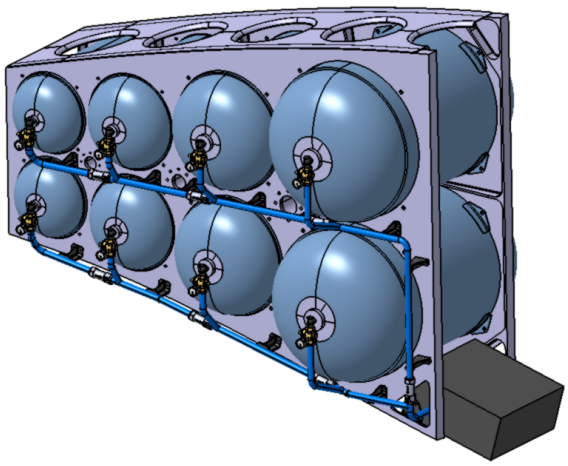

Figure 9.13: Detailed render of multi-cell concept

Since the multi-cell concept is made up of Type IV geodesic pressure vessels built using the toolbox for conceptual design the same assumptions apply (See Section 7.1). An overview of the design parameters per cell can be found in Table 9.1.

Table 9.1: Overview of design parameters for multi-cell concept

Property	Cell 1& 5	Cell 2& 6	Cell 3& 7	Cell 4& 8	Total
Cell mass [kg]	26.9	36.7	62.1	126.8	503.2
Hydrogen mass [kg]	2.8	4.1	7.3	15.6	59.5
Wall mass [kg]	14.2	20.2	35.2	74.4	287.4
Liner mass [kg]	5.0	5.6	8.0	12.9	62.0
Bosses mass [kg]	0.3	0.6	1.1	2.4	8.8
BOP mass [kg]	4.6	6.2	10.6	21.6	85.5
Total cell volume [L]	86.7	125.2	220.3	469.2	1801.6
Hydrogen volume [L]	69.7	102.6	182.6	393.5	1496.8
Wall volume [L]	9.0	12.8	22.4	47.3	182.7
Liner volume [L]	5.3	5.9	8.4	13.5	64.9
Bosses volume [L]	0.1	0.2	0.4	0.9	3.1
BOP volume [L]	2.6	3.8	6.6	14.1	54
Cell length [mm]	900.8	915.0	1013.9	1269.1	NA
Cell outer radius [mm]	187.3	222.5	277.5	362.2	NA
Cell LD ratio	2.4	2.1	1.8	1.7	NA

Similar to the preliminary design the three main efficiencies can be computed per cell and for the whole multi-cell concept, this is shown in Table 9.2. Note that for now the mass of the outer structure is neglected, this will be considered in Section 10.1.2.

Table 9.2: Overview of system efficiencies for the multi-cell concept

Efficiency	Cell 1& 5	Cell 2& 6	Cell 3& 7	Cell 4& 8	Total
Gravimetric [%]	10.2	10.6	11.2	11.8	11.3
Volumetric [g-H2L^{-1}]	30.9	31.2	31.6	32.0	31.7
Fill [%]	2.0	2.9	5.2	11.2	42.5

Finally, the mass and volume breakdown of the whole multi-cell concept can be obtained. This is shown in Figure 9.14 and 9.15.

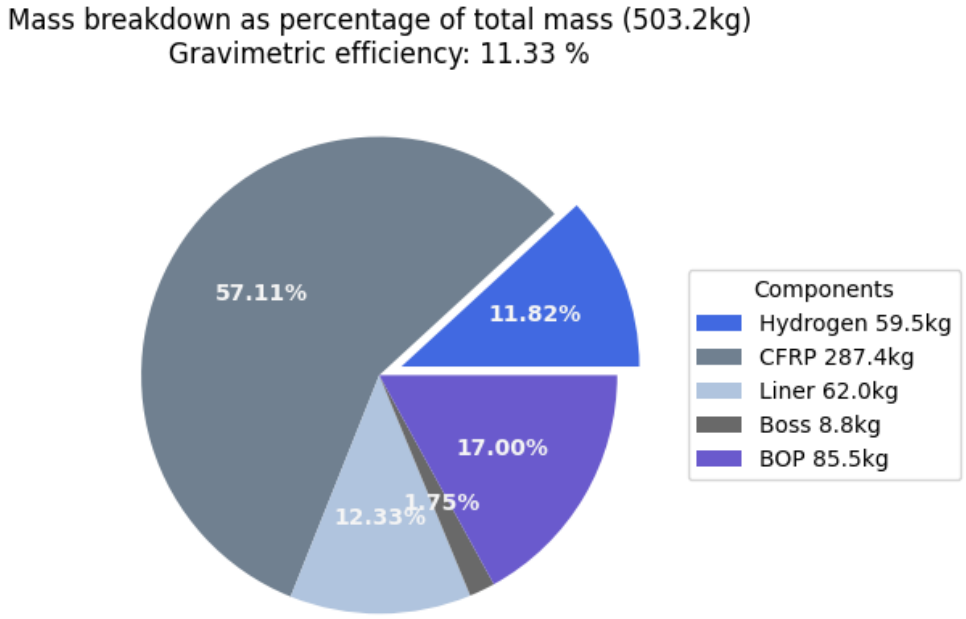

Figure 9.14: Mass breakdown of multi-cell concept

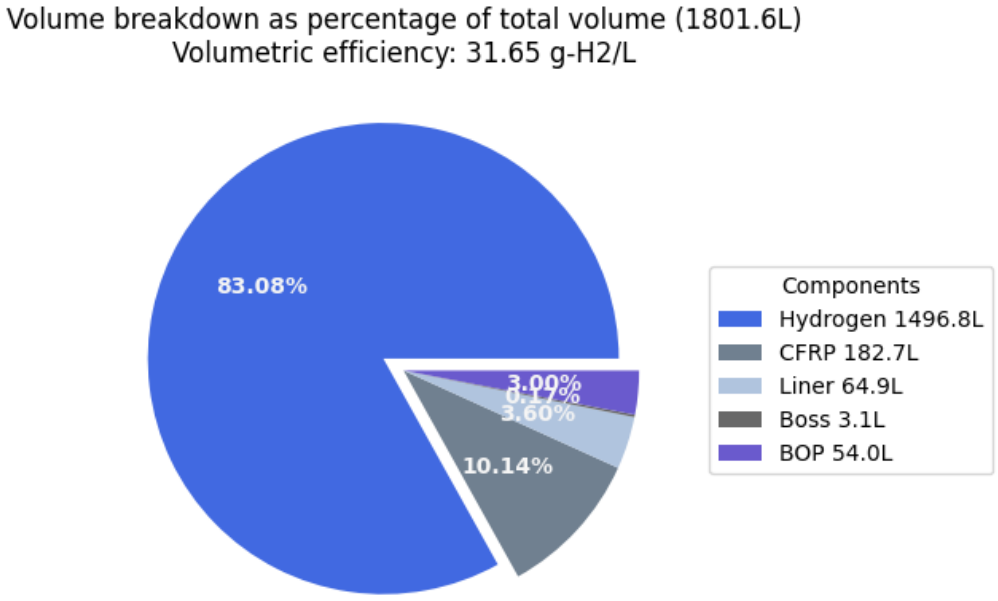

Figure 9.15: Volume breakdown of multi-cell concept

10. Results & discussion

The conventional and multi-cell conformable concept designs have been completed using the toolbox for conceptual design. This started with preliminary sizing followed by a series of thermal, structural, and hydrogen mass verifications before evaluating each concept's various performance criteria and efficiencies. At this stage, the results of the research project will be discussed.

First, a comparative analysis between the conventional and conformable concepts will be performed. This analysis will look at the various efficiencies and how they are defined before comparing the concepts. Then an alternative multi-cell concept will be discussed. Finally, the chosen design will be verified against the system requirements. This is the final step of the research project.

10.1. Comparative analysis

To determine whether the conformable concept is advantageous it must be compared to the conventional design. However, to do this the various performance criteria and efficiencies must first be defined. This will be treated in the next subsection.

10.1.1. Performance criteria & efficiencies

One of the key objectives of compressed hydrogen storage is to reduce the system mass and volume as much as possible. This is due to hydrogen's very low density despite its high specific energy. To quantify the system mass and weight for a given amount of hydrogen two parameters are used, mainly the gravimetric and volumetric efficiency. The definition of gravimetric and volumetric efficiency can be found in Equation 10.1 and 10.2.

$$\eta_{grav} = \frac{m_{H2}}{m_{tot}} \tag{10.1}$$

$$\eta_{vol} = \frac{m_{H2}}{V_{tot}} \tag{10.2}$$

Where η is efficiency, m_{H2} is the usable hydrogen mass, m_{tot} is the total system mass and V_{tot} is the total system volume.

The gravimetric efficiency measures how much hydrogen mass is stored over the total system mass which includes the BOP components, the pressure vessel wall, the liner, and the aluminum inserts. The ultimate DOE target for gravimetric capacity is 5.5 [%] [46].

The volumetric efficiency is similar to the gravimetric one since it measures how many kilograms of hydrogen are stored for a given system volume. It indicates how much space storing a kilogram of hydrogen takes. The ultimate goal of the DOE is 50 [g-H2L^{-1}] [46].

For this research project, another efficiency will be defined, it is called the fill efficiency. The fill efficiency represents the volume of stored hydrogen over the total available volume. In this case, the available volume is determined by the volume of the tail bounding box. This efficiency represents how much volume is used to store hydrogen by a concept, a higher value means that the space is used more efficiently. This efficiency is relevant when the design cannot be altered and the hydrogen storage must be contained within a pre-determined volume. The fill efficiency is defined in Equation 10.3.

$$\eta_{fill} = \frac{V_{H2}}{V_{avbl}} = \frac{V_{H2}}{V_{tail}} \tag{10.3}$$

Where V_{H2} is the usable hydrogen volume, V_{avbl} is the available volume and V_{tail} is the volume inside the tail bounding box.

All the relevant system efficiencies have been determined however these are not the only criteria that will be used to compare the concepts. A set of performance parameters will be defined to measure a concept's capability.

The first performance parameter that will be used to determine a concept's performance will be the total mass increase. This is defined in Equation 10.4. It represents the percentage increase in total vehicle mass. To estimate this the concept mass is added to the original vehicle mass. It is assumed that the fuel stack array will weigh as much as the current battery array and that the hydrogen storage solution is added to the overall system mass. Furthermore, a coefficient is added to the concept mass, this coefficient represents the mass required to integrate the concept to its environment. This coefficient is set to 1.2 which means that 20 [%] of the total system weight is additional structural mass.

$$M_{incr} = \frac{m_{tot} \cdot c_{str} + m_{EVTOL}}{m_{EVTOL}} \tag{10.4}$$

Where M_{incr} represents the percentage increase in vehicle mass, m_{tot} is the concept mass, c_{str} is the structural coefficient and m_{EVTOL} is the mass of Varuna.

Another performance criterion will be the hydrogen mass in the system. This represents how much hydrogen can be stored using the proposed concept. This will be compared to the minimum required amount of hydrogen from the preliminary sizing.

Finally, the last performance criterion will be adjusted flight time. This represents how much flight time can be expected from the converted EVTOL using a given concept. Since the concept mass is added to the original EVTOL mass, this increases the overall vehicle mass which in turns leads to an increase in required power. This mass and power increase can be translated into an adjusted flight time. The definition of adjusted flight time and its derivation can be found in Equation 10.5. This assumes that the increase in required power is linear with mass. This is accurate since a quadrotor drone needs to overcome its mass in order to ascend and hover. As such thrust is greater than or equal to vehicle mass.

$$p_{adj} = p_{avg} \cdot M_{incr} \qquad t_{adj} = \frac{m_{H2}}{m_{req}} \frac{p_{avg}}{p_{adj}} t_0 \tag{10.5}$$

Where p_{adj} is the adjusted required power, p_{avg} is the required average power, t_{adj} is the adjusted flight time, m_{req} is the required usable hydrogen mass from preliminary sizing and t_0 is the initial flight time.

Now that the various concept efficiencies and performance criteria have been defined the concepts can be compared. This will be done in the next subsection.

10.1.2. Design comparison

To select a concept and determine whether conformable compressed pressure vessels are advantageous over conventional pressure vessels, each concept must evaluated and compared according to the criteria defined in Section 10.1.1. An overview of the criteria per concept and their percentage difference can be found in Table 10.1.

Table 10.1: Performance criteria and efficiencies per concept

Property	conventional concept	Multi-cell concept	Percentage difference
Gravimetric efficiency [%]	12.1	11.3	-6.6 [%]
Volumetric efficiency [g-H2L^{-1}]	32.3	31.6	-2.0 [%]
Fill efficiency [%]	24.7	42.5	72.1 [%]
Vehicle mass increase [%]	10.3	18.8	7.7 [%]
Total concept mass [kg]	330.6	603.8	82.7 [%]
Hydrogen mass [kg]	34.8	59.5	70.5 [%]
Adjusted flight time [min]	28.4	43.2	52 [%]

When looking at the values in the table above it is clear that the multi-cell concept leads to a significant increase in flight time and on-board hydrogen at a reasonable vehicle mass increase. The total vehicle mass increase is less than 8 [%] for over 70 [%] increased hydrogen mass which in turn represents a 52 [%] increase in flight time.

In Chapter 7 the endurance requirement of 1 [h] was reduced to 30 [min] due to the conventional pressure vessel size. With the multi-cell concept, the total flight time is much closer to the initial requirement.

Additionally, it is clear that the gravimetric and volumetric efficiency of the system is similar for both concepts, this is because each cell of the multi-cell concept is an optimized geodesic cylindrical pressure vessel. The gravimetric efficiency decreases more than the volumetric one, this can be explained via Figure 9.5. There is a significant decrease in gravimetric efficiency as the number of cells increases.

It is clear that the multi-cell concept is much more fill efficient than the conventional concept with over 70 [%] increase. The multi-cell concept achieves a 42.5 [%] fill efficiency, which could be increased even further by reducing the cell size and increasing the number of cells. This would lead to a significant increase in mass compared to the increase in hydrogen mass.

Finally, it is clear that the multi-cell concept is much heavier than the conventional concept, this is expected since the cylindrical concept is a more optimal shape in terms of structural efficiency.

Note that currently, the multi-cell concept has been designed to maximize the amount of hydrogen inside the tail section. Another approach would be to increase the usable volume inside the tail. The proposed conventional pressure vessel concept uses up all the space inside the tail volume, this does not leave room for added systems or to increase the cabin space. An alternative multi-cell concept will be discussed in Section 10.2.

Overall the multi-cell concept significantly increases the amount of hydrogen that can be stored within a pre-determined volume at a reasonable increase in mass. This shows that the multi-cell concept is advantageous for vehicular applications where volume is restricted and cannot be changed.

10.2. Alternative multi-cell concept

One of the major advantages of the multi-cell concept is its filling efficiency, which can be used to increase the amount of on-board hydrogen. However, another application for this technology would be to free up space inside a given volume by optimizing the cell arrangement. Using a multi-cell configuration instead of a single-tank configuration leads to increased usable cabin space or reduced vehicle size.

Figure 10.1 shows a multi-cell concept whose adjusted flight time equals the conventional design. This configuration frees up 1280 [L] of tail volume for a total length of 500 [mm] (represented by green area in Figure 10.1), this volume can then be used to install systems, increase cabin space, reduce vehicle size... Note that since the multi-cell concept is heavier than a conventional pressure vessel concept, the required hydrogen mass is higher to achieve a similar flight time.

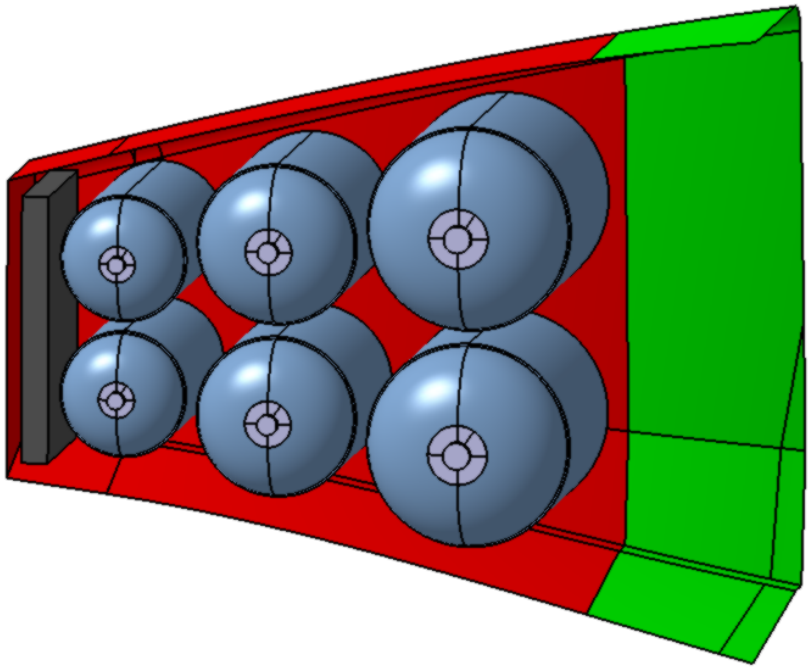

Figure 10.1: Multi-cell design with equivalent flight time compared to the conventional design

Using the multi-cell concept to achieve an equivalent flight time leads to an increase in system mass and volume. An overview of the performance criteria and efficiencies for both the conventional and equivalent multi-cell design can be found in Table 10.2. Overall, the increase in mass is negligible compared to the increase in usable volume. Since the mass increase is small the required hydrogen is similar for the conventional and equivalent multi-cell concepts.

Table 10.2: Performance criteria and efficiencies for the alternative concept

Property	conventional concept	Equivalent multi-cell	Percentage difference
Gravimetric efficiency [%]	12.1	11.0	-9.1 [%]
Volumetric efficiency [g-H2L^{-1}]	32.3	31.5	-2.5 [%]
Fill efficiency [%]	24.7	24.9	0.8 [%]
Vehicle mass increase [%]	10.3	10.9	0.6 [%]
Total concept mass [kg]	330.6	350.0	5.8 [%]
Hydrogen mass [kg]	34.8	35.0	0.6 [%]
Adjusted flight time [min]	28.4	28.4	0 [%]

The equivalent multi-cell concept can be integrated inside the tail section in a similar way to the original multi-cell concept. The difference is that the BOP can be located at the back since there is more free space there. The structure and vehicle integration of the concept can be found in Figure 10.2.

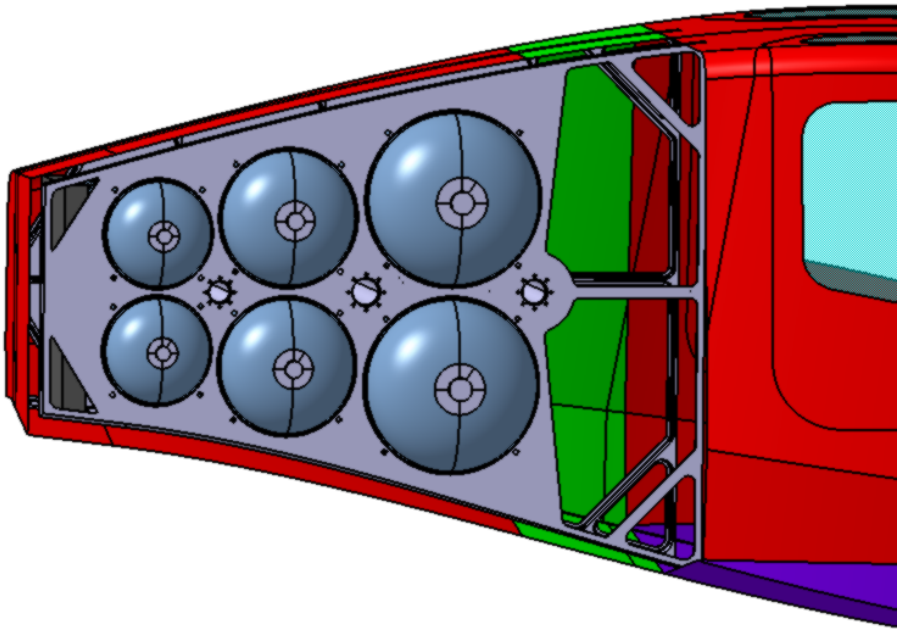

Figure 10.2: Equivalent multi-cell concept structural integration inside Varuna

Overall the multi-cell concept can be used to increase cabin size or reduce vehicle size at an equivalent hydrogen mass. This comes at a negligible increase in mass. This additional volume can be used to install other systems. If the vehicle size is reduced using a multi-cell concept a total vehicle mass decrease can be expected.

10.3. Requirement verification

The final step of the research project is to verify whether the preliminary design of the chosen concept meets the system requirements. This will be done sequentially. The chosen concept is the multi-cell concept made up of 8 individual cells. This concept maximizes onboard hydrogen.

Firstly, requirements SYS-THERM-01, SYS-THERM-02 are verified according to Section 8.2. From the figures it is clear that the wall temperature stays between 85 [C°] and -40 [C°]. This is not necessarily true for the hydrogen temperature which reaches low temperatures of up to -70 [C°]. However, this is most likely due to the adiabatic assumption which leads to very low temperatures when hydrogen mass is low. Note that this requirement has been verified for the conventional pressure vessel which is much larger than the individual cells of the multi-cell design. The hydrogen temperature rise and range increases as the hydrogen mass and volume increase, meanwhile the thermodynamic parameters are scaled with size and shape. Since the individual cells are smaller than the conventional design and similar in shape it is expected that the thermal behavior of the multi-cell concept will be less extreme than the conventional vessel.

Next, SYS-OPS-01, SYS-OPS-02, SYS-OPS-03 and SYS-OPS-04 are also verified accoriding to Section 8.1 and Section 8.3. The hydrogen mass and volume model which has been used to size the hydrogen pressure and mass required have been verified. Furthermore, the hydrogen pressure increase during filling has been shown to stay below 125 [%] of nominal pressure with thermal verification.

SYS-SAFE-01 has been verified via Section 8.3 which has proven that netting analysis is a suitable sizing method for composite pressure vessels. SYS-SAFE-02 has not been verified, the liner thickness has been taken from the literature but experiments need to be performed to verify the permeation rate

is lower than the specified limit.

SYS-MAT-01 and SYS-MAT-02 are verified, the wall material is carbon epoxy. Meanwhile, the liner is Polyamide6 which is a polymer material.

Finally, SYS-GEN-01 is verified as the multi-cell concept is located within the tail. SYS-GEN-02 is not verified as the maximum endurance achievable with the multi-cell concept is 45 minutes instead of 1 hour. However, this requirement was reduced to 30 minutes since the conventional design for 1-hour endurance was too large to fit within the tail section.

Overall, most requirements have been verified except for requirements SYS-SAFE-02 and SYS-GEN-02. This shows that the multi-cell pressure vessel is a suitable solution to store compressed hydrogen on board Varuna. A more in-depth verification of the thermal and structural requirements will be required in the future.

11. Conclusion

This research project aimed to investigate the potential of Type IV conformable compressed hydrogen pressure vessels to enhance the efficiency and performance of UAM vehicles, specifically the Varuna EVTOL. This was achieved by proposing a conceptual design for a conformable high-pressure hydrogen storage system which was compared to a conventional Type IV storage vessel.

The comparative analysis demonstrated that conformable pressure vessels could significantly increase the hydrogen mass stored within a predetermined volume, optimize space utilization, and improve the operational range of UAM vehicles compared to conventional pressure vessels. This will be shown by addressing the research sub-questions.

The first sub-question investigated how conformable pressure vessels could increase the hydrogen mass stored within a predetermined volume compared to conventional pressure vessels. The findings indicate that conformable pressure vessels, due to their ability to fit irregular spaces more effectively, can store a greater mass of hydrogen within the same volume. Using the Varuna EVTOL as a use case, the implementation of a conformable hydrogen storage system leads to a 70% increase in onboard hydrogen compared to a conventional Type IV storage system. This technology allows for a higher fill efficiency, contributing to longer flight duration and increased operational range for UAM vehicles.

The second sub-question examined the extent to which conformable pressure vessels can make better use of available space in UAM vehicles. Conformable vessels can adapt to the unique geometry of the Varuna EVTOL, integrating into the aircraft's design. This adaptability leads to improved space utilization, which is critical in the compact and weight-sensitive environment of UAM vehicles. Enhanced space efficiency not only improves overall vehicle design but also allows for additional components, increased payload capacity, or a decrease in vehicle size. Using a conformable storage system in Varuna saves up to 1200 [L] of cabin space compared to an equivalent conventional storage system.

Addressing the third sub-question, the study evaluated how conformable pressure vessels affect the operational range of UAM vehicles. The increased hydrogen mass storage and better space utilization contribute to a significant improvement in the operational range of the Varuna EVTOL. Overall, the conformable design provides a 52 [%] increase in flight time compared to the conventional design. By maximizing hydrogen storage capacity, conformable vessels enhance the vehicle's endurance, making it more viable for various urban mobility applications.

The final sub-question explored how the weight of conformable pressure vessels affects the overall weight and balance of UAM vehicles compared to conventional pressure vessels. The study found that while conformable pressure vessels tend to increase the overall mass of the vehicle due to their heavier construction compared to optimized conventional pressure vessels, this weight increase is acceptable. The slight increase in vehicle mass (+7.7 [%]) is outweighed by the substantial gains in operational range (+52 [%]) and hydrogen storage efficiency.

These findings suggest that conformable hydrogen storage systems can play a crucial role in advancing hydrogen-powered UAM technology, offering practical solutions to the challenges of hydrogen storage in aerospace applications. Additionally, these insights have broader implications for the transportation sector, potentially enhancing hydrogen-powered ground vehicle technology.

However, one limitation of the study was the reliance on theoretical models, which may not fully capture the complexities of real-world applications. The research focused on the preliminary design phase, and hence, some values and findings might change during the detailed design phase. Additionally, the study did not consider the economic and environmental aspects of implementing these technologies, which could impact the feasibility and adoption of the proposed solutions.

In conclusion, this research project has demonstrated the potential benefits of conformable hydrogen storage systems for UAM vehicles. By addressing key challenges in hydrogen storage, this research contributes to the advancement of sustainable aerospace technologies and sets the stage for further innovations in the field.

12. Recommendations & future work

Based on the findings of this research, several recommendations can be made for the further development and optimization of conformable hydrogen storage systems for UAM vehicles like the Varuna EVTOL. This is especially important as the research project focuses on the preliminary design stage.

The first recommendation is regarding the geodesic dome contour, the current method uses a numerical integration which only works up to a certain radius. Once the local radius is equal to 1.22 times the polar opening an asymptote is reached and the method becomes inaccurate. Improving the geodesic contour algorithm via another method such as Wang's cubic interpolation method would be desirable. This will lead to a more accurate dome contour, particularly around the polar opening. This will have a positive impact on the structural and mass sizing.

Another recommendation would be to consider alternative filament winding patterns. The current design uses a geodesic winding, the use of non-geodesic winding can lead to a more optimal dome design. This will increase the burst pressure and decrease the mass of the design. Non-geodesic paths allow more flexibility in the dome design and can potentially improve the design further.

The current hydrogen mass sizing assumes that the hydrogen is in a perfect gaseous state and at a constant temperature. The hydrogen is modeled using a variety of equations of state but does not model the phase of hydrogen inside the vessel. A potential recommendation would be to improve the accuracy of the hydrogen state modeling by considering multiple phases of hydrogen inside the tank (i.e. liquid, gaseous, supercritical...). Furthermore, accounting for the temperature variation of hydrogen inside the tank would yield more accurate mass and pressure results.

Another recommendation would be to consider a triple-zone heat model. This will improve the thermal analysis of the design by also simulating the liner of the pressure vessel. This would result in more accurate thermal modeling and account for the thermodynamic behavior of the liner. Currently, the model only accounts for the wall and hydrogen thermodynamic properties and behaviors.

To further improve the thermal model a proper estimation of the heat transfer coefficient must be derived. The model assumes a constant heat transfer coefficient which is not true in reality. This lowers the accuracy of the thermal model which is undesirable.

The thermal model has been used to verify the large conventional design, it is recommended to thermally verify the conformable design as well. Currently, the thermal behavior of the conformable design is assumed to be less extreme than the larger conventional design. However, this should be verified using the proposed model.

The thermal model is adiabatic and assumes no heat loss to the environment. This is accurate for short operational phases like filling but not during emptying. The thermal model can be further improved by accounting for the heat loss to the environment.

Another recommendation is regarding the structural verification of the conformable design, the current FEM analysis is not comprehensive enough to verify the design. It is recommended to derive an analytical structural model to compare the FEM results.

Furthermore, the current FEM model does not include the aluminum bosses or the liner. The accuracy of the results would improve if all the components of the pressure vessel were modeled.

The current FEM analysis only looks at the stresses and moments at the element level without any applied failure criteria. It is recommended to look at stresses and moments at the individual ply level and to include failure criteria for the burst pressure. The implementation of the maximum stress or Tsai-Wu criteria at the ply level would improve the structural model and allow proper verification of the design.

The final recommendation is regarding the evaluation of the performance and efficiency of the conventional and conformable design where the structural mass of the design is assumed via a coefficient. In

the future, it is recommended to design and evaluate the structural mass per concept to provide a more accurate mass and volume comparison.

In the future, several key steps must be taken to finish the design and implement it into the Varuna EVTOL. These steps must be taken after the recommendations have been implemented.

The first step concerns the detailed design. Moving beyond the preliminary design phase, it is necessary to perform a detailed design and prototype. This will allow for the validation of theoretical models and provide a more accurate assessment of performance and integration challenges.

Secondly, a cost and life cycle analysis must be performed. This will provide new metrics to compare the design and can be used to further evaluate the feasibility of conformable storage technologies in aerospace systems.

Next, the structural integration of the design must be further detailed. This includes a clash analysis within the Varuna environment. During this step, issues such as crashworthiness and maintainability must be investigated.

Finally, a manufacturing plan and philosophy are required to successfully realize the design. This will detail the time, processes, and resources required to manufacture the design and integrate it into the Varuna EVTOL.

In conclusion, the recommendations outlined in this section provide a roadmap for advancing the design and implementation of conformable hydrogen storage systems in UAM vehicles, offering practical solutions to address current challenges and paving the way for sustainable aerospace technologies in the future.

References

[1] B Gabriel, *Présentation Projet E VTOL*, French, Presentation, Expleo Toulouse, Jan. 2023. (visited on 10/20/2023).

[2] *SAE J 2601/2:2023-07-06*, fr. [Online]. Available: https://www.normadoc.com/french/sae-j-2601-2-2023-07-06.html (visited on 06/04/2024).

[3] H. Barthelemy, M. Weber, and F. Barbier, "Hydrogen storage: Recent improvements and industrial perspectives," *International Journal of Hydrogen Energy*, Special issue on The 6th International Conference on Hydrogen Safety (ICHS 2015), 19-21 October 2015, Yokohama, Japan, vol. 42, no. 11, pp. 7254–7262, Mar. 2017, ISSN: 0360-3199. DOI: 10.1016/j.ijhydene.2016.03.178. [Online]. Available: https://www.sciencedirect.com/science/article/pii/S0360319916305559 (visited on 10/24/2023).

[4] T. Hua *et al.*, "Technical assessment of compressed hydrogen storage tank systems for automotive applications," *International Journal of Hydrogen Energy*, vol. 36, pp. 3037–3049, Feb. 2011. DOI: 10.1016/j.ijhydene.2010.11.090.

[5] A. N. A. Mubin, M. H. Bahrom, M. Azri, Z. Ibrahim, N. A. Rahim, and S. R. S. Raihan, "Analysis performance of proton exchange membrane fuel cell (PEMFC)," en, *IOP Conference Series: Materials Science and Engineering*, vol. 210, no. 1, p. 012 052, Jun. 2017, Publisher: IOP Publishing, ISSN: 1757-899X. DOI: 10.1088/1757-899X/210/1/012052. [Online]. Available: https://dx.doi.org/10.1088/1757-899X/210/1/012052 (visited on 06/04/2024).

[6] S. Sulaiman, S. Borazjani, and S. H. Tang, "Finite element analysis of filament-wound composite pressure vessel under internal pressure," en, *IOP Conference Series: Materials Science and Engineering*, vol. 50, no. 1, p. 012 061, Dec. 2013, ISSN: 1757-899X. DOI: 10.1088/1757-899X/50/1/012061. [Online]. Available: https://dx.doi.org/10.1088/1757-899X/50/1/012061 (visited on 06/04/2024).

[7] R. M. Gheshlaghi, M. H. Hojjati, and H. R. M. Daniali, "Analysis of Composite Pressure Vessels," en, in *Fracture of Nano and Engineering Materials and Structures*, E. E. Gdoutos, Ed., Dordrecht: Springer Netherlands, 2006, pp. 335–336, ISBN: 978-1-4020-4972-9. DOI: 10.1007/1-4020-4972-2_165.

[8] K. W. Harrison, R Remick, and G. D. Martin, "Hydrogen Production: Fundamentals and Case Study Summaries; Preprint," en, National Renewable Energy Laboratory, Jan. 2010.

[9] H. Chen, J. Zheng, P. Xu, L. Li, Y. Liu, and H. Bie, "Study on real-gas equations of high pressure hydrogen," *International Journal of Hydrogen Energy*, 2008 International Hydrogen Forum (HyForum2008), vol. 35, no. 7, pp. 3100–3104, Apr. 2010, ISSN: 0360-3199. DOI: 10.1016/j.ijhydene.2009.08.029. [Online]. Available: https://www.sciencedirect.com/science/article/pii/S0360319909012749 (visited on 06/04/2024).

[10] P. Chatzinas, E. Bilalis, A. Papadakis, and N. Tsouvalis, "Effect of manufacturing parameters on the mechanical properties of filament wound composite materials," in Nov. 2021, pp. 377–385, ISBN: 978-1-00-323037-3. DOI: 10.1201/9781003230373-43.

[11] Q. Zhang, H. Xu, X. Jia, L. Zu, S. Cheng, and H. Wang, "Design of a 70 MPa type IV hydrogen storage vessel using accurate modeling techniques for dome thickness prediction," *Composite Structures*, vol. 236, p. 111 915, Mar. 2020, ISSN: 0263-8223. DOI: 10.1016/j.compstruct.2020.111915. [Online]. Available: https://www.sciencedirect.com/science/article/pii/S0263822319344897 (visited on 06/04/2024).

[12] M. Madhavi, "Design and Analysis of Filament Wound Composite Pressure Vessel with Integrated-end Domes," en, *Defence Science Journal*, vol. 59, no. 1, pp. 73–81, Jan. 2009, Number: 1, ISSN: 0976-464X. DOI: 10.14429/dsj.59.1488. [Online]. Available: https://publications.drdo.gov.in/ojs/index.php/dsj/article/view/1488 (visited on 06/04/2024).

[13] S. Sulaiman, S. Borazjani, and S. H. Tang, “Finite element analysis of filament-wound composite pressure vessel under internal pressure,” en, *IOP Conference Series: Materials Science and Engineering*, vol. 50, no. 1, p. 012 061, Dec. 2013, ISSN: 1757-899X. DOI: 10.1088/1757-899X/50/1/012061. [Online]. Available: https://dx.doi.org/10.1088/1757-899X/50/1/012061 (visited on 06/04/2024).

[14] M. J. Siddiqui, P. K. Balguri, K. Haripriya, A. R. Rajendran, and I. V. Patil, “Analysis of type IV hydrogen pressure vessel with S-glass, Carbon fiber T700 and Kevlar composite materials,” *Materials Today: Proceedings*, Sep. 2023, ISSN: 2214-7853. DOI: 10.1016/j.matpr.2023.09.036. [Online]. Available: https://www.sciencedirect.com/science/article/pii/S2214785323046989 (visited on 06/04/2024).

[15] *H-Mat R&D Activities*. [Online]. Available: https://h-mat.org/research-and-development/ (visited on 06/04/2024).

[16] Y. Su, H. Lv, W. Zhou, and C. Zhang, “Review of the Hydrogen Permeability of the Liner Material of Type IV On-Board Hydrogen Storage Tank,” en, *World Electric Vehicle Journal*, vol. 12, no. 3, p. 130, Sep. 2021, Number: 3 Publisher: Multidisciplinary Digital Publishing Institute, ISSN: 2032-6653. DOI: 10.3390/wevj12030130. [Online]. Available: https://www.mdpi.com/2032-6653/12/3/130 (visited on 06/04/2024).

[17] P. Blanc-Vannet *et al.*, “Sample scale testing method to prevent collapse of plastic liners in composite pressure vessels,” *International Journal of Hydrogen Energy*, Special issue on The 7th International Conference on Hydrogen Safety (ICHS 2017), 11-13 September 2017, Hamburg, Germany, vol. 44, no. 17, pp. 8682–8691, Apr. 2019, ISSN: 0360-3199. DOI: 10.1016/j.ijhydene.2018.10.031. [Online]. Available: https://www.sciencedirect.com/science/article/pii/S0360319918332087 (visited on 06/04/2024).

[18] Y. Su, H. Lv, C. Feng, and C. Zhang, “Hydrogen permeability of polyamide 6 as the liner material of Type □ hydrogen storage tanks: A molecular dynamics investigation,” *International Journal of Hydrogen Energy*, vol. 50, pp. 1598–1606, Jan. 2024, ISSN: 0360-3199. DOI: 10.1016/j.ijhydene.2023.10.154. [Online]. Available: https://www.sciencedirect.com/science/article/pii/S036031992305262X (visited on 06/04/2024).

[19] C. Dong *et al.*, “Hydrogen Permeability of Polyamide 6 Used as Liner Material for Type IV On-Board Hydrogen Storage Cylinders,” *Polymers*, vol. 15, no. 18, p. 3715, Sep. 2023, ISSN: 2073-4360. DOI: 10.3390/polym15183715. [Online]. Available: https://www.ncbi.nlm.nih.gov/pmc/articles/PMC10534423/ (visited on 06/04/2024).

[20] *Hydrogen Tank Liner*, en, May 2023. [Online]. Available: https://hyfindr.com/en/hydrogen-knowledge/hydrogen-tank-liner (visited on 06/04/2024).

[21] H. Barthelemy, M. Weber, and F. Barbier, “Hydrogen storage: Recent improvements and industrial perspectives,” en, *International Journal of Hydrogen Energy*, vol. 42, no. 11, pp. 7254–7262, Mar. 2017, ISSN: 03603199. DOI: 10.1016/j.ijhydene.2016.03.178. [Online]. Available: https://linkinghub.elsevier.com/retrieve/pii/S0360319916305559 (visited on 06/04/2024).

[22] R. Rejab, K. Kadirgama, M. Noor, S. Sani, and R. Daud, “Modification and Testing of Four Axes Filament Winding Machine,” Jan. 2008.

[23] D. I. Kis and E. Kókai, “A review on the factors of liner collapse in type IV hydrogen storage vessels,” *International Journal of Hydrogen Energy*, vol. 50, pp. 236–253, Jan. 2024, ISSN: 0360-3199. DOI: 10.1016/j.ijhydene.2023.09.316. [Online]. Available: https://www.sciencedirect.com/science/article/pii/S0360319923050310 (visited on 06/04/2024).

[24] A. Kayran and C. S. İbrahimo□lu, “Preliminary study on the applicability of semi-geodesic winding in the design and manufacturing of composite towers,” en, *Journal of Physics: Conference Series*, vol. 555, no. 1, p. 012 059, Dec. 2014, ISSN: 1742-6596. DOI: 10.1088/1742-6596/555/1/012059. [Online]. Available: https://dx.doi.org/10.1088/1742-6596/555/1/012059 (visited on 06/04/2024).

[25] *Aluminum 2024-T4 Material Data Sheet*. [Online]. Available: https://asm.matweb.com/search/SpecificMaterial.asp?bassnum=ma2024t4 (visited on 06/04/2024).

[26] *Overview of materials for Nylon 6, Cast*. [Online]. Available: https://www.matweb.com/search/DataSheet.aspx?MatGUID=8d78f3cfcb6f49d595896ce6ce6a2ef1&ckck=1 (visited on 06/04/2024).

[27] *Thermoset Epoxy Prepreg - Toughened PRepreg System - Fast Cure Prepreg | Toray Composite Materials America*. [Online]. Available: https://www.toraycma.com/products/prepreg/ (visited on 06/04/2024).

[28] H.-C. Wu and C. D. Eamon, "3 - Composite mechanics," in *Strengthening of Concrete Structures using Fiber Reinforced Polymers (FRP)*, H.-C. Wu and C. D. Eamon, Eds., Woodhead Publishing, Jan. 2017, pp. 19–34, ISBN: 978-0-08-100636-8. DOI: 10.1016/B978-0-08-100636-8.00003-X. [Online]. Available: https://www.sciencedirect.com/science/article/pii/B978008100636800003X (visited on 06/04/2024).

[29] M. Nebe, A. Johman, C. Braun, and J. M. J. F. van Campen, "The effect of stacking sequence and circumferential ply drop locations on the mechanical response of type IV composite pressure vessels subjected to internal pressure: A numerical and experimental study," *Composite Structures*, vol. 294, p. 115 585, Aug. 2022, ISSN: 0263-8223. DOI: 10.1016/j.compstruct.2022.115585. [Online]. Available: https://www.sciencedirect.com/science/article/pii/S0263822322003725 (visited on 06/04/2024).

[30] A. Tcharkhtchi, S. Villalonga, N. Zirak, A. Lucas, S. Farzaneh, and M. Shirinbayan, "Optimal dome design for 700 bar hydrogen tank type IV: Hyperelliptic functions and shape factor," en, *Energy Storage*, vol. 5, no. 7, e469, 2023, _eprint: https://onlinelibrary.wiley.com/doi/pdf/10.1002/est2.469, ISSN: 2578-4862. DOI: 10.1002/est2.469. [Online]. Available: https://onlinelibrary.wiley.com/doi/abs/10.1002/est2.469 (visited on 06/04/2024).

[31] Z. Padovec, D. Vondráček, and T. Mares, "The Analytical and Numerical Stress Analysis of Various Domes for Composite Pressure Vessels," *Applied and Computational Mechanics*, vol. 16, pp. 151–166, Jan. 2023. DOI: 10.24132/acm.2022.781.

[32] R. Wang, W. Jiao, W. Liu, and F. Yang, "Dome Thickness Prediction of Composite Pressure Vessels by a Cubic Spline Function and Finite Element Analysis," *Polymers and Polymer Composites*, vol. 19, no. 2-3, pp. 227–234, Mar. 2011, Publisher: SAGE Publications Ltd STM, ISSN: 0967-3911. DOI: 10.1177/0967391111019002-327. [Online]. Available: https://doi.org/10.1177/0967391111019002-327 (visited on 06/04/2024).

[33] M. Kormann and I. L. Krüger, "Application of a real gas model by van-der-waals for a hydrogen tank filling process," in *Proceedings of the 13th International Modelica Conference, Regensburg, Germany, March 4–6, 2019*, ser. Modellica, Linköing University Electronic Press, Feb. 2019. DOI: 10.3384/ecp19157665. [Online]. Available: http://dx.doi.org/10.3384/ecp19157665.

[34] E. W. Lemmon, M. L. Huber, and J. W. Leachman, "Revised Standardized Equation for Hydrogen Gas Densities for Fuel Consumption Applications," *Journal of Research of the National Institute of Standards and Technology*, vol. 113, no. 6, pp. 341–350, 2008, ISSN: 1044-677X. DOI: 10.6028/jres.113.028. [Online]. Available: https://www.ncbi.nlm.nih.gov/pmc/articles/PMC4652867/ (visited on 06/05/2024).

[35] J. Xiao, X. Wang, X. Zhou, P. Bénard, and R. Chahine, "A dual zone thermodynamic model for refueling hydrogen vehicles," *International Journal of Hydrogen Energy*, Special issue on The 7th International Conference on Hydrogen Safety (ICHS 2017), 11-13 September 2017, Hamburg, Germany, vol. 44, no. 17, pp. 8780–8790, Apr. 2019, ISSN: 0360-3199. DOI: 10.1016/j.ijhydene.2018.10.235. [Online]. Available: https://www.sciencedirect.com/science/article/pii/S0360319918335183 (visited on 06/05/2024).

[36] J. Xiao *et al.*, "Thermodynamic and heat transfer models for refueling hydrogen vehicles: Formulation, validation and application," *International Journal of Hydrogen Energy*, vol. 52, pp. 172–190, Jan. 2024, ISSN: 0360-3199. DOI: 10.1016/j.ijhydene.2023.06.081. [Online]. Available: https://www.sciencedirect.com/science/article/pii/S0360319923029385 (visited on 06/05/2024).

[37] A. Couteau, P. Dimopoulos Eggenschwiler, and P. Jenny, “Heat transfer analysis of high pressure hydrogen tank fillings,” en, *International Journal of Hydrogen Energy*, vol. 47, no. 54, pp. 23 060–23 069, Jun. 2022, ISSN: 03603199. DOI: 10.1016/j.ijhydene.2022.05.127. [Online]. Available: https://linkinghub.elsevier.com/retrieve/pii/S0360319922021905 (visited on 06/05/2024).

[38] V. Molkov, M. Dadashzadeh, and D. Makarov, “Physical model of onboard hydrogen storage tank thermal behaviour during fuelling,” en, *International Journal of Hydrogen Energy*, vol. 44, no. 8, pp. 4374–4384, Feb. 2019, ISSN: 03603199. DOI: 10.1016/j.ijhydene.2018.12.115. [Online]. Available: https://linkinghub.elsevier.com/retrieve/pii/S0360319918340837 (visited on 06/05/2024).

[39] D. G. Casey, J. M. Rovner, R. M. Roberts, and C. L. Krause, “Method for calculating hydrogen temperature during vehicle fueling,” pat. US7647194B1, Jan. 2010. [Online]. Available: https://patents.google.com/patent/US7647194B1/en (visited on 06/05/2024).

[40] J. Jadoon, A. Shazad, M. Muzamil, M. Akhtar, and M. Sattar, *Finite Element Analysis of Composite Pressure Vessel Using Reduced Models.* | *Tecciencia* | *EBSCOhost*, en, ISSN: 1909-3667 Issue: 33 Pages: 49 Volume: 17, Jul. 2022. DOI: 10.18180/tecciencia.2022.33.5. [Online]. Available: https://openurl.ebsco.com/contentitem/doi:10.18180%2Ftecciencia.2022.33.5?sid=ebsco:plink:crawler&id=ebsco:doi:10.18180%2Ftecciencia.2022.33.5 (visited on 06/05/2024).

[41] H. Kang *et al.*, “Stress–strain and burst failure analysis of fiber wound composite material high-pressure vessel,” en, *Polymers and Polymer Composites*, vol. 29, no. 8, pp. 1291–1303, Oct. 2021, Publisher: SAGE Publications Ltd STM, ISSN: 0967-3911. DOI: 10.1177/0967391120965387. [Online]. Available: https://doi.org/10.1177/0967391120965387 (visited on 06/05/2024).

[42] S. Aceves, G. Berry, A. Weisberg, F. Espinosa-Loza, and S. Perfect, “Advanced Concepts for Vehicular Containment of Compressed and Cryogenic Hydrogen,” *16th World Hydrogen Energy Conference 2006, WHEC 2006*, vol. 3, Jan. 2006.

[43] Y. Choi, J. Ahn, and D. Chang, “Time-Dependent Reliability Analysis of Plate-Stiffened Prismatic Pressure Vessel with Corrosion,” en, *Mathematics*, vol. 9, no. 13, p. 1544, Jan. 2021, Number: 13 Publisher: Multidisciplinary Digital Publishing Institute, ISSN: 2227-7390. DOI: 10.3390/math9131544. [Online]. Available: https://www.mdpi.com/2227-7390/9/13/1544 (visited on 06/05/2024).

[44] R. Du, P. Zhang, and G. Xu, “Multi-cell hydrogen storage devices with extra volumetric capacity,” *Journal of Power Sources*, vol. 185, no. 2, pp. 1322–1327, Dec. 2008, ISSN: 0378-7753. DOI: 10.1016/j.jpowsour.2008.09.030. [Online]. Available: https://www.sciencedirect.com/science/article/pii/S0378775308018235 (visited on 10/11/2023).

[45] T. Propulsion, “High-Pressure Conformable Hydrogen Storage For Fuel Cell Vehicles,” en, *Proceedings of the 2000 Hyrogen Program Review*,

[46] *DOE Technical Targets for Onboard Hydrogen Storage for Light-Duty Vehicles*, en. [Online]. Available: https://www.energy.gov/eere/fuelcells/doe-technical-targets-onboard-hydrogen-storage-light-duty-vehicles (visited on 06/05/2024).